UNIVERSITY OF OKLAHOMA

GRADUATE COLLEGE

IDENTIFICATION AND ISOLATION OF BIOACTIVE NATURAL PRODUCT COMPOUNDS TARGETING OXYSTEROL-BINDING PROTEINS

A THESIS

SUBMITTED TO THE GRADUATE FACULTY

in partial fulfillment of the requirements for the

Degree of

MASTER OF SCIENCE

By

INES FORREST
Norman, Oklahoma
2020

IDENTIFICATION AND ISOLATION OF BIOACTIVE NATURAL PRODUCT

COMPOUNDS TARGETING OXYSTEROL-BINDING PROTEINS

A THESIS APPROVED FOR THE
DEPARTMENT OF CHEMISTRY AND BIOCHEMISTRY

BY THE COMMITTEE CONSISTING OF

Dr. Robyn Biggs, Chair

Dr. Adam S. Duerfeldt

Dr. Daniel T. Glatzhofer

Dr. Isabelle Ripoche

Dr. Isabelle Thomas

To my parents, to whom I owe everything.

To my grandmother and aunt, whose inspirational fight is and will forever be the reason for my passion and dedication to scientific research.

Acknowledgements

This thesis is the result of an incredible experience. I would not have been able to complete my Master's year without the help of several people who actively contributed to its successful completion. I would like to express my gratitude and respect to them.

Firstly, I would like to thank my advisor Dr. Anthony Burgett, for giving me the opportunity to join his laboratory and above all, for his confidence in regard to the projects I worked on. That being said, I also thank the former and current members of the Burgett Research Group, who have been not just colleagues, but friends and daily support. Special thanks to Dr. Anh Le-McClain and Dr. Cori Malinky for being great mentors in lab, for always having my back in the most difficult times, for all the good times outside of lab and for contributing to my development both as a person and scientist. I would also like to acknowledge my biochemist colleagues, namely Zach, Matt and Dr. Ryan Bensen, for their enthusiasm and willingness to teach me more about their field, and for helping me since I arrived.

I wish to thank the Department of Chemistry and Biochemistry, and to individually thank my committee members, namely Dr. Adam Duerfeldt for everything he thought me especially in medicinal chemistry, for helping me since day one and for giving me new opportunities to grow as a scientist, and Pr. Daniel Glatzhofer, for his constant motivation, his kindness and for allowing me to continue practicing my German now and then (Vielen Dank!). I express my warm thanks to Dr. Isabelle Ripoche and Dr. Isabelle Thomas, for their support during my two years at Sigma-Clermont, for their faith in me and for their encouragements to participate in this program, nothing would have been possible without them and their colleagues in the Chemistry Department.

Many thanks to Dr. Si Wu and Dr. Laura-Isobel McCall, for their support and for giving me more knowledge in the different ‘omics’ fields. I address my sincere thanks to Pr. George Richter-Addo, for taking me under his wing outside of work, for the long and motivational talks, for his valuable advice, for sharing his joy and passion for music and above all, for being a friend.

Last but not least, my everlasting gratitude goes to my parents, for their unconditional support even miles away, and for making me the person I am today.

Table of Contents

List of Tables

List of Figures

List of Abbreviations

μM: micromolar concentration (10^{-6} M)

ACE: angiotensin-converting enzyme

AcOH: acetic acid

Ala: alanine

ALS: amyotrophic lateral sclerosis

ANK: ankyrin

BuOH: butanol

cAMP:cyclic adenosine monophosphate

CC: column chromatography

CD3: cluster of differentiation 3

$CHCl_3$: chloroform

DAG: diacylglycerol

DEPT: distortionless enhancement of polarization transfer spectroscopy

DI: deionized

EMCV: encephalomyocarditis virus

ER: endoplasmic reticulum

ESI: electrospray ionization

EtOAc: ethyl acetate

EtOH: ethanol

FAB: fast atom bombardment

FDA: Food and Drug Administration

GI_{50}: half maximal cell growth inhibition

Gln: glutamine

GNPS: global natural product social molecular networking

$G_{\alpha q/11}$: G protein αq/11 subunit

HCV: hepatitis C virus

HPLC: high performance liquid chromatography

IC_{50}: half maximal inhibitory concentration

IP_3: inositol 1,4,5 triphosphate

IR: infrared spectroscopy

ITZ: itraconazole

K_D: dissociation constant

K_i: inhibition constant

LC_{50}: half maximal lethal concentration

Leu: leucine

LSC: leukemia stem cells

Lys: lysine

MDR: Multi-drug resistant

MeCN: acetonitrile

MeOH: methanol

MS: mass spectrometry

N: unaltered natural product

NB: botanical natural product (defined mixture)

NCI: National Cancer Institute

ND: natural product derivative

NM: mimic of natural product

nM: nanomolar concentration (10^{-9} M)

NMR: nuclear magnetic resonance spectroscopy

NOE: nuclear Overhauser effect

NP: natural product

ODS: octadecylsilanzied

OHC: hydroxycholesterol

ORD: oxysterol-binding domain

ORP4: OSBP-related protein 4

OSBP: oxysterol-binding protein

PDE: phosphodiesterase

PI4KIIIβ: type III phosphatidylinositol-4-kinase β

PIP: phosphatidylinositol phosphate

PLC: phospholipase C

RNA: ribonucleic acid

RO: replication organelle

S*: synthetic drug with natural product pharmacophore

S: synthetic drug

SAR: structure activity relationship

T-ALL: T-cell acute lymphoblastic leukemia

TCS: tumor cell survival

TM: transmembrane

UV: ultraviolet spectroscopy

VAP: vesical associate protein

List of Cancer Cell Lines

Blood Cancer (Leukemia): CCRF-CEM (acute lymphoblastic leukemia), HL-60 (acute promyelocytic leukemia), MOLT-4 (acute lymphoblastic leukemia), Jurkat (T acute lymphoblastic leukemia), K562 (acute promyelocytic leukemia).

Bone Cancer: HOS (osteosarcoma)

Brain Cancer: T98 (glioblastoma)

Breast Cancer: MCF7 (adenocarcinoma), MDA-MB-231 (adenocarcinoma), T-470 (Ductal Carcinoma)

Cervical Cancer: HeLa (epithelioid carcinoma)

Colorectal Cancer: HCT-116 (carcinoma), DLD-1 (adenocarcinoma)

Endometrial Cancer: Ishikawa (adenocarcinoma)

Gastric Cancer: AGS (adenocarcinoma), BGC-823 (carcinoma)

Liver Cancer: 7404 (hepatoma), HepG2 (hepatoma)

Lung Cancer: A549 (adenocarcinoma), NCI-H460 (carcinoma, large cell lung cancer)

Other: BJ (human fibroblasts)

Prostate Cancer: PC-3 (grade IV, adenocarcinoma)

Renal Cancer: A498 (adenocarcinoma)

Skin Cancer: G-361 (malignant melanoma), ARN8 (malignant melanoma)

Abstract

OSW-1, a plant-derived cholestane glycoside, has been shown to exhibit broad-spectrum antiviral activity by targeting oxysterol-binding protein (OSBP) and potent antiproliferative activity by targeting OSBP-related protein 4 (ORP4). In order to develop OSW-1 and OSW-1-derived compounds as potential antiviral or anticancer therapeutics, an understanding of OSW-1 structure-activity relationships (SAR) for binding to OSBP and ORP4 must be established. This SAR will allow for the identification of compounds with improved pharmacological properties and the development of selective OSBP- or ORP4-targeting compounds. To date, there are no reported protein structures of OSBP or ORP4, and the published research on OSW-1 only provides partial insight on the compound SAR. The major goal of this research project is to purify and identify OSW-1-related natural product compounds from *Ornithogalum saundersiae* bulbs. The new OSW-1-related compounds can then be subjected to biological testing, including binding to OSBP and ORP4, anticancer assays, and antiviral assays. Through the development of an efficient analytical method for the purification of natural products from *Ornithogalum saundersiae,* several OSW-1-related compounds, including newly discovered compounds, were purified and structurally characterized. Testing the isolated OSW-1-related compounds for OSBP and ORP4 binding will provide further SAR understanding, and progressively guide the discovery and synthesis of new OSBP and ORP4 specific compounds for pre-clinical drug development as new antiviral and anticancer drugs.

Chapter I: Introduction and Background

I.1 Overview of Naturally Occurring Small-Molecules in Drug Discovery

For millennia, natural products isolated from plants have provided health remedies.[1] Natural product compounds form the basis of highly sophisticated systems of traditional medicine, including Traditional Chinese, African and Ayuverdic Medicine (India).[2] In the modern scientific era, many pharmaceutical therapeutics are based on natural products (NPs), with the discovery of new natural products continuing to supply new therapeutic molecules.[3] According to a recently published review, 1,881 new drugs were approved by the FDA and similar organizations between January 1981 and September 2019. Of these approved therapeutics, 1,394 were small molecule drugs, among which, 713 are unaltered NPs (N), NP-derived (NB and ND), or synthetic drugs with NP pharmacophores (S*or S*/NM). An additional 681 are total synthetic drugs or mimics of NPs (S or S/NM). The evolution of the source of small molecules has been followed over the last 38 years (**Figure 1**, adapted from Newmann and Cragg).[4]

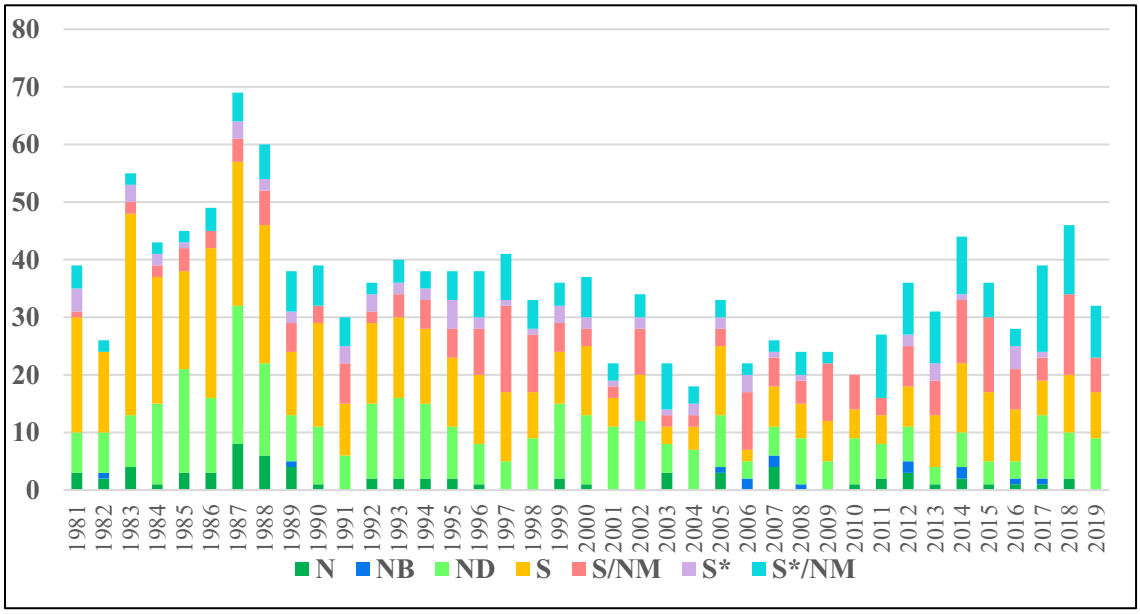

Figure 1. Source evolution of small-molecule approved drugs from 1981 to 2019.

Several structurally diverse molecules isolated from plant extracts have proven their effectiveness. For example, Artemisinin, isolated from Chinese sweet wormwood (*Artemisia annua*) is an essential antimalarial drug.[5] Paclitaxel, discovered from the bark of the Pacific yew tree (*Taxus baccata*) is a standard of care anticancer drug.[6] Galantamine is an alkaloid isolated from Snowdrops (*Galanthus nivalis*), which is used in the treatment of mild to moderate forms of Alzheimer's disease (**Figure 2**).[7]

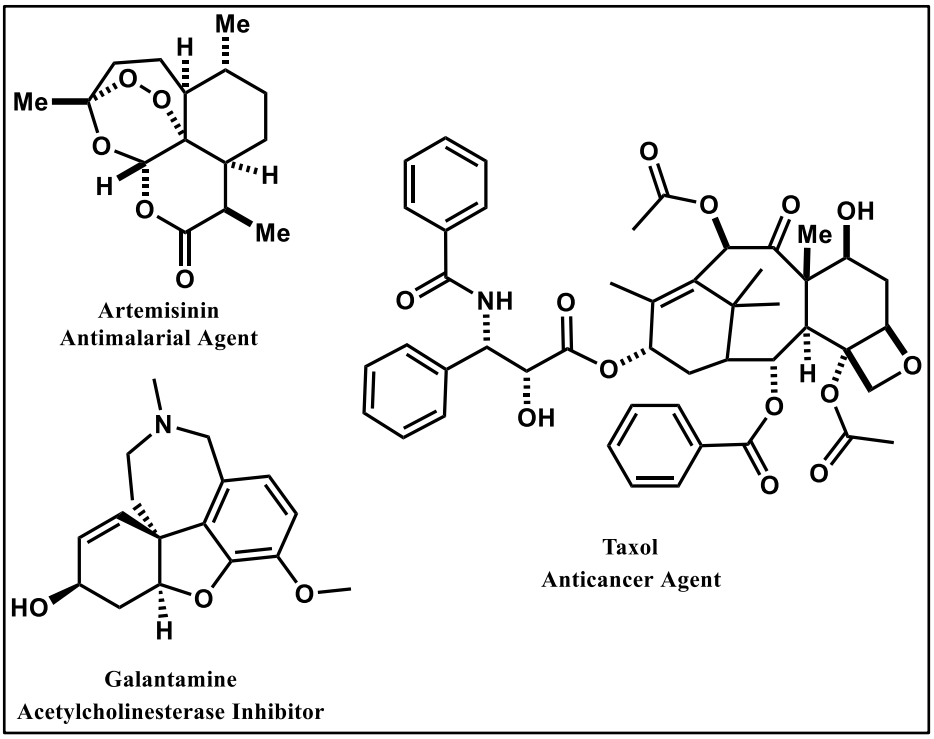

Figure 2. Structurally diverse bioactive natural products

The power of naturally occurring small-molecules lies in both their complexity, structural diversity, and disease-relevant biological activity.[8] Even today, Nature remains our greatest source of molecular inspiration, and new natural product molecules continue to be discovered in plants.[9] One specific family of bioactive NPs isolated from plants with potential therapeutic applications are the cholestane glycosides.

I.2 Saponins and Cholestane Glycosides

Saponins are a class of naturally occurring bioorganic compounds found in particular abundance in the plant kingdom. More specifically, they are glycosides described by the soap-like foaming (from Latin *sapo* meaning soap).[10] Structurally, these compounds have at least one glycosidic linkage between a hydrophobic aglycone (steroidal-C_{27} or triterpenoid-C_{30} skeleton) and varying numbers of hydrophilic sugar moieties (**Figure 3**).[10–13]

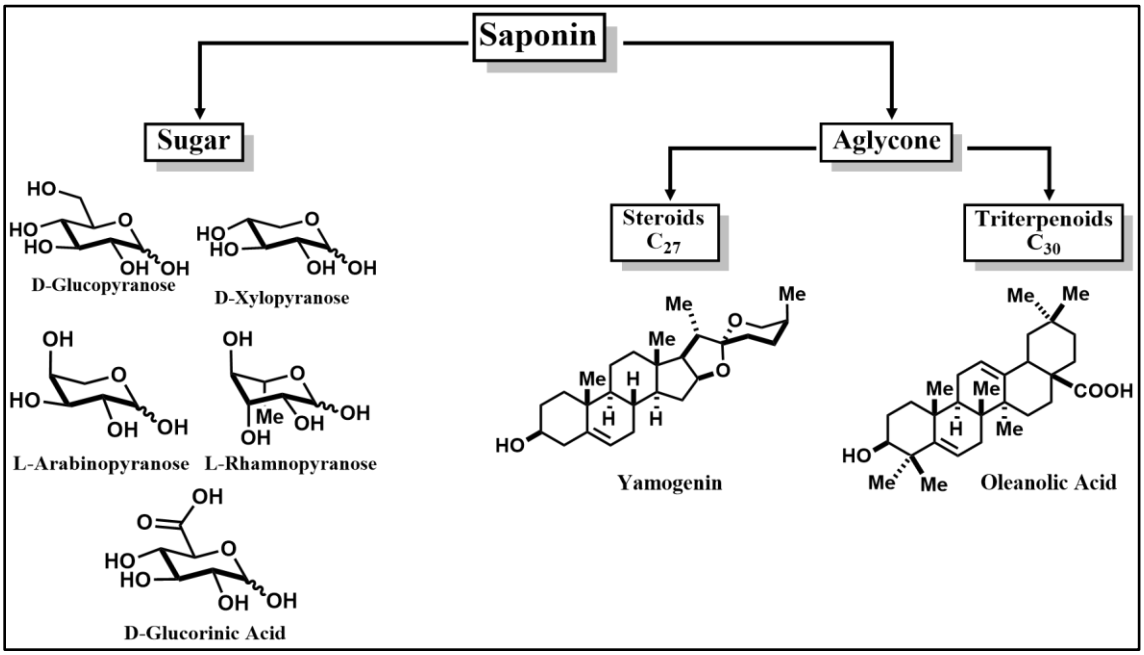

Figure 3. General saponin structure

Individual saponins display a range of exceptional medicinal properties and biological activities such as hemolytic, molluscicidal, anti-inflammatory, antifungal, antibacterial, antiviral, anticancer and cytotoxicity.[11] These properties represent the increasing importance of saponins in prospective therapeutic uses.[14] The discovery of Digitalis and Digoxin is a good example. These two steroidal saponins isolated from Foxglove (*Digitalis purpurea*) are cardiac glycosides used in the treatment of certain heart conditions such as congestive heart failure and heart rhythm problems.[15]

Likewise, the *Ornithogalum* plant genus (**Figure 4**) has drawn considerable attention over the past 15 years due to its production of steroidal saponins.[13] Although most *Ornithogalum* species do not exhibit medicinal properties, and some are even poisonous,[16] *Ornithogalum* bulbs produce a number of cholestane glycosides with promising biological activity, especially selective activity against malignant cancer cells versus non-transformed cells[17]).

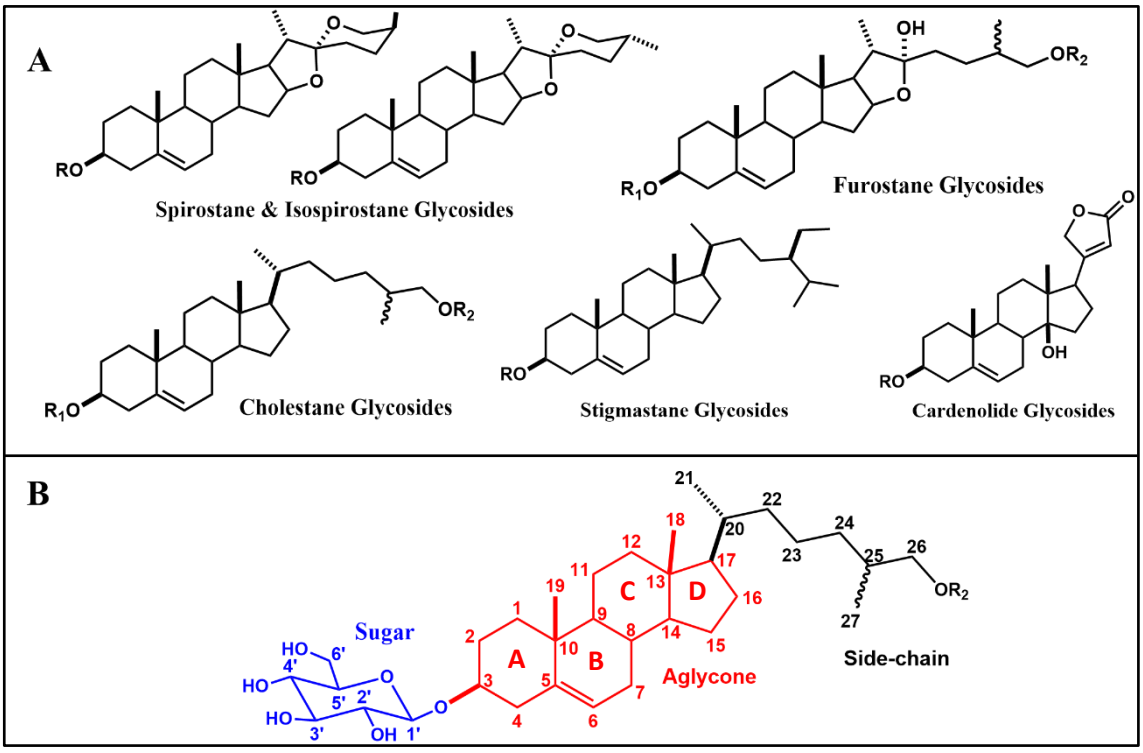

Figure 4. Steroidal saponin subfamilies from the Ornithogalum Genus (A) and cholestane glycoside numbering convention (B)

Despite their general structure similarity, these natural compounds are different in their aliphatic side chains, in the composition of the glycoside moiety and in their activity.[18–29]

I.3 The OSW-1 Natural Product

The *Ornithogalum saundersiae* flowering plant, also called the African Lily, is a perennial garden plant species native to the African Drakensberg Mountains, located in the Highveld region of South Africa and Swaziland.[17,30] In 1992, the Sashida group from the Tokyo College of Pharmacy disclosed the discovery and structural characterization of a group of cholestane glycosides isolated from a methanolic extract of *O. saundersiae* bulbs. The main component of this mixture was termed OSW-1 (**Figure 5**).[19]

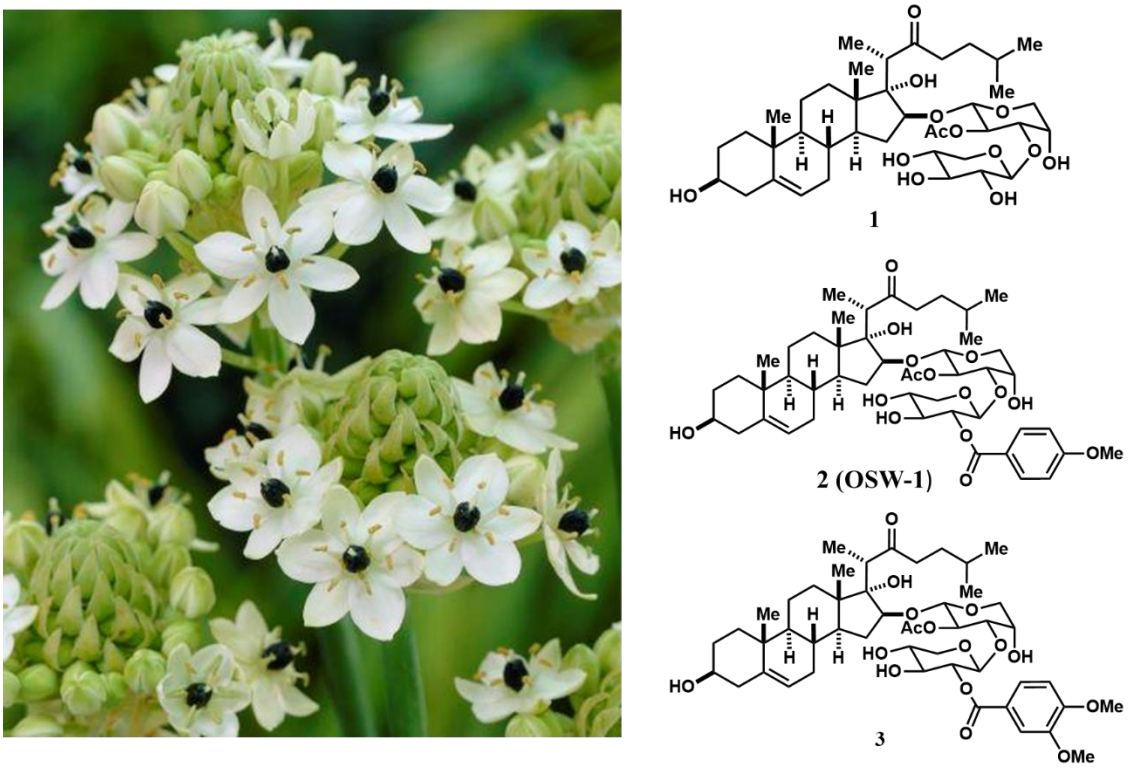

Figure 5. First group of cholestane glycosides (right) isolated from *Ornithogalum saundersiae* plant (left)

Upon isolation, OSW-1 was identified as a micromolar inhibitor (IC_{50} = 50 μM) of cyclic adenosine monophosphate (cAMP) phosphodiesterase (PDE).[17,19] Cyclic AMP is a nucleotide, which acts as a key second messenger in many signal transduction pathways involved in regulating various cellular functions, including cell growth, differentiation,

gene transcription and protein expression.[31] A PDE is an enzyme that degrades cAMP, thus influencing a vast array of pharmacological processes (e.g, pro-inflammatory mediator production, ion channel function, muscle contraction, differentiation, apoptosis). Inhibition of this enzyme causes cAMP increase, thus for example preventing heart failure or antagonizing malignant tumors in myeloid and lymphoid tissue.[32]

Five years later, OSW-1 was identified as the main cytotoxic compound contained in the bulbs, due to its exceptional potent cytotoxic activity against various malignant tumor cells, including HL-60 human promyelocytic leukemia cells.[33] In comparison with clinically applied anticancer agents, such as etoposide (IC_{50} = 25 nM), Adriamycin (IC_{50} = 7.2 nM) and methotrexate (IC_{50} = 12 nM), OSW-1 strongly suppresses HL-60 cell proliferation with an IC_{50} value of approximately 0.25 nM.[28,33] Moreover, OSW-1 demonstrated exceedingly potent activities when tested in the National Cancer Institute 60 cancer cell lines (NCI-60), with the mean growth inhibition (GI_{50}) of 0.78 nM, which is 10-100 times more potent than cisplatin, Taxol and mitomycin C.[33]

The OSW-1 compound has received great scientific attention because of its potent cytotoxic activities against various cultured tumor cell lines and cell growth inhibitory activities against experimental animal tumors.[17] These *in vitro* cytotoxic and *in vivo* antitumor screenings of OSW-1 have revealed that it is a possible novel anticancer drug candidate.[17,34] However, at that time, the lack of identification of the cellular targets and mechanism of action of OSW-1 limited its anticancer drug development.[35–47]

I.4 OSW-1's Cellular Targets: The OSBP and ORP Protein Family

In 2011, Burgett *et al.* identified oxysterol-binding protein (OSBP) and OSBP-related protein 4 (ORP4) as the cellular targets of OSW-1.[40] Subsequent to that discovery,

ORP4 has been recognized as a driver of cancer cell proliferation, including in patient isolated leukemias.[40,44,45] Unexpectedly, OSBP was recently discovered to be essential for RNA viral replication, and OSW-1 was reported to potently inhibit RNA viral replication by targeting OSBP.[48,49]

Oxysterol-binding protein (OSBP) and OSBP-related-proteins (ORPs) constitute a conserved family of eukaryotic proteins, from yeast to humans.[50–56] The OSBP/ORPs are involved in diverse cellular activities, including regulation of signaling pathways, lipid transport between organelles and lipid metabolism. The human OSBP/ORP family consists of 12 proteins (splicing generates 15 proteins), which can be subdivided into 6 subfamilies based on gene organization and amino acid homology (**Figure 6**). All members of this protein family possess a conserved sterol- or ligand-binding domain, named the OSBP-related domain (ORD).[50–56] The ORD contains conserved signature fingerprint region (EQVSHHPP). Outside of the ORD, several other regulatory domains are present in individual OSBP/ORPs. The N-terminal pleckstrin homology (PH) domain recognizes phosphatidylinositol phosphates (PIPs) with varying degrees of affinity.[51,57] The "two phenylalanines in an acidic tract" (FFAT) sequence motif allows for proteins to associate with the endoplasmic reticulum (ER) by binding vesical associate proteins (VAP).[53,58] The ankyrin repeats (ANK) allow ORP1L to associate with late endosomes.[59] Instead of FFAT motifs, ORP5 and ORP8 possess transmembrane (TM) domains that anchor the protein to membranes. [60] Additionally, some OSBP/ORP proteins have both short (S) variants, which lack the N-terminal PH domain and others present in the long (L) variants. The ORP short and long variants arise transcriptional initiation at different start-sides of the gene. [54]

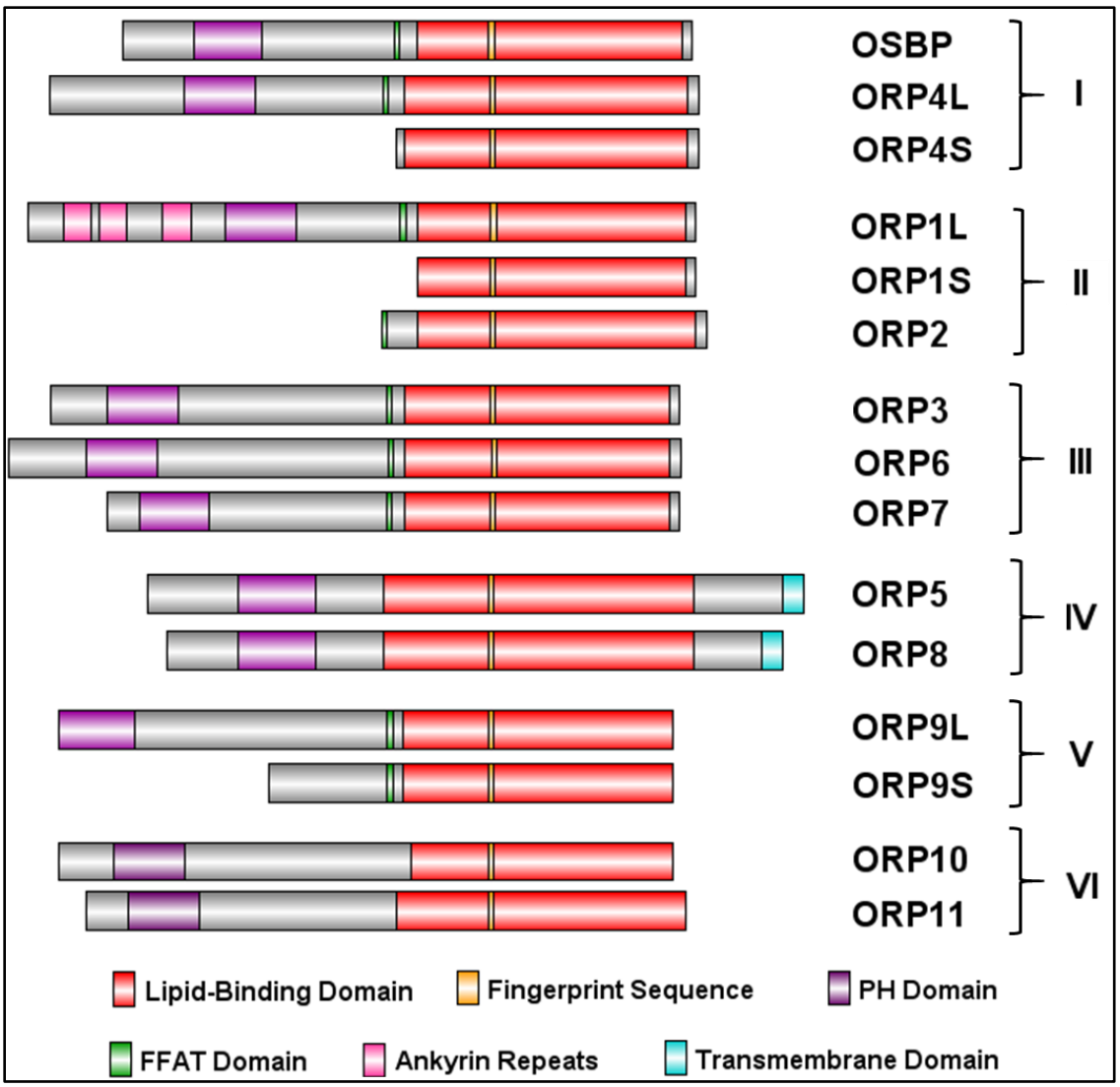

Figure 6. Domain homology diagrams of the human ORPs superfamily. Graphs were generated using DOG 2.0 software

Among this protein family, two members of subfamily I, OSBP and ORP4L, have drawn particular interest for the reasons stated above. These proteins share similar features such as the PH and FFAT domains and 68% identity in the ORD, resulting in 59% overall sequence homology (**Figure 7**).[51] However, OSBP and ORP4L have significantly different biological activities.[40,61]

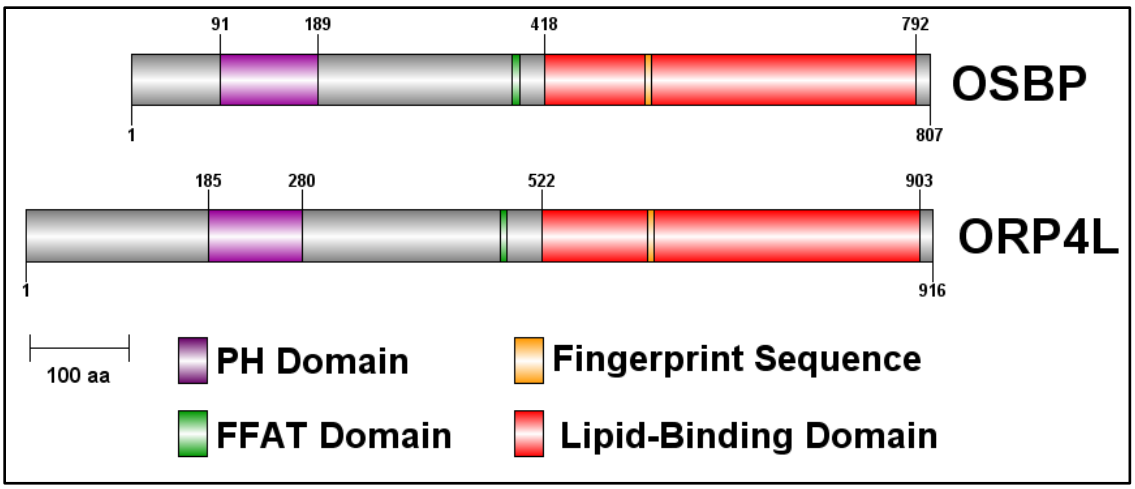

Figure 7. OSBP and ORP4L domain homology diagrams. Graphs were generated using DOG 2.0 software

I.4.1 OSBP and ORP4 as Druggable Targets

OSBP was originally discovered due to its ability to bind oxysterols.[62] These steroidal compounds are oxygenated derivatives of cholesterol involved in various cellular signaling responses.[50,53,56,63] Disruption of oxysterol activity can promote malignant cell proliferation.[50,53,56,63] OSBP particularly binds 25-hydroxycholesterol (25-OHC) with high affinity (K_D = 22 ± 5 nM)[64] in comparison to cholesterol (K_D ≈ 173 nM)[65,66]. Likewise, ORP4L binds to 25-OHC with similar affinity (K_D = 17 nM)[40] and to cholesterol at lower affinity (K_D = 63 nM).[42,62,67] There are no protein structures of OSBP or ORP4, making ligand binding on the molecular level unclear. There are only protein structures of *Saccharomyces cerevisiae* yeast OSBP homologs (i.e., Osh proteins), which share approximately 55% overall sequence homology.[56,59,68,69] Im *et al.* reported the first structure of Osh4 co-crystalized with several oxysterols including 25-OHC.[56,59,68] According to this co-crystal structure, the ligand-binding pocket contains a hydrophobic tunnel and a flexible N-terminal lid capable of shielding the bound ligand sterol from the aqueous environment.[70] After lipid transport, the lid opens and has a flat surface allowing

for contact with the cell membrane and possible sterol injection into the membrane (**Figure 8A**).[70] The C3-hydroxyl group of 25-OHC forms direct hydrogen bonding with Gln96 residue and water-mediated hydrogen bonds to a polar cluster of amino acids at the bottom of the ligand binding pocket. Likewise,C25-hydroxyl group interacts with a water molecule that mediates interactions with Leu24, Leu27, Lys109 and Ala29 residues in the lid putative region (**Figure 8B**).[70–73]

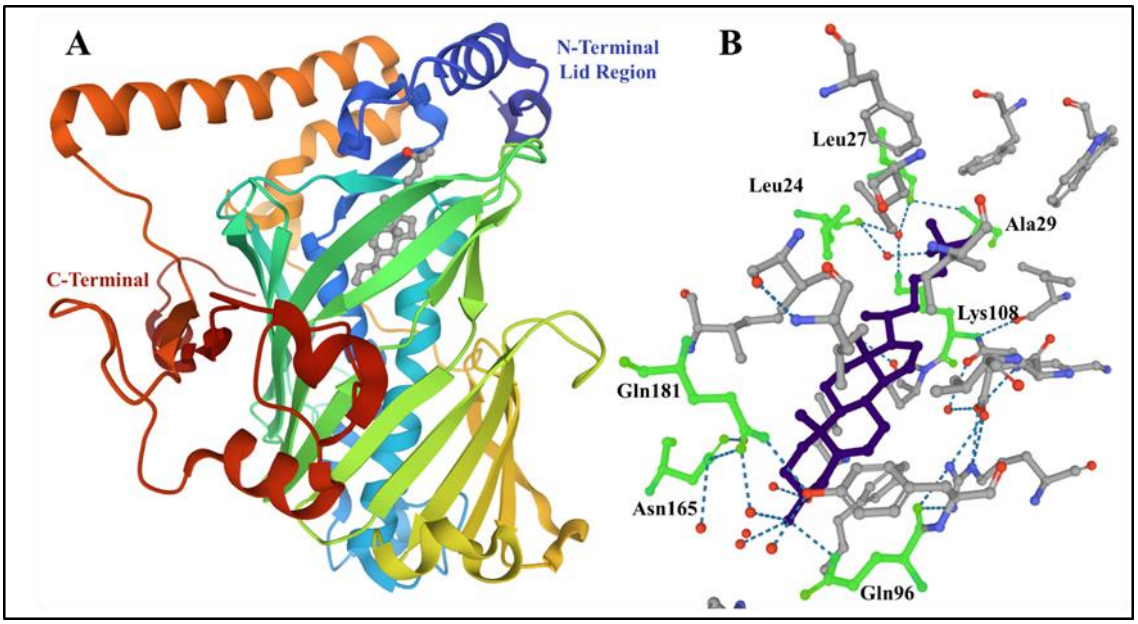

Figure 8. (A) Structure of Osh4 co-crystallized with 25-OHC. Protein backbones and sidechains are colored according to residue sequence identity, from blue (N-terminal), to red (C-terminal). **(B) 25-OHC interacting with tunnel entrance and N-terminal lid region residues.** 25-OHC is highlighted in purple and residues that interact with 25-OHC are highlighted in green. Figures were generated using RCSB Protein Data Bank.

In addition to oxysterols, Burgett *et al*. were able to demonstrate, through affinity purification and proteomic analysis, that OSBP and ORP4L are the specific cellular targets of a group of structurally diverse naturally-occurring small molecules, including OSW-1, cephalostatin[74], ritterazine B[74,75], schweinfurthin A[76] and stellettin E[77] (**Figure 9**). These natural products have been named the ORPphilins, based on their ability to interact with OSBP and ORPs.[40]

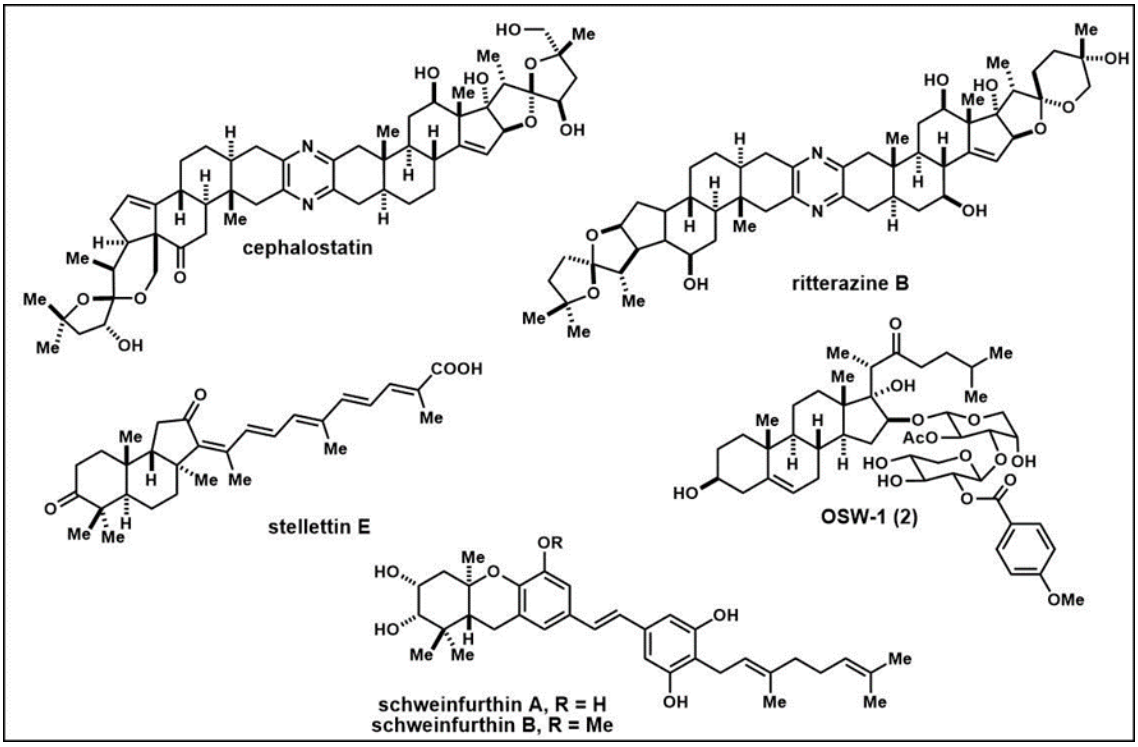

Figure 9. Chemical structures of ORPphillins

As mentioned above, 25-OHC is a high affinity ligand of OSBP and ORP4L. Therefore, to assess each ORPphilin's OSBP and ORP4L binding affinity, competitive binding assays were carried out with [^{3}H]25-OHC. Results for OSW-1, cephalostatin, ritterazine B and schweinfurthin A are summarized in **Table 1**. Ritterazine B binds to OSBP with higher affinity than ORP4 in the 25-OHC competitive binding assay. Stellettin E was not available for testing and putatively assigned as an ORPphilin based on similar antiproliferative profiles to the ORPphilin.[40]

	25-OHC	Cephalostatin	OSW-1	Ritterazine B	Schweinfurthin A
OSBP	32 ± 14	39 ± 10	26 ± 9	28 ± 4	68 ± 23
ORP4L	54 ± 23	78 ± 15	54 ± 11	>350	2,600 ± 570

Table 1. ORPphilins inhibitory constant (K_i) values (nM) compared to 25-OHC

These results indicate that the ORPphilins indeed bind to both OSBP and ORP4L with high affinity.[40] Schweinfurthin A and Ritterazine B are outliers in that their affinity for ORP4L was considerably lower than their affinity for OSBP.[40]

I.4.2 Potential Anticancer Drug Development by targeting ORP4L

ORP4L was demonstrated to be overexpressed in cancer and to drive cancer proliferation. ORP4L is reported to be essential for mitochondrial bioenergetics in T-cell acute lymphoblastic leukemia (T-ALL).[44,45,78] The protein is proposed to function as a scaffold for inositol triphosphate (IP_3) signaling, which ultimately results in calcium (Ca^{2+}) uptake into the mitochondria.[44,45,78] More precisely, ORP4L assembles CD3ε, $G_{\alpha q/11}$ and PLCβ3 into a complex that activates PLCβ3.[44,45,78] PLCβ3 catalyzes IP_3 production in T-ALL, as opposed to PLCγ1 in normal T-cells, allowing Ca^{2+} release from the ER and thus increased oxidative phosphorylation. (**Figure 10**).[36,41,42,44,47]

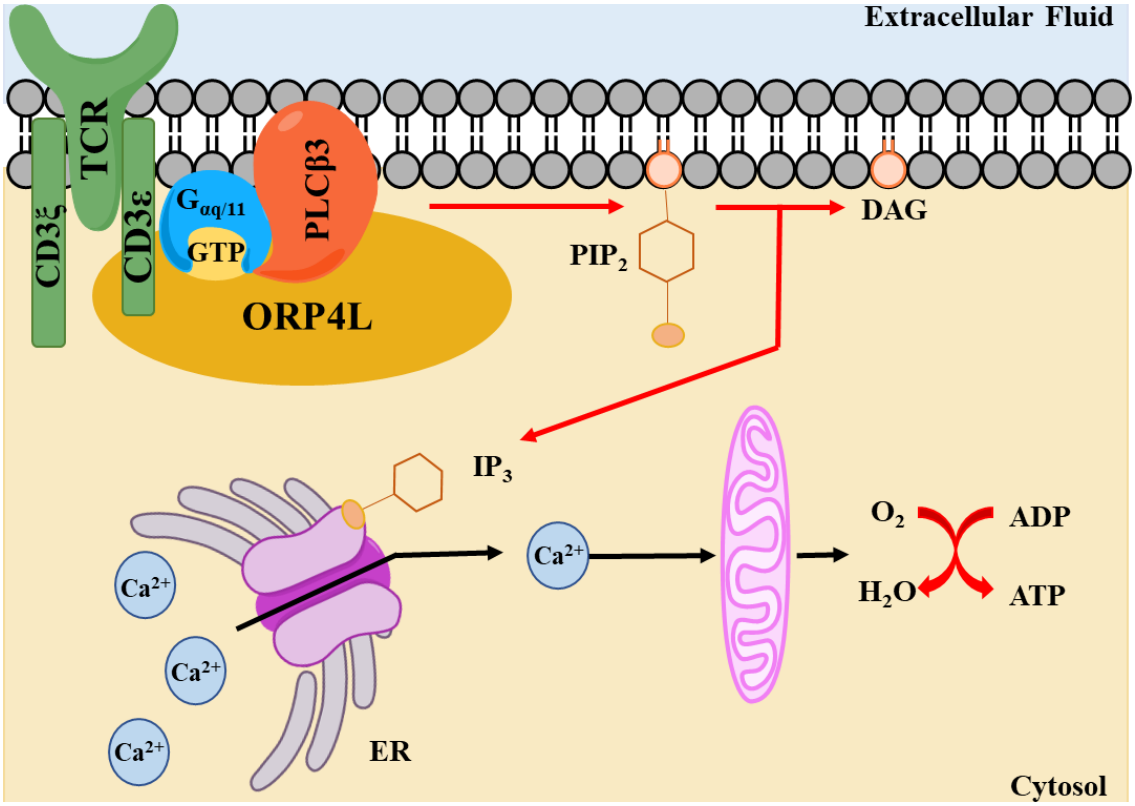

Figure 10. ORP4L mediates G protein-coupled ligand-induced PLCβ3 activation, resulting in an increase of mitochondrial respiration for cell survival

Inhibition of ORP4L expression in T-ALL cells prevents malignant cell proliferation and leads to apoptosis.[45] Hence, ORP4L can serve as a precision cancer therapeutic target.[79]

I.4.3 Potential Antiviral Drug Development by targeting OSBP

In contrast with ORP4L, OSBP is present in all human tissues.[53,80,81] It is localized in the cytosol at the Golgi-ER interface, and recently, OSBP has been reported to play a pivotal role in PI(4)P and cholesterol counterflow transport between the ER and Golgi.[53,80,81] OSBP is able to contact both the ER membrane with its FFAT domain and the Golgi membranes with its PH domain.[81] Tethered by the PH and FFAT domains, the ORD is able to transfer cholesterol from the ER to the Golgi, and back transfer PI(4)P from the Golgi to the ER. PI(4)P is then hydrolyzed by the ER protein Sac1 to provide energy which drives the sterol transfer (**Figure 11**).[81] In addition to these cellular activities, OSBP is implicated in multiple human diseases, including neurological disorders, such as amyotrophic lateral sclerosis (ALS), as well as viral infection, replication and release[51,53,56,78,82]. Hence, OSBP-targeting compounds can lead to the development of anti-viral therapeutics.[49,64,83]

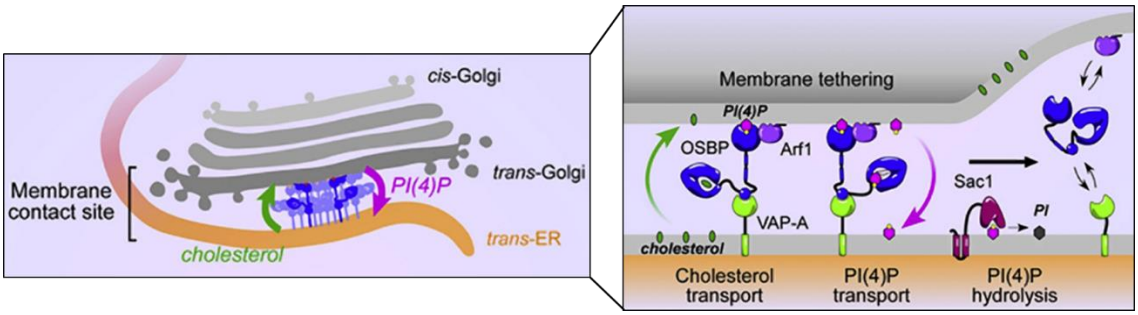

Figure 11. OSBP-mediated back transfer of PI(4)P coordinates the transfer of lipid species at the ER-Golgi interface (reproduced from Mesmin *et al.* with permission)[81]

As mentioned above, OSBP is implicated as an essential host protein in a wide variety of RNA viral infections, namely Hepatitis C (HCV), Enteroviruses—a family of positive-strand RNA viruses implicated in a panel of diseases) — Zika virus, Dengue fever virus, and encephalomyocarditis (EMCV).[84–89] Currently, there are no direct antiviral treatments available for any of these viral pathogens, limiting the clinical intervention to supportive therapy.[90] The clear need to develop effective therapeutics for these serious RNA viral pathogens has driven substantial progress in identifying candidate targets for anti-viral drugs.[91] In that respect, compounds including OSW-1, itraconazole (ITZ), T-001270HEV2 (THEV), and TTP-8307 (TTP) demonstrate potent anti-viral activity through targeting OSBP (**Figure 12**).[48,49,64,83,92]

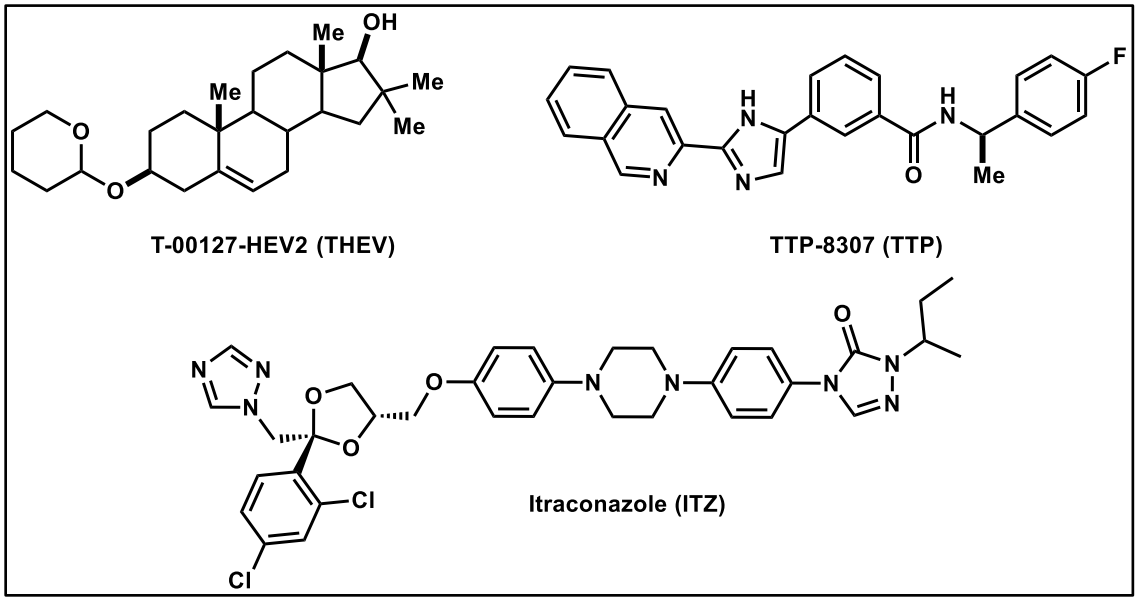

Figure 12. Structurally diverse anti-viral small molecules

OSBP is postulated to play an essential role in the formation of viral replication organelles (ROs).[83] The ROs are membrane wrapped structures that allow viral components to hide from the cellular anti-viral innate immunity factors.[83] For many viruses, the viral genome is replicated by assemblies of viral and host proteins located in

ROs formed at ER-Golgi interface.[83] RNA viral replication is particularly associated with dysregulation of lipid homeostasis, in which OSBP plays a role. Through viral recruitment of the type III phosphatidylinositol-4-kinase β (PI4KIIIβ) enzyme, PI4P is generated at ROs, and in the case of *Enteroviruses*, the cholesterol shuttling ability of OSBP is hijacked to make the viral ROs, in order to carry out efficient replication within the host cell.[53,93,94] Strating *et al.* reported that ITZ, an anti-fungal agent, perturbates this process by binding OSBP, which results in an arrest of cholesterol shuttling between membranes and ultimately inhibits viral replication (**Figure 13**).[83]

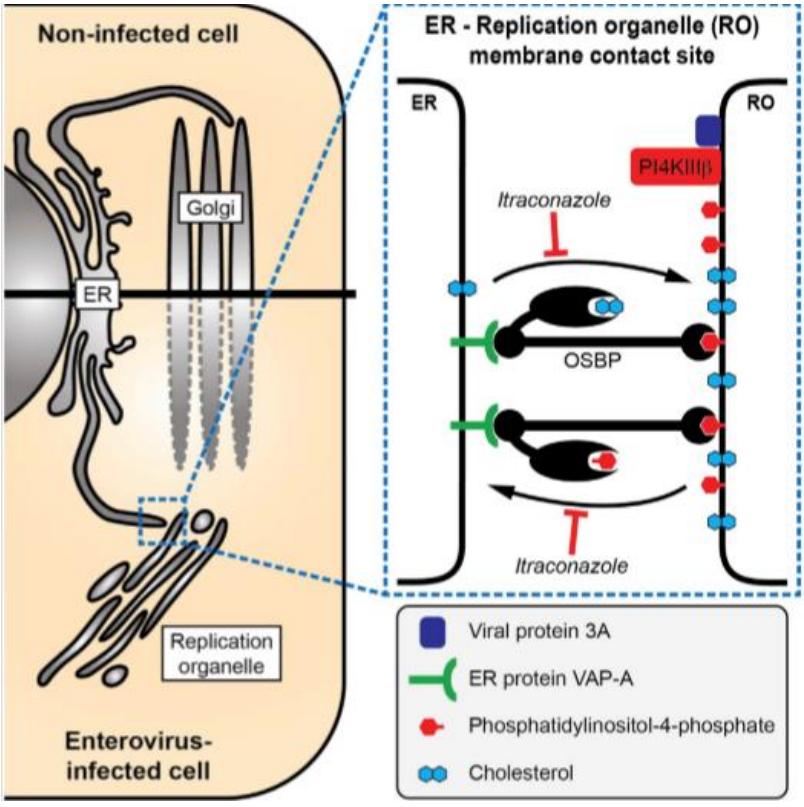

Figure 13. Enterovirus replication inhibition mechanism of action (reproduced from Strating *et al.* with permission)[83]

Most recently, the Burgett Research group investigated the effects of the structurally-diverse antiviral small molecule compounds (**Figure 12**) and their ability to interact with and modulate OSBP's cellular activity through different mechanisms.

Interestingly, ITZ and TTP, which are reported to target OSBP, do not inhibit the binding of 25-OHC to OSBP, indicating that these compounds bind OSBP at a different ligand binding site.[64] Both THEV and OSW-1 inhibit binding of 25-OHC with nanomolar K_i values. Moreover, OSW-1 is the only compound among all that causes a ~90% reduction in cellular OSBP levels and induces a prophylactic antiviral response in cells.[95] Although the exact mechanism of the OSW-1-induced OSBP repression has not been identified yet, OSW-1 is the example of a potential broad spectrum prophylactic anti-viral through targeting a human protein.[64,95]

The drug development potential of OSW-1 has drawn particular interest due to its exceptional antiproliferative and antiviral activities through targeting ORP4L and OSBP respectively.[35–37,40,64] However, as shown in **Table 1**, the OSW-1 compound binds to both proteins with comparable affinity, which could result in unwanted side effects.[40] There are currently no direct experimental results characterizing the binding of OSW-1 to OSBP, ORP4L or any other OSBP/ORP protein. Computational models have docked OSW-1 on to the OSBP and ORP4 homology models built off the Osh protein structures, but these models are of unclear value due to the lack of protein structural and functional information. This renders the understanding of OSW-1's interaction within the binding pocket challenging. Furthermore, the OSW-1 compound has been extensively studied for its anti-proliferative properties by testing related analogs on various cancer cell lines (discussed in **Section I.5**), but very few binding activities have been reported.[51,54–56] Identifying how it binds to OSBP/ORP4L could allow us to supplement current SAR models and efficiently modulate its components, with the ultimate goal of novel small-molecule precision therapeutic development.

I.5 Reported Biological Activities of OSW-1-Related Compounds

As stated previously, OSW-1 has mainly been studied for its anti-cancer activity. Cytotoxic (or cell-killing) agents capable of directly destroying tumor cells constitute a vital treatment for cancer.[96] Despite meaningful improvements in cancer drug development and biomedical research, most anti-cancer agents remain toxic to normal cells.[97] Cytotoxic chemotherapeutic agents have severe side effects, and the therapeutic administration of these drugs is often limited by the side effects. Simultaneous resistance of tumor cells to cytotoxic drugs is also a major limitation. Multi-drug resistant (MDR) cells exhibit reduced accumulation of drugs, altered expression and/or activity of certain cellular proteins, physiological changes that alter the intracellular milieu, and a high rate of mutation that decreases the affinity of receptors/enzymes for the drug.[98] The failure of existing chemotherapy drugs to provide an effective treatment with acceptable side effects fuels the pursuit of new cancer-selective agents functioning through novel modes of action. OSW-1, through targeting ORP4L, has shown promising preclinical anticancer efficacy and cancer selectivity.[17,33,34] As a result, between 1992 and 2019, a multitude of analogs have been tested *in vitro* for their cytotoxic activities on various cancer cell lines.[17,19,20,22–25,27,29,33,99–101] These experiments provide a starting point for defining OSW-1's SAR. As with any cytotoxic compounds, the cytotoxicity is cell line-dependent. All compounds with IC_{50} values greater than 10,000 nM are considered inactive.[10,12-25]

I.5.1 Biological Activities of Natural OSW-1 Analogs

The OSW-1 natural analogs can be classified into two major structural types (**Figure 14**).

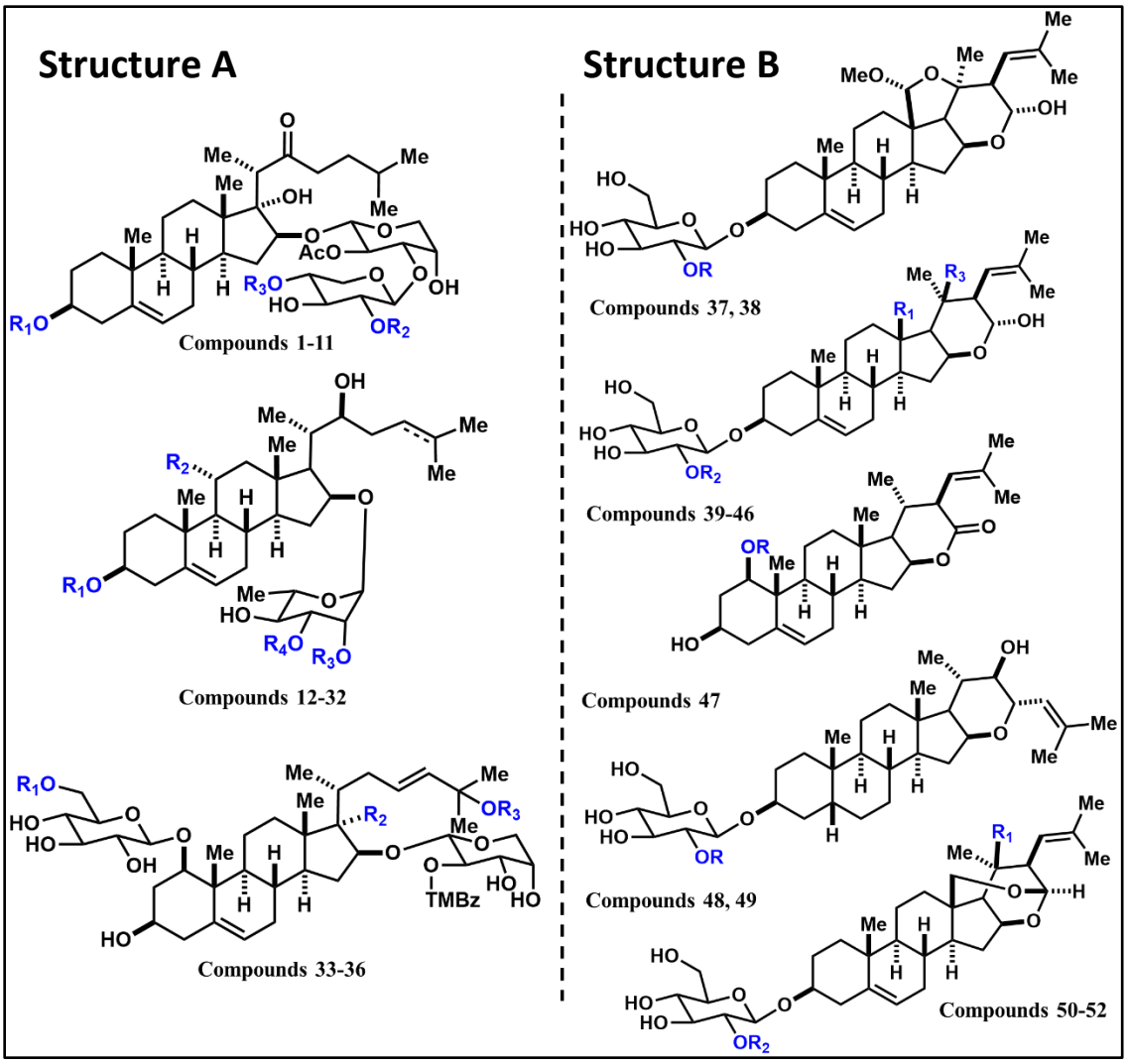

Figure 14. Isolated cholestane glycosides (1-52) structural classes (A and B)

The **Structure A** class (**Figure 14A**) is related to OSW-1, as the 3β,16β,17α dihydroxyl steroid core is largely unmodified.[17,19,28,29,33] Compounds with **Structure A** are either monodesmosidic or bisdesmosidic, depending on the sugar fraction having one or two attachment points respectively. Natural products with **Structure B** (**Figure 14B**) all possess a fused oxygen-containing E-ring instead of an aliphatic side chain. Interestingly, the C-21 methyl is retained with identical stereochemistry to OSW-1. Moreover, all compounds with **Structure B** are monodesmosidic, as the saccharide component (mainly β-D-glucopyranoside) is linked to the C-1 or C-3 position of the

steroidal core .[17,22,100,101] The isolated *O. saundersiae* natural products were tested for antiproliferative activity on various cancer cell lines, including HL-60 and A549 (**Figure 15**).[17,19,20,22–25,27,29,33,99–101] Detailed structures of all OSW-1 natural analogs and their cytotoxic activities can be found in **Appendix A and B**.

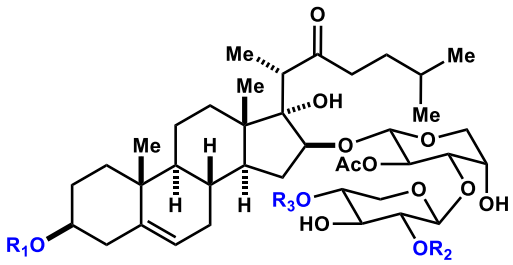

	Substituents			IC50 values (nM)	
Compounds	**R1**	**R2**	**R3**	**HL-60**	**A549**
1	H	H	H	3.4 ± 0.076	98 ± 8.0
2 (OSW-1)	H	PMBz	H	0.19 ±0.0026	1.7 ± 005
3	H	DMBz	H	0.077 ±0.0070	0.68 ±0.057
4	H	(E)-CNM	H	0.24	NT
5	glc	PMBz	H	0.12	NT
6	glc	(E)-CNM	H	16	NT
7	H	DMBz	glc	14	NT
8	H	TMBz	glc	0.20 ± 0.0074	3.6 ± 0.37
9	H	PHBz	H	0.55 ± 0.013	6.2 ± 0.10
10	H	TMBz	H	3.4 ± 0.076	98 ± 8.0
11	H	PHBz	H	NT	NT

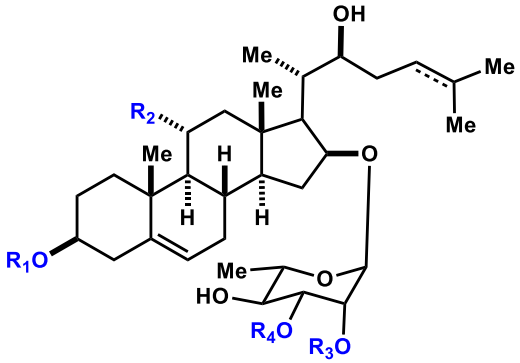

	Substituents				IC50 values (nM)	
Compounds	**R1**	**R2**	**R3**	**R4**	**HL-60**	**A549**
16	H	OH	H	Ac	0.99	NT
19	H	OH	H	TMBz	50 ± 10	270 ± 40
20	H	OH	H	PMBz	60 ± 2	370 ± 90

Figure 15. Cytotoxic Activities of a selection of OSW-1 analogs with Structure A tested against HL-60 and A549 cancer cell lines. NT: not tested

The most cytotoxic analogs were the ones that retained the OSW-1 structure (**Structure A**, **Figure 14**) with IC_{50} values ranging from 0.077 nM to 98 nM, but none were more potent than OSW-1 (**Figure 15**). Interestingly, compound **4** (**Figure 15**) comprised of an (E)-cinnamoyl group instead of a benzoyl group at the C-2 position of the D-xylopyranoside is almost as potent as OSW-1 (0.077 nM). Cholestane rhamnosides (**16, 19 and 20, Figure 15**) were less potent. The hydrophilic substituents of the hydroxyl group at C-11 and/or the glucosyl group at C-3 in the steroidal frame reduced the cytotoxicity of these compounds and rendered them inactive (**Appendix A, B**). Compounds with **Structure A** lacking the C-22 ketone (**33-36**, **Figure 14**) showed no activity (**Appendix A,B**). Moreover, most analogs with **Structure B (37-52**, **Figure 14**) were somewhat active against HL-60 cell lines (**Appendix C, D**), although the deacyl derivatives were significantly less potent (**Figure 16**). [17,19,20,22–25,27,29,33,99–101]

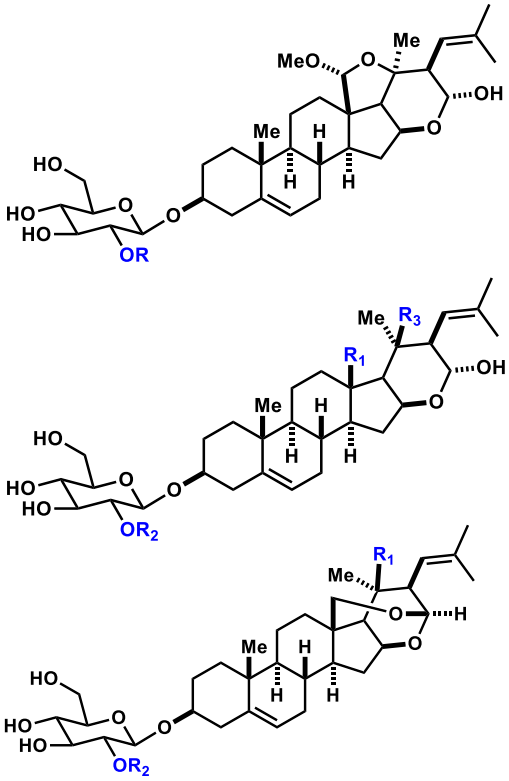

	Substituents	IC_{50} values (nM)
Compounds	**R**	**HL-60**
37	$glc^2 \rightarrow {}^1rha$	1,800
38	$^4rha \rightarrow PMBz$	9.2

	Substituents			IC_{50} values (nM)
Compounds	**R_1**	**R_2**	**R_3**	**HL-60**
39	CHO	$glc^2 \rightarrow {}^1rha$	H	inactive
40	CHO	rha	H	inactive
41	CHO	$rha^4 \rightarrow PHBz$	H	21
42	CHO	$rha^4 \rightarrow PMBz$	H	19
43	CH_2OH	$rha^4 \rightarrow PHBz$	H	63
44	CH_2OH	$rha^4 \rightarrow PMBz$	H	52
45	CH_2OH	$rha^4 \rightarrow PHBz$	OH	37 ± 4.4
46	CH_2OH	$rha^4 \rightarrow PMBz$	OH	90 ± 14

	Substituents		IC_{50} values (nM)	
Compounds	**R_1**	**R_2**	**HL-60**	**A549**
50	H	$glc^2 \rightarrow {}^1rha$	58 ± 2.0	900 ± 11
51	OH	$rha^4 \rightarrow$ PHBz	67 ± 0.23	850 ± 15
52	H	$rha^4 \rightarrow PMBz$	170 ± 5.1	5,500 ± 170

Figure 16. Cytotoxic Activities of a selection of OSW-1 analogs with Structure B tested against HL-60 and A549 cancer cell lines.

More recently, Chen *et al*. reported the isolation of 15 new compounds from *O. saundersiae* bulbs (**Figure 17**, nomenclature was adapted from Chen *et al.*).[21,103] These new oxygenated cholestane glycosides were named osaundersiosides. Interestingly, all the compounds had structures similar to **Structures A and B** (**Figure 14**)**,** but are mainly different in the positions of the various substituents. [21,103] These compounds (**53-67, Figure 17**) were tested on five different cancer cell lines (A549, BGC-823, HepG2, HCT-116, MCF-7) and were surprisingly found to all be inactive (**Appendix E**).[21,103]

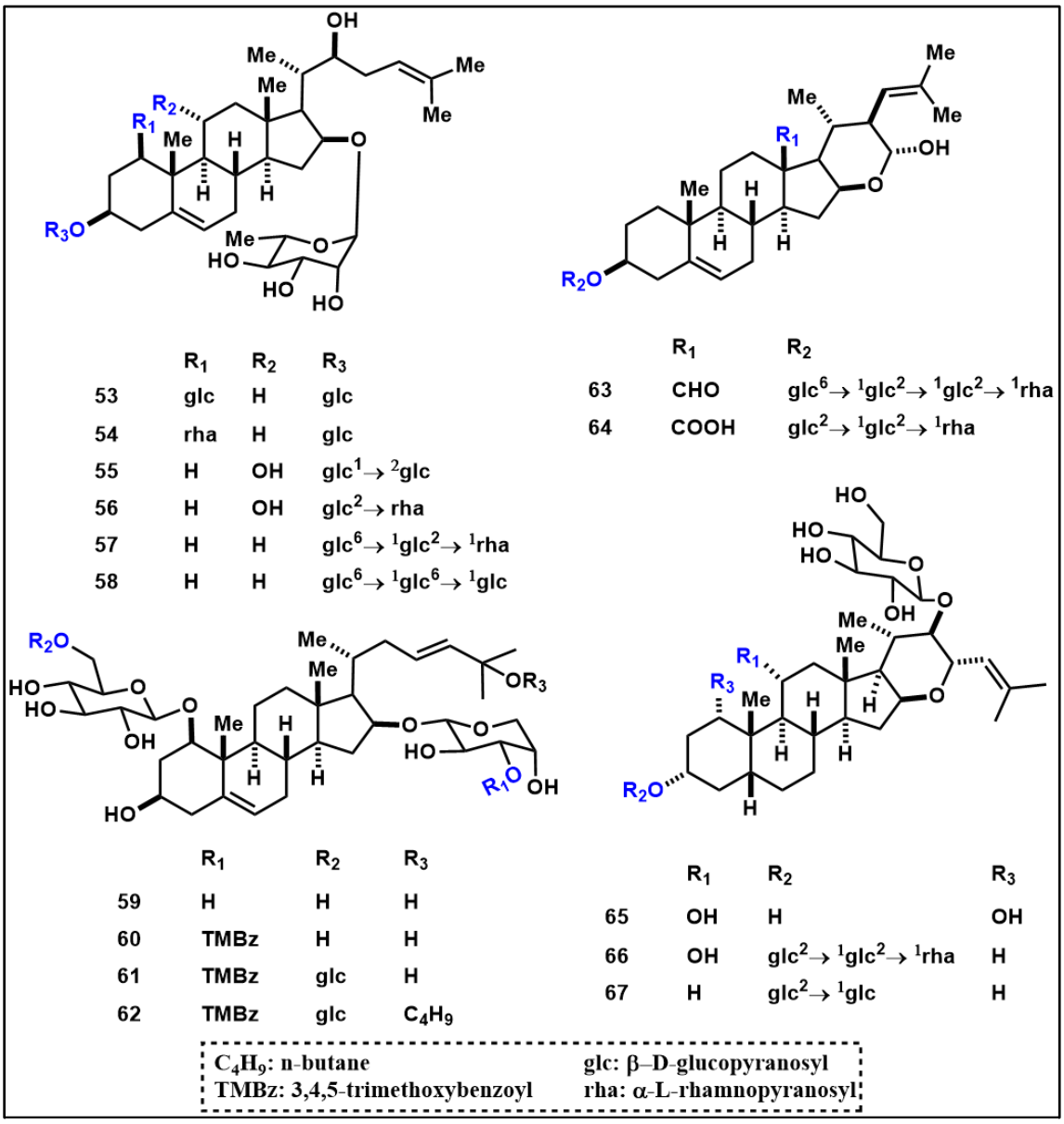

Figure 17. New inactive cholestane glycosides isolated from *O. saundersiae* bulbs

I.5.2 Biological Activities of Synthetic OSW-1 Analogs

Several OSW-1 total syntheses have been reported.[104–106] An efficient total synthesis of a natural product compound can supply significant quantities of a compound and provided for the generations of analog compounds.[30,107–123] The first total synthesis of OSW-1 was accomplished seven years after its discovery by the Yu group, in 27 steps with the longest linear sequence being 14 steps, and in 6% overall yield.[104] Most recently, the Guo group was able to scale up the synthesis and afford the OSW-1 compound in 10 steps with an overall yield of 6.4%.[106] Likewise, many synthetic analogs have been developed to access new OSW-1-congeners for SAR studies. Synthetic OSW-1 analogs either had a modified steroidal nucleus, a different side chain and/or an altered disaccharide moiety.[30,107–123] These OSW-1-related compounds were also tested for biological activity.[17,117,120] Detailed structures of all OSW-1 synthetic analogs and their cytotoxic activities can be found in **Appendix F-I.**

There is an overall lack of consistency in biological testing, which renders comparison challenging. However, in summary, based on the reported results, it seems that extension of the aliphatic side chain or changes to C22 functional groups (ester, amide, thioester, ether, unfunctionalized C-22 position) leads to mixed results, with potency or inactivity depending on the cancer cell line.[111,116,119,122] Conversely, shortening of the aliphatic side chain significantly decreases potency (**Appendix G, H**).[111,116,119,122]

The disaccharide moiety can also be modulated to understand its utility within the molecule. Most recently, Sakurai *et al.* reported that the disaccharide component was found as a structural scaffold required for biologically functionalities.[17,124] In other terms, the arabinose and xylose moieties are hypothesized to serve as a spacer for the extension

of the critical benzoate moiety to the desired position near the side chain component, while the C-17 hydroxyl, C-22 ketone and the acetate moiety on the arabinose participate in a hydrogen-bonding network to provide the optimal conformation of the OSW-1 molecule (**Figure 18**).[17,124]

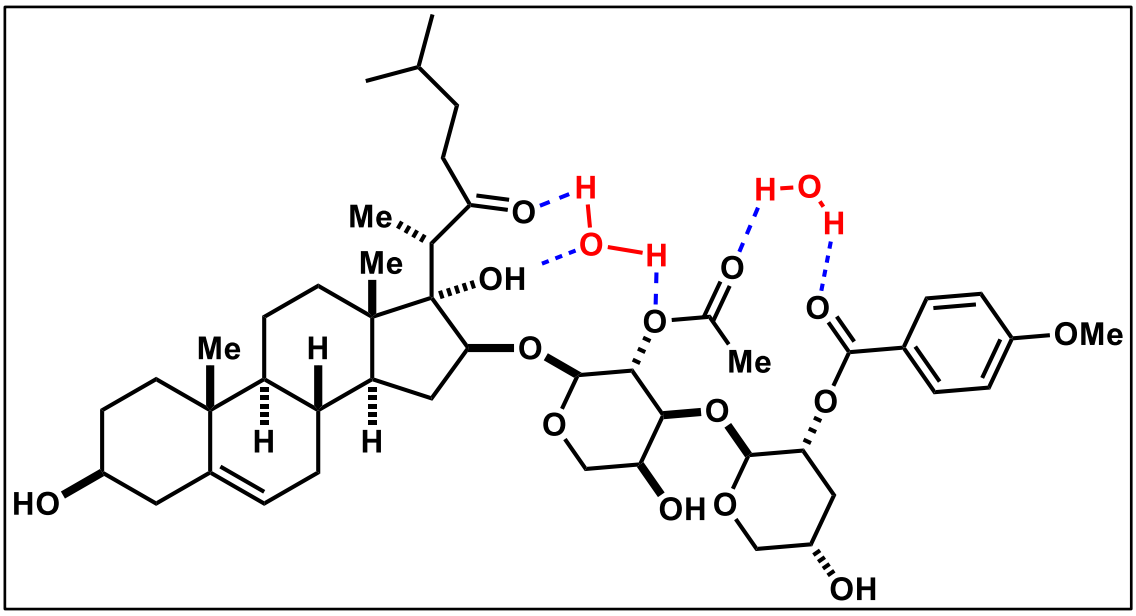

Figure 18. Hypothesized model of OSW-1's hydrogen bonding network. Hydrogen bonds are shown in blue. Figure was adapted from Cori Malinky's dissertation

Recently, the most promising results related to OSW-1 anti-cancer research involves the development of an analog named LYZ-81 (**107, Figure 19**) by the Lei group. When tested against mice leukemia cells *in vitro* and *in vivo*, both compounds were well tolerated, but LYZ-81 interestingly shows increased efficacy in comparison to OSW-1.[109,113] Most importantly, LYZ-81 differs from OSW-1 by the presence of a hydroxyl group at the C-26 position and the absence of one at the C-17 position. This compound selectively targets ORP4L with high affinity (K_D= 1.05 ± 0.26 nM) over OSBP (K_D = 5,900 ± 1,860 nM), which suggests the possibility to develop new OSW-1-derived compounds that selectively bind to either OSBP or ORP4L.[109,113]

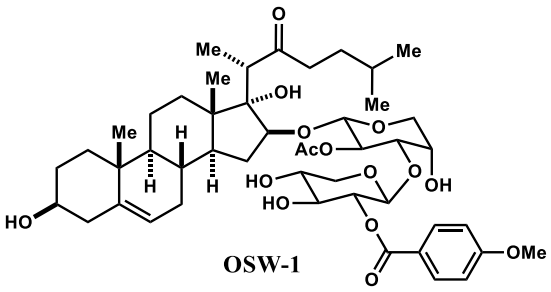

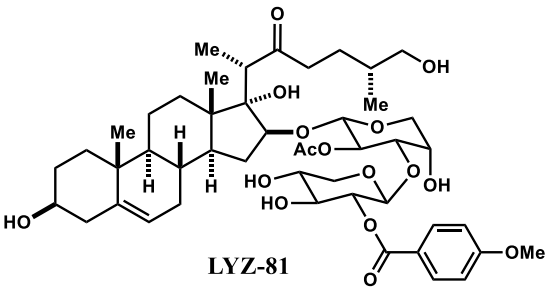

	IC_{50} values (nM)	K_D values (nM)	
Compounds	**Leukemia Stem Cells (LSCs)**	**OSBP**	**ORP4L**
OSW-1	0.152	1.49 ± 0.26	0.85 ± 0.17
LYZ-81	3.27	5,900 ± 1,860	1.05 ± 0.24

Figure 19. Comparison of OSW-1 and LYZ-81 cytotoxic activities against Leukemia Stem Cells (LSCs) and binding affinities to OSBP and ORP4L[109,113]

The discovery and synthesis of all these diverse *O. saundersiae* cholestane glycosides provides important information to determine the SAR of OSW-1. The OSW-1-related compounds, either synthesized or isolated from the natural source, have provided valuable insights for the derivatization of OSW-1 to the potential development of antiviral and anticancer agents through targeting the OSBP and ORP4 proteins.

I.5.3 Current OSW-1 SAR

Because of OSW-1's biomedical interest, several groups have achieved its total synthesis and a number of its analogs have been tested.[28-40,42–45,65,99,100] These analogs can contribute to deciphering OSW-1's SAR, which is basis to explore more potent analogs.[28-40,42–45,65,99,100] In 2013, based on all the reported cytotoxic activities, Tang *et al.* proposed a model of OSW-1's SAR (**Figure 20**).[17]

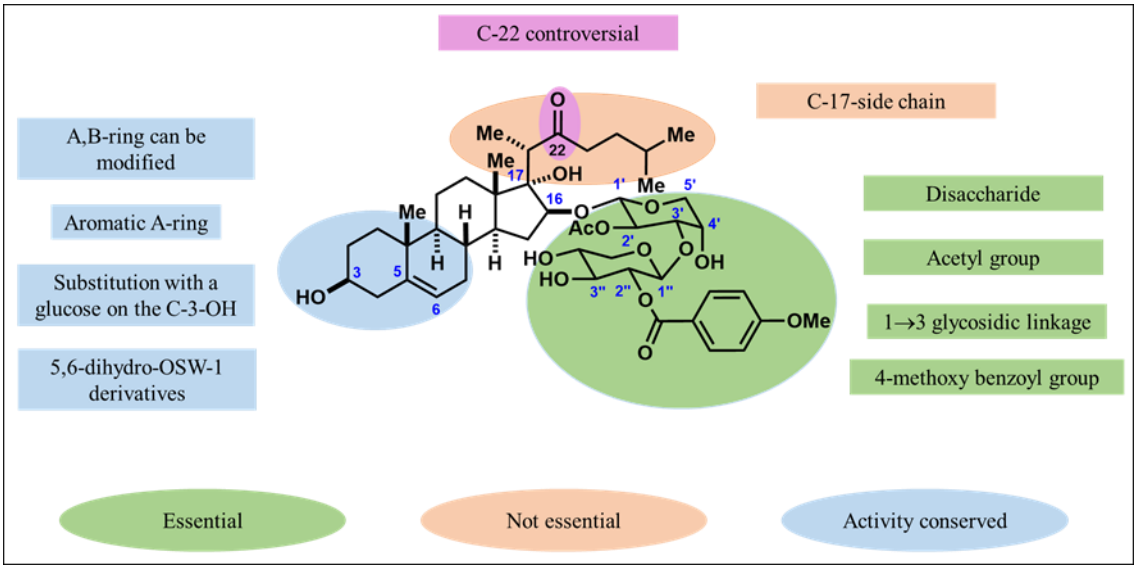

Figure 20. Most recent OSW-1 SAR model

Based on literature, both acyl groups on the disaccharide are critical for the bioactivity.[17] The A,B-ring system can be modified without significant loss of activity. Moreover, it has been determined that the disaccharide component is essential for the anti-cancer activity.[17,124] Homology modeling and molecular docking studies suggest that the sugar does not directly bind to the protein, but rather acts as a spacer unit that gives the correct conformation to OSW-1 via hydrogen bonding, forming a stable complex within the binding pocket, and allowing OSW-1 to interact with the protein.[17,124]

For the past three decades, many studies related to OSW-1's anti-proliferative activity have been carried out, but nothing has been reported for binding activities. It has been hypothesized that the side chain is essential for binding activity, but more SAR studies are needed to confirm this hypothesis. As mentioned previously, the way OSW-1 binds to OSBP and ORP4 is not necessarily understood. Moreover, the protein structures remain unsolved, which renders the understanding of these binding interactions unclear. Determining what is responsible for the binding of OSW-1 at the molecular level will allow for the development of selective OSBP-targeting anti-viral drugs, and likewise,

ORP4-targeting precision therapeutics. The best way of doing that is by modulating specific components of the molecule and developing concise structure activity relationships. In order to supplement the current SAR model, more analogs are needed, and two approaches are considered to obtain them: synthesis, which can be very time-consuming, especially for these complex scaffolds, or direct isolation from the plant. Testing of these analogs will allow to further supplement OSW-1's SAR and understand how it binds to the proteins to ultimately develop potential selective high affinity antiviral drugs and anticancer precision therapeutics.

Chapter II: Isolation, Characterization and Evaluation of OSW-1 Related Compounds

II.1 Abstract

The OSW-1 natural product demonstrates antiviral activity through interacting with OSBP and anti-proliferative activity through interacting with ORP4L. However, OSW-1 binds to both proteins with comparable affinities. As a result, OSW-1 itself cannot be developed into a drug, as unwanted side effects may arise. To this day, the way OSW-1 binds to OSBP and ORP4L remains unknown. Although many OSW-1-related compounds have been isolated from *O. saundersiae* bulbs and evaluated for their cytotoxic activity, the binding affinities of these related compounds have not been tested. This is essential to further supplement SAR studies and develop a complete OSW-1 SAR model. Obtaining natural OSW-1-derived products is the most direct source of compounds to study how OSW-1 interacts with its cellular targets OSBP and ORP4L; the chemical synthesis of the diverse and structurally complex OSW-1 compounds is much more demanding. Herein, a novel and efficient isolation procedure to isolate many OSW-1 natural product compounds, including new compounds, from *O. saundersiae* bulbs is reported. The procedure is different from previously reported methods by the use of alternative extraction and purification methods and especially by the development of a novel detailed analytical method allowing the isolation of multiple compounds in a reproducible manner. A diverse library of known and newly discovered natural products are structurally characterized, and the future testing of these OSW-1-related compounds will provide important SAR understanding of OSBP and ORP4L compound binding and potential drug development.

II.2 Introduction

Natural products and their derivatives provide an unprecedented range of chemical structure diversity.[126] Naturally-occurring small molecules have been recognized as an outstanding source of chemical probes used to interrogate biological functions, and further serve as therapeutic leads in drug discovery and development.[127] Due to an increasing demand for chemical diversity, seeking therapeutic drugs from natural products has continued to increase.[128]

Phytochemical analysis of *Ornithogalum saundersiae* bulbs has yielded a significant amount of potent cytotoxic cholestane glycosides, including OSW-1.[10,12-27] Bioactive cholestane glycosides derived from *Ornithogalum saundersiae* bulbs have been discovered through a series of extraction, isolation and purification processes.[17,19,28] The approach to isolate natural products starts with identification, collection and preparation of the biological material **(Figure 21**).

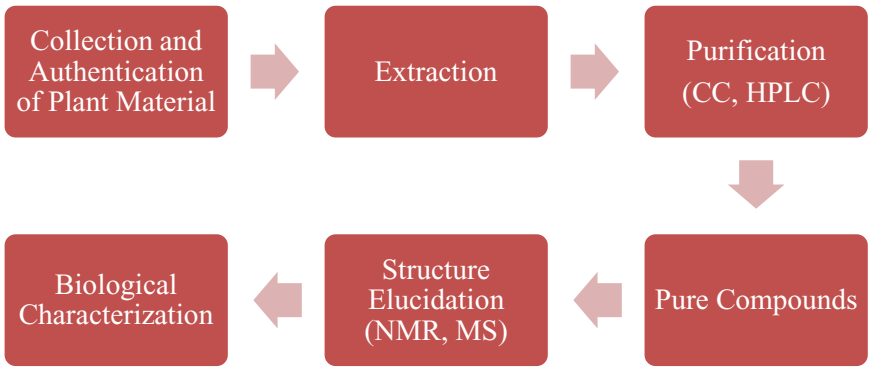

Figure 21. General approaches in extraction of bioactive compounds from plants

Organic solvent extraction is an essential step in the isolation of natural products.[128] Several extraction methods exist, including maceration, percolation, decoction, infusion, reflux, hydro distillation, or through use of a Soxhlet apparatus (**Table 1**).[129]

Method	Solvent	Time	Specifics
Maceration	Water, aqueous and organic solvents	Long	Solid plant material is placed in a stoppered container with the whole of the solvent and allowed to stand for a period of 3 to 7 days with frequent agitation, until soluble matter is dissolved.
Percolation	Water, aqueous and organic solvents	Long	Process of extracting soluble constituents of a powdered substance by slow passage of a liquid through it.
Decoction	Water	Moderate	Powdered plant material is boiled in a specified volume of water for a defined time; it is then cooled and strained or filtered.
Infusion	Water	Short	Plant material is macerated for a short period of time with either cold or boiling water.
Reflux Extraction	Aqueous and organic solvents	Moderate	Plant material is treated with boiling solvent.
Soxhlet Extraction	Organic solvents	Long	Continuous extraction of plant material by a hot solvent.
Hydro distillation	Water	Long	Plant material is soaked in boiling water. This is the widely used process for isolation of essential oils.

Table 2. Brief summary of various extraction methods for natural products

Determination of total plant contents can then be proceeded via individual extraction in a solvent (e.g, *n*-butanol), or by consecutive extraction in solvents of increasing polarity (e.g, n-hexane, petroleum ether, chloroform, ethyl acetate, ethanol, acetone and water).[130] Pure bioactive compounds are further obtained by separation and purification methods such as Thin Layer Chromatography (TLC), Column Chromatography (CC) or HPLC.[127,131] Due to a combination of various types of phytochemicals that differ in composition and polarities, their separation and purification remain key challenges in natural product drug discovery and development.[129] The chemical structures of the pure compounds are then elucidated using a wide range of spectroscopic techniques, including UV, IR, NMR and MS, prior to biological evaluation.[127,129,131]

II.3 Results and Discussion

II.3.1 Extraction

The discovery of OSW-1 and other OSW-1-related cytotoxic cholestane glycosides suggested that further phytochemical analysis of *O. saundersiae* bulbs could be beneficial.[19] For the original isolation in 1992, 16.2 kg of bulbs were first extracted in methanol under reflux, and the methanolic fraction was then extracted with 1-butanol. The combined organic extractions were fractionated over silica gel column chromatography using $CHCl_3$-MeOH gradient mixture as eluent. The partially-fractionated components were further purified using a combination of chromatographic techniques, namely octadecyl-silica (ODS) column chromatography and preparative HPLC, to yield 25 mg of **1**, 439 mg of **2** (**OSW-1**), and 23.5 mg of **3** (**Figure 5**).[19] The detailed step-by-step procedure is summarized in **Figure 22.**

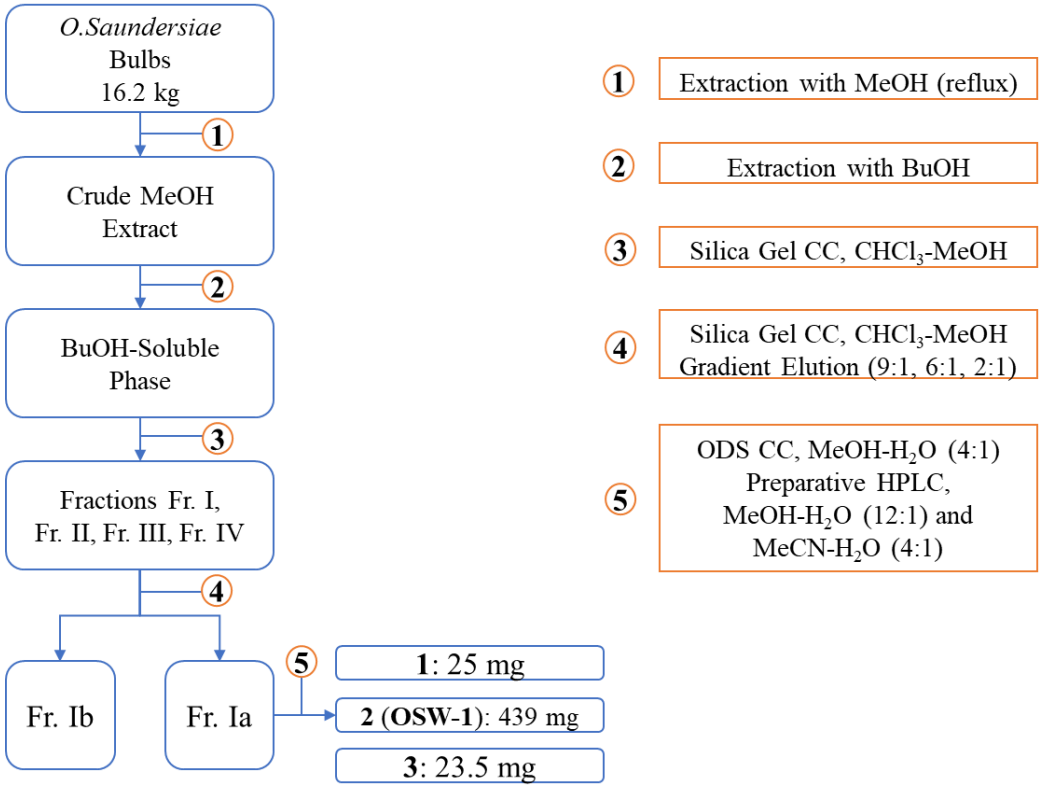

Figure 22. Original isolation procedure summary

The bulbs used in this work were cultivated in the OU Greenhouse by Mr. Lynn Nichols, harvested in June 2019 and stored at 0°C prior to extraction. To facilitate extraction, remove water, and increase yield by breaking cell integrity, the *O. saundersiae* bulbs were lyophilized overnight and physically ground using mortar and pestle. Two major extraction methods were investigated: one using a reflux condenser as performed in the literature[19], and the other one involving a Soxhlet apparatus, method never reported for this plant (**Figure 23**).

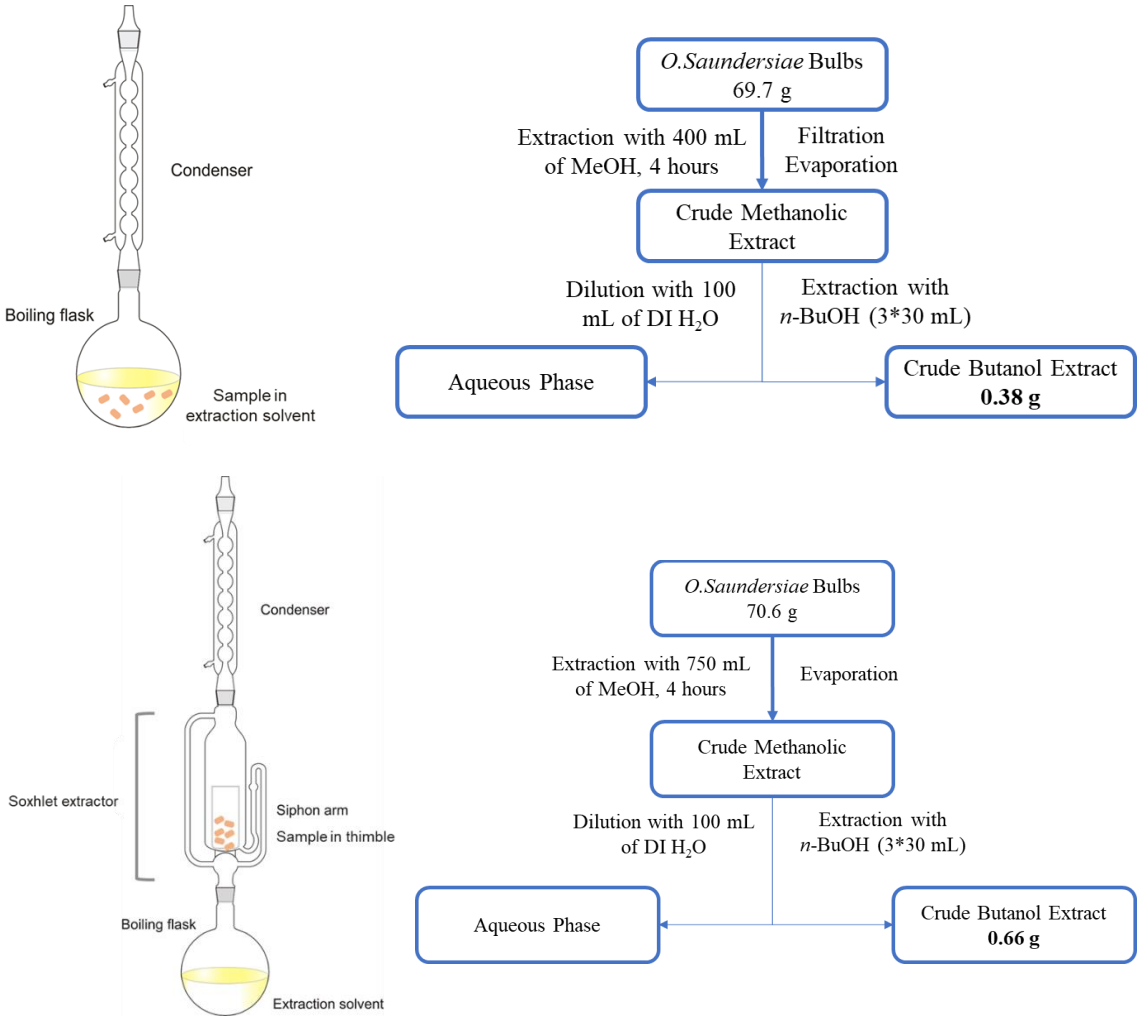

Figure 23. Comparison of extraction methods summary

Similar amounts of *O. saundersiae* plant material were subjected to both extraction methods. In order to compare and validate results, the procedure was carried out 8 times.

A higher mass of extracted compounds was constantly observed by using a Soxhlet apparatus compared to a simple reflux condenser. This is presumably due to the fact that the compounds are extracted multiple times in a Soxhlet extraction. The advantage of this system is that instead of many portions of warm solvent being passed through the sample, just one batch of solvent is continuously recycled. Based on the larger amount of material extracted, the preliminary results supported use of the Soxhlet extraction method.

With the selected extraction method, a larger scale procedure was performed with more plant material. Ten *O. saundersiae* bulbs (308.6 g) were lyophilized overnight, resulting in a final mass of 153.3 g of bulk material. Dried bulbs were chopped into small pieces and extraction was carried out in 750 mL of hot MeOH using Soxhlet apparatus for 48 hours. After evaporation *in vacuo*, 63.9 g of crude methanolic liquid extract was obtained. The crude mixture was then diluted with 100 mL of DI H_2O and partitioned three times with *n*-BuOH. The resulting combined organic phase was condensed to a crude butanol extract (1.51 g) while the aqueous phase was lyophilized to afford white powder (**Figure 24**).

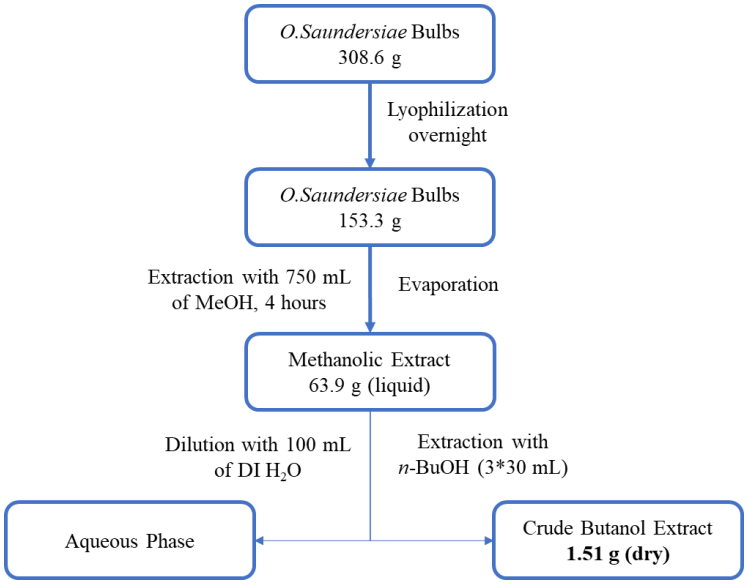

Figure 24. Optimized extraction method summary

In order to indicate the presence of saponins and qualitatively verify the composition of both phases, a frothing test was performed.[1] For that, 1 mL of the butanol extract was diluted with 20 mL of DI H_2O and shaken in a graduated cylinder for 15 minutes. Development of stable foam suggests the presence of saponins.[1] As expected, no foam formed in the aqueous phase, meaning that it did not contain any saponins. The butanol extract showed clear frothing. Natural products from the crude butanol extract were further separated through a developed, multi-stage purification processes.

II.3.2 Purification and Analytical Method Development

Due to the unavailability of equipment described in the literature,[19] a novel purification procedure was developed. The butanol extract was first analyzed by TLC prior to establishing an appropriate chromatographic separation method. Multiple elution conditions were tested (**Figure 25**).

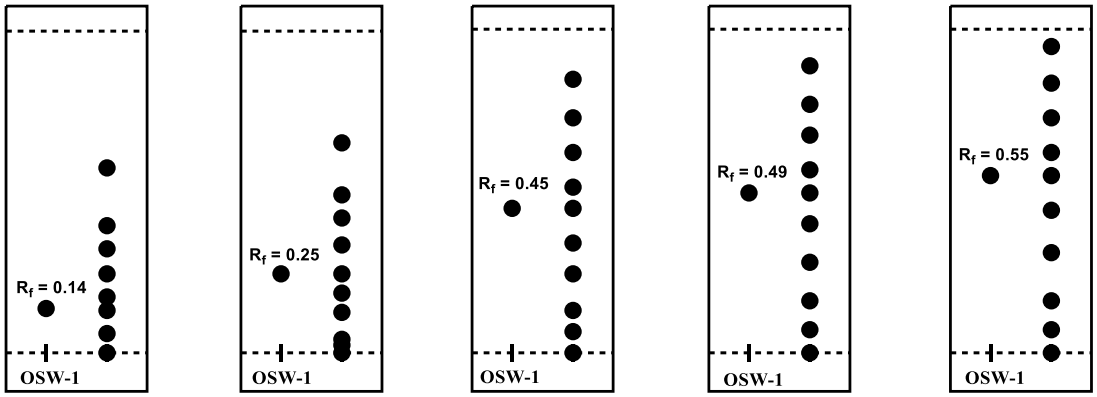

Figure 25. TLCs of the butanol extract compared to OSW-1 tested with different elution conditions

Separation was optimal between 10-15% MeOH/$CHCl_3$. In order to increase reproducibility of the method and obtain a consistent separation pattern, the 300 mg of the crude butanol extract was fractionated on automated silica gel column using Biotage Isolera, with linear gradient elution from 0-30% MeOH/$CHCl_3$ and washed with EtOAc.

Fractions with similar TLC profiles were combined and divided into 8 subfractions (**Figure 26**).

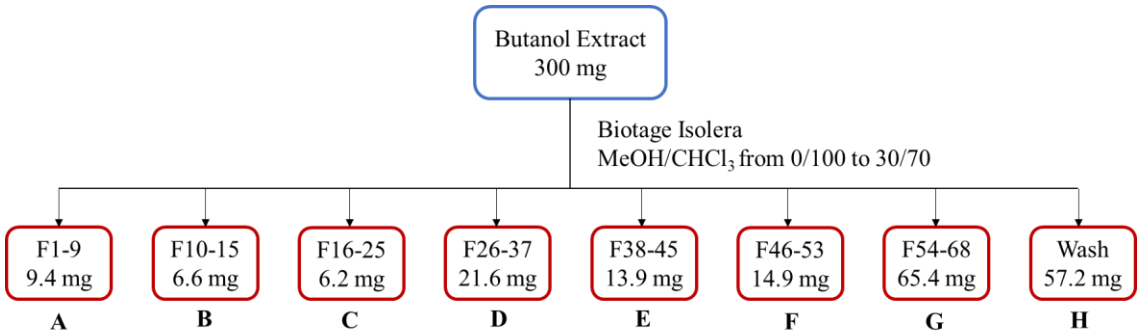

Figure 26. First purification and fractionation of the crude butanol extract

Each subfraction was then further purified and analyzed by reverse phase LC-MS Different separation conditions were investigated (**Table 3**). Variable parameters include column (C_8, C_{18}), mobile phase composition (MeCN, MeOH) and elution (isocratic, linear/step gradient).

Column	Solvent A	Mobile Phase Composition (Solvent A/H_2O)	Elution	Resolution Factor
C_8	MeOH	80/20	Isocratic	0.60
C_8	MeOH	80/20 to 95/5	Linear gradient	0.61
C_8	MeCN	80/20	Isocratic	0.63
C_8	MeCN	80/20 to 100/0	Linear gradient	0.64
C_8	MeOH	75/25	Isocratic	0.68
C_8	MeOH	75/25 to 95/5	Linear gradient	0.67
C_8	MeCN	75/25	Isocratic	0.82
C_8	MeCN	75/25 to 100/0	Linear gradient	0.82
C_8	MeOH	70/30	Isocratic	0.71
C_8	MeOH	70/30 to 95/5	Linear gradient	0.72
C_8	MeCN	70/30	Isocratic	0.84
C_8	MeCN	70/30 to 100/0	Linear gradient	0.85
C_8	MeOH	65/35	Isocratic	0.65
C_8	MeOH	65/53 to 95/5	Linear gradient	0.62
C_8	MeCN	65/35	Isocratic	0.79
C_8	MeCN	65/53 to 100/0	Linear gradient	0.77
C_8	MeOH	75/25 to 85/15 to 95/5	Step gradient	1.02
C_8	MeCN	75/25 to 85/15 to 100/0	Step gradient	1.24

C_{18}	MeOH	80/20	Isocratic	0.72
C_{18}	MeOH	80/20 to 95/5	Linear gradient	0.72
C_{18}	MeCN	80/20	Isocratic	0.88
C_{18}	MeCN	80/20 to 100/0	Linear gradient	0.89
C_{18}	MeOH	75/25	Isocratic	0.75
C_{18}	MeOH	75/25 to 95/5	Linear gradient	0.73
C_{18}	MeCN	75/25	Isocratic	0.94
C_{18}	MeCN	75/25 to 100/0	Linear gradient	0.94
C_{18}	MeOH	70/30	Isocratic	0.78
C_{18}	MeOH	70/30 to 95/5	Linear gradient	0.80
C_{18}	MeCN	70/30	Isocratic	1.02
C_{18}	MeCN	70/30 to 100/0	Linear gradient	1.03
C_{18}	MeOH	75/25 to 85/15 to 95/5	Step gradient	0.98
C_{18}	MeCN	75/25 to 85/15 to 100/0	Step gradient	1.32
C_{18}	MeOH	70/30 to 85/15 to 95/5	Step gradient	1.08
C_{18}	**MeCN**	**70/30 to 85/15 to 100/0**	**Step gradient**	**1.43**

Table 3. Screening of optimum HPLC separation conditions

In order to quantitatively assess the best separation conditions, resolution factors were calculated for each chromatogram. A resolution factor of 1.5 or more is indicative of optimal peak separation.[132] Compared to MeOH/H_2O, MeCN/H_2O gave overall superior HPLC separation quality (**Table 3**). Due to the heterogeneity of samples, a step gradient was preferred over a linear gradient and isocratic elution. Peak separation was ideal with a step gradient from 70/30 to 85/15 to 100/0 MeCN/H_2O (with 0.1% formic acid), as resolution factor is close to 1.5.

The coupling of HPLC with MS is a powerful tool to identify both naturally-occurring cholestane glycosides and their synthetic analogs. Three cholestane glycosides, including OSW-1 and two new analogs with modified steroidal side chains, thienyl-OSW-1 (**116, Appendix J**) and silylated thienyl-OSW-1 (**117, Appendix J**), were analyzed by using optimized, reversed phase HPLC with electrospray ionization and atmospheric pressure chemical ionization quadrupole MS[133,134] To the best of our knowledge, this is the only study that reported optimized MS techniques to complement

traditional characterization methods (NMR, IR) of OSW-1-derived compounds. Yet, this technique gives useful information, especially for the isolation, identification and structural elucidation of naturally-occurring analogs.[135]

In this work, monoisotopic masses were determined by MS via positive and negative electrospray ionization (ESI^+ and ESI^-). The following adducts of compounds were detected: $[M+H]^+$, $[M+Na]^+$, $[M+K]^+$, $[M+NH_4]^+$, $[M+HCOO]^-$, $[M+CH_3COO]^-$. Positive ESI mode showed superior sensitivity and consistency in the MS detecting of OSW-1-related compounds than the negative ESI mode. As stated above, 0.1% formic acid (pK_A= 3.75) was added to the water phase, thus promoting protonation of the hydroxyl groups (pK_A≈16). Interestingly, sodium adducts peaks ($[M+Na]^+$) were predominantly detected in comparison with protonated adduct peaks ($[M+H]^+$), despite the 0.1% of formic acid present. This is presumably due to the fact that sodium is one of the most abundant contaminants in all commercially available HPLC grade solvents.[136] Moreover, sodium can come from a number of sources, mainly during sample preparation and analysis: residual salts can be present on the column, in the HPLC system (injector, tubing, etc…) or sodium can leach from the glassware used to prepare the solvents.[136]

Based on all isolation studies, targeted cholestane glycosides have a molecular mass approximately ranging from 680-1100 g/mol.[17,19,20,22–25,27,29,33,99–101] Therefore, all compounds with molecular ion peaks outside of this bracket were not considered relevant. Once the molecular ion peak was determined, a unique fragmentation pattern allowed us to further assess a compound's structure (discussed in **Section II.3.3 below**). Relevant natural products were identified in subfractions F26-37 (D) and F38-45 (E). The ultimate

step of the entire procedure was to fractionate these subfractions by HPLC, resulting in isolated amounts of the various natural product compounds (**Figure 27**).

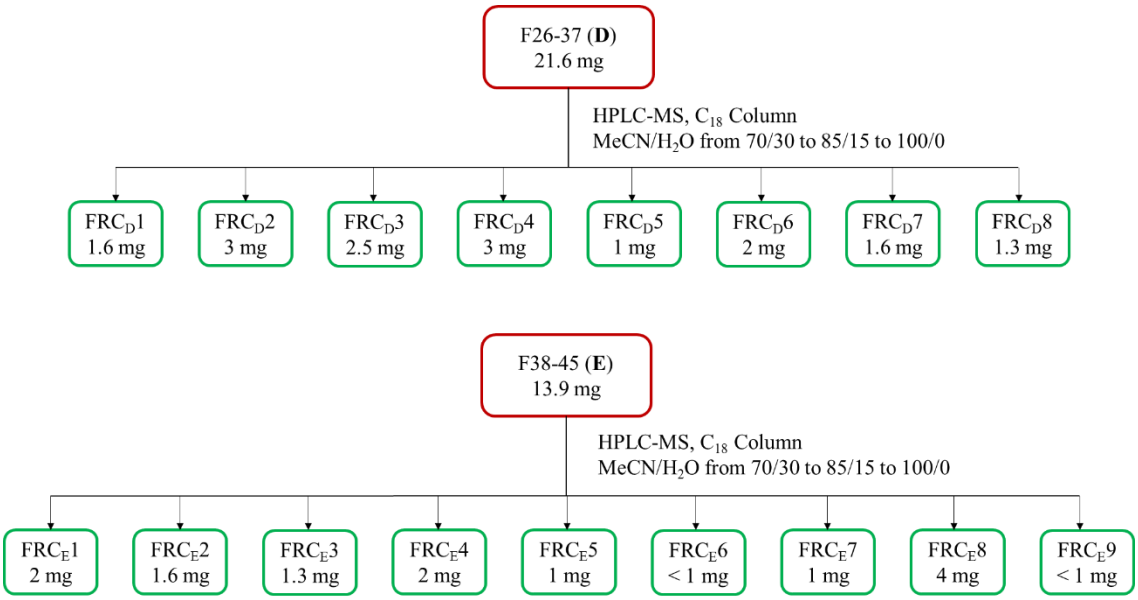

Figure 27. Ultimate step of the isolation procedure: fractionation of F26-37 (top) and F38-45 (Bottom)

Purity was assessed by re-submitting isolated compound to HPLC analysis prior to preliminary characterization. Based on peak areas, compound was considered pure when purity ≥ 95%.

II.3.3 Preliminary Characterization

Approximately 100 OSW-1 analogs were purified via reverse-phase HPLC (**Appendix L-O**), 6 of which were characterized (**Figure 28**). After purification and identification of molecular masses, preliminary characterization of each isolated natural product was achieved by ^{1}H-NMR, MS, and by comparison with spectral data reported in literature. [17,19,20,22–25,27,29,33,99–101]

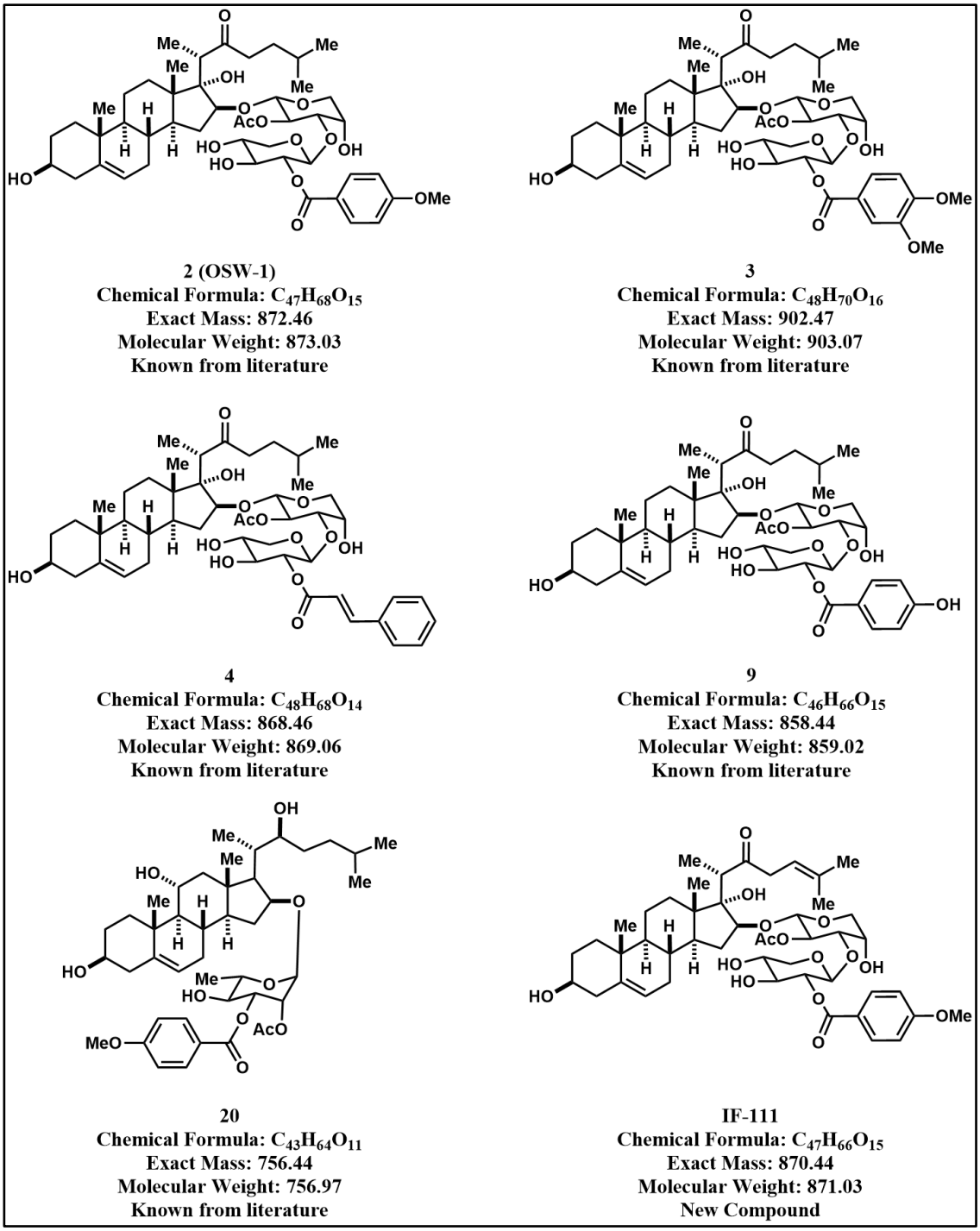

Figure 28. Overview of known and new characterized compounds

Characterization of 2 (OSW-1)

Compound **2** (**Figure 28**) was isolated as an amorphous solid by HPLC and had an *m/z* value of $[M+Na]^+$ 895.25 and $[M+H]^+$ 873.25 in ESI^+ and 917.15 $[M+HCOO]^-$ in ESI^- corresponding to a molecular weight of 873.03 g/mol and molecular formula $C_{47}H_{68}O_{15}$. In accordance with literature, compound **2** was identified as OSW-1.[19,133] The ^{1}H-NMR data matched with the structure originally isolated.[19] Moreover, the MS fragmentation pattern of OSW-1 was extensively studied in order to identify how the natural product is fragmented in the mass spectrometer, and to further help determine what part of the OSW-1-related compounds had changed in regard to OSW-1 (**Figure 29**). This is not a common method, and to the best of our knowledge, the hypothesized fragmentation pattern of OSW-1 has only been reported once.[133,134]

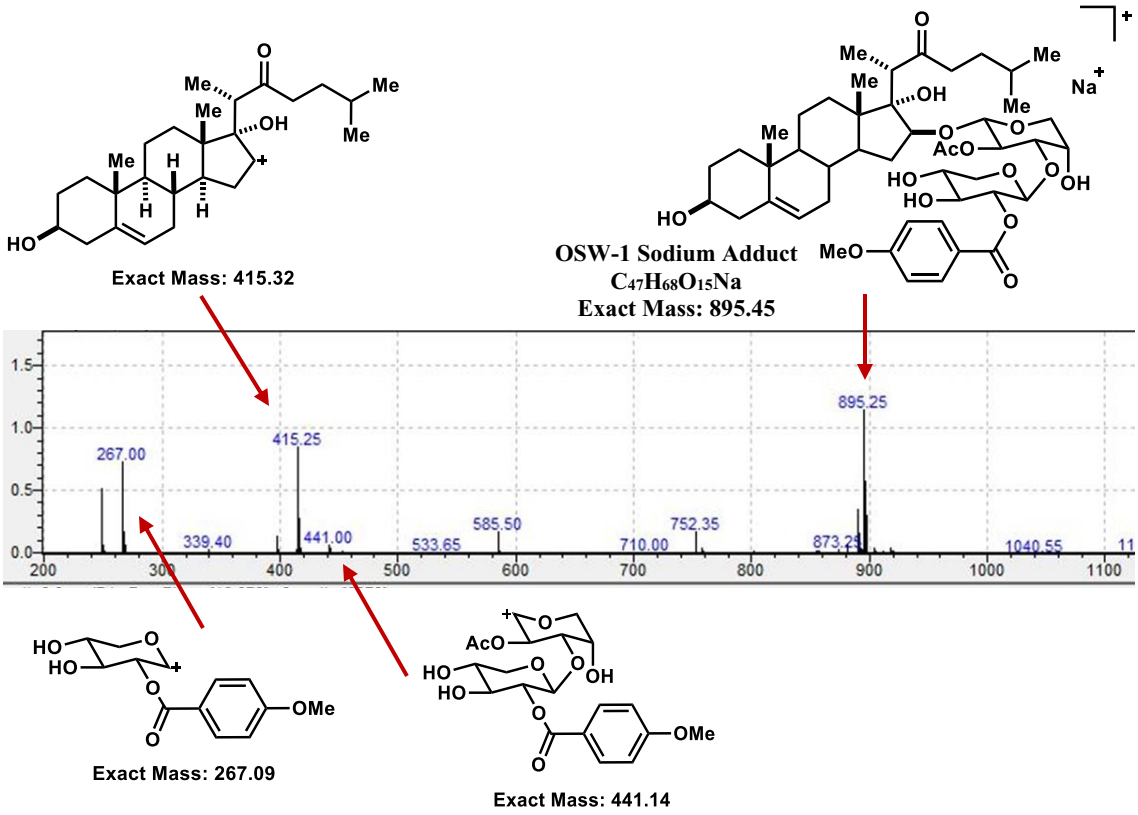

Figure 29. OSW-1 mass spectrum and fragmentation pattern

With the procedure being reiterated 8 times, OSW-1 was isolated multiple times. Due to the reproducibility of the analytical method, retention times recorded by HPLC were similar, and a total amount of 12 mg of OSW-1 was isolated.

Characterization of 3

Compound **3** (**Figure 28**) was isolated as an amorphous solid by HPLC had an *m/z* value of 925.30 $[M+Na]^+$ in ESI^+ and 947.10 $[M+HCOO]^-$ in ESI^-, corresponding to a molecular weight of 903.07 g/mol and molecular formula $C_{48}H_{70}O_{16}$. This molecular formula matched the 3,4-dimethoxybenzoate analog of OSW-1.[19] In a similar manner as described above, the MS fragmentation pattern of **3** was determined for the first time (**Figure 30**).

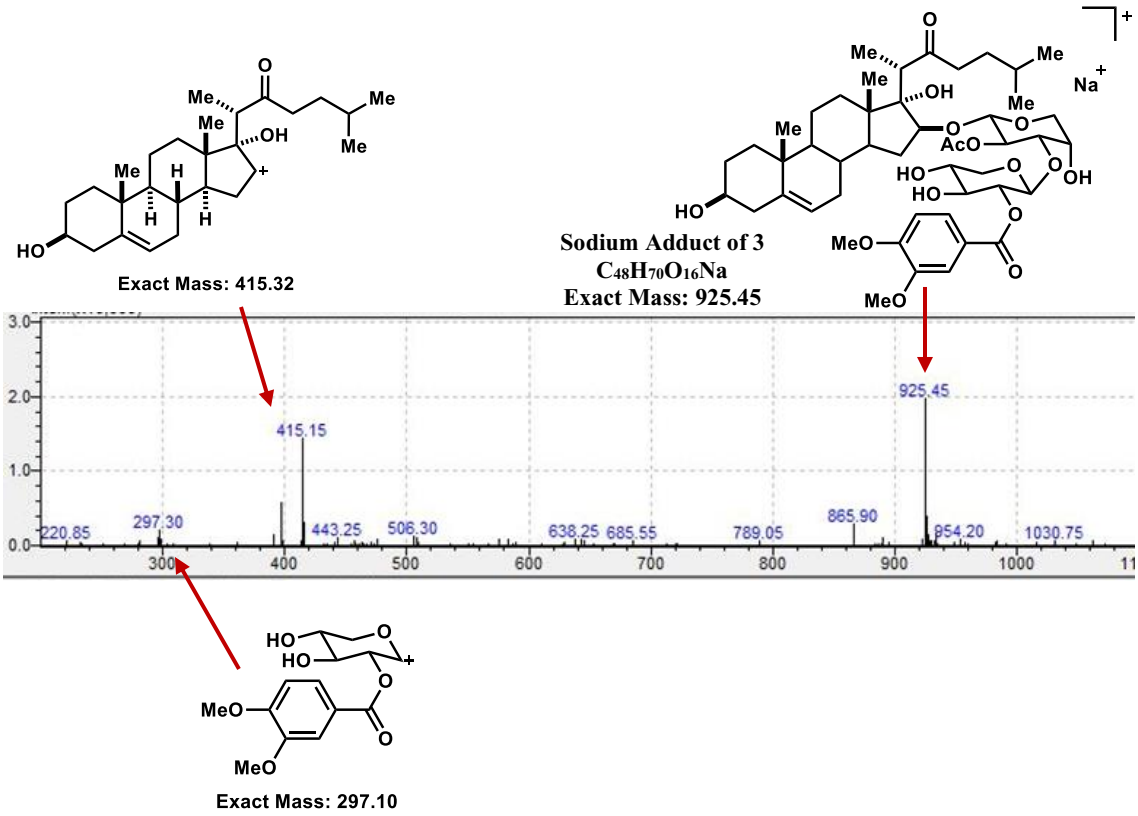

Figure 30. Mass spectrum and fragmentation pattern of 3

Spectral data of **3** was almost identical with those of OSW-1. Comparison of the ^{1}H spectra of **2** (OSW-1) and **3** in deuterated acetonitrile (**Figure 31**) showed minor signal changes at δ 7.73 (dd, J = 8.5, 2.0 Hz, 2H), δ 7.61 (d, J = 2.0 Hz, 2H), and δ 7.06 (d, J = 8.5 Hz, 1H) in the aromatic region, due to the disubstituted benzoyl moiety.

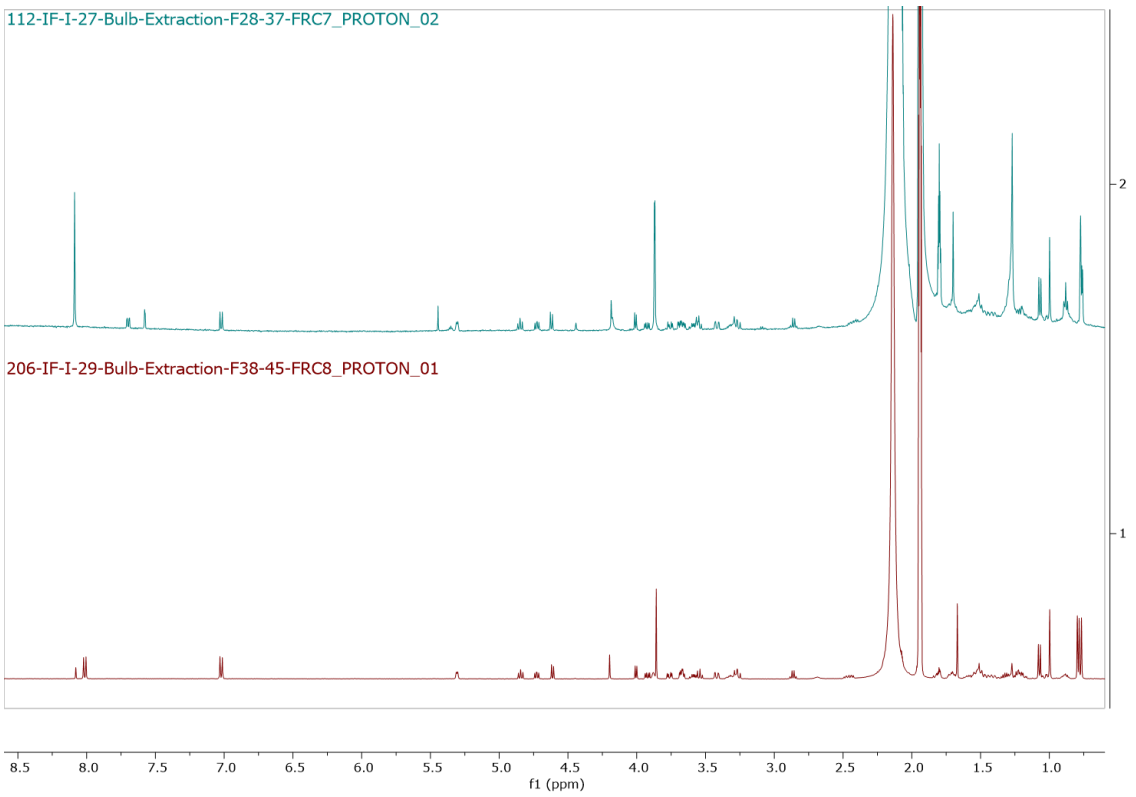

Figure 31. ^{1}H-NMR spectra comparison of OSW-1 (bottom) and IF-112 (top)

With the procedure being reiterated 8 times, **3** was isolated multiple times. Due to the reproducibility of the analytical method, retention times recorded by HPLC were similar, and a total amount of 4 mg of **3** was isolated. Additionally, bulbs used in the original isolation procedure were not necessarily the same as the ones used in this work. Therefore, in order to assess whether the amount of **3** in regard to **2** (OSW-1) was similar to the literature, the ratio of **3** with respect to **2** was calculated and compared to literature. Originally, 23.5 mg of **3** and 439 mg of **2** were isolated, which is equivalent to a ratio of 5.4%. In this work, the peak areas were used to determine that ratio (peak area of **3**:

134,137; peak area of **2**: 2,105,820), resulting in a value of 6.4%. These results are indicative of a consistent amount of **3** in regard to **2**, regardless of the type of bulbs.

Characterization of 4

Compound **4** (**Figure 29**) was isolated as an amorphous solid by HPLC and had an *m/z* value of $[M+Na]^+$ 891.20 in ESI^+, corresponding to a molecular weight of 869.06 g/mol and molecular formula $C_{48}H_{68}O_{14}$. This molecular formula matched the (E)-Cinnamoyl analog of OSW-1.[33] In a similar manner as described above, the MS fragmentation pattern of **4** was determined for the first time (**Figure 32**).

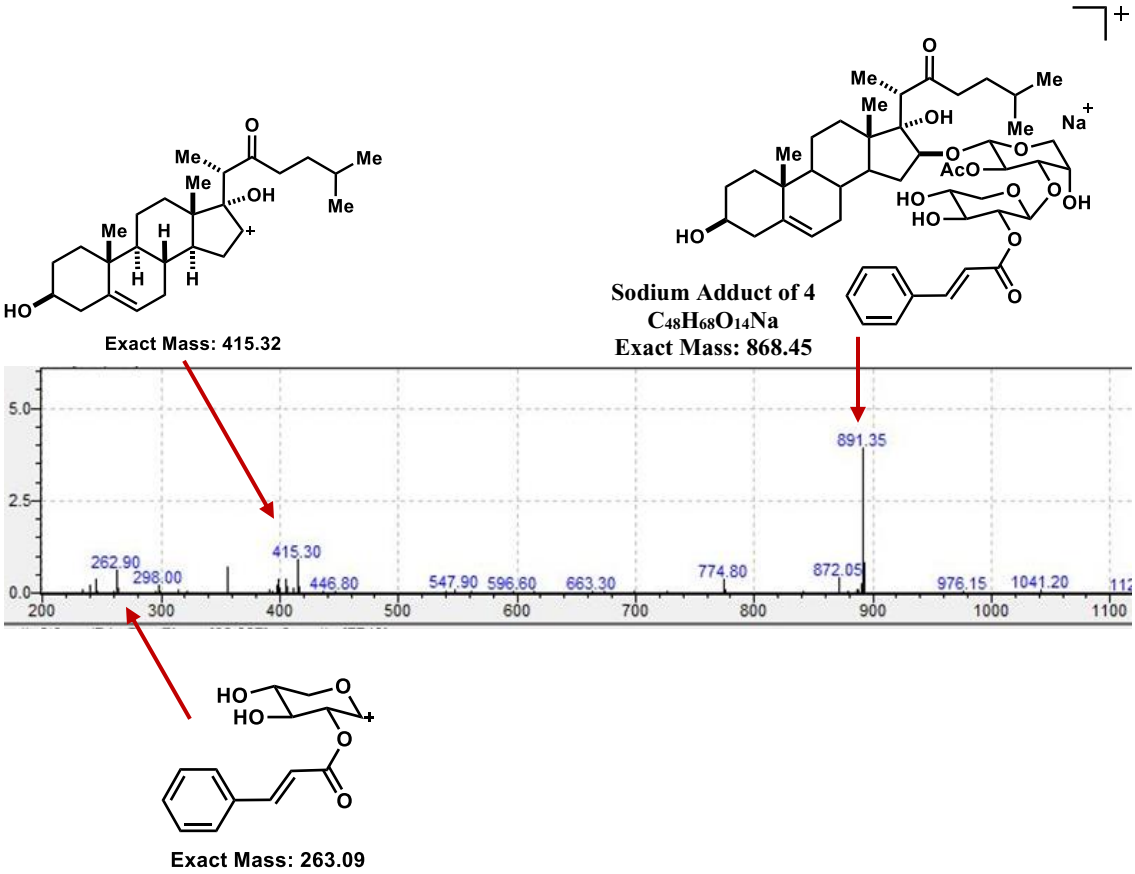

Figure 32. Mass spectrum and fragmentation pattern of 4

Analysis of the ^1H spectrum of **4** and comparison with **2** (OSW-1) (**Figure 33**) implied that **4** differed from OSW-1 only in terms of the aromatic constituent. The absence of the $-CH_3$ peak at δ 3.86 indicated that 4 is not comprised of a 4-methoxybenzoyl group.

Moreover, a significant change of signal was observed in the aromatic region at δ 7.65 (m, 2H) and 7.46 – 7.40 (m, 4H), indicative of a non-substituted benzene ring, and at δ 7.73 (d, J = 16.1 Hz, 1H), 6.52 (d, J = 16.0 Hz, 1H), indicative of a the presence of alkene in trans configuration, supported by the coupling constants.

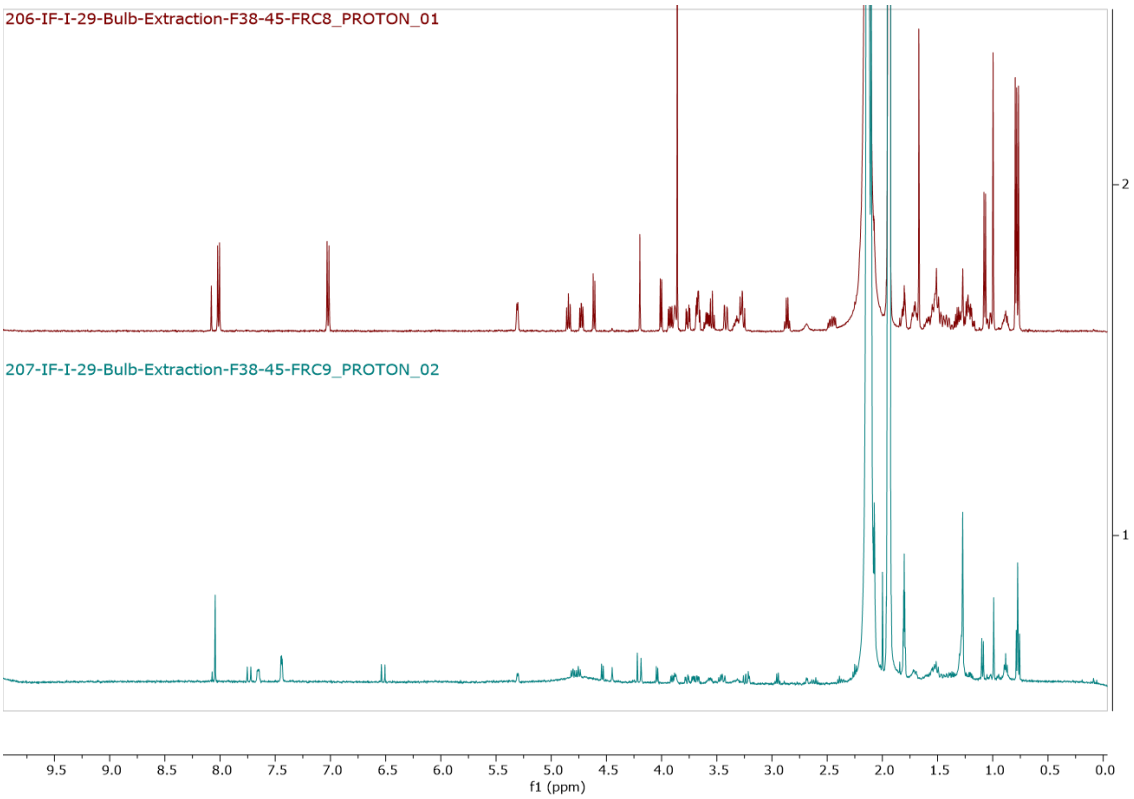

Figure 33. ^{1}H-NMR spectra comparison of OSW-1 (top) and IF-207 (bottom)

With the procedure being reiterated 8 times, **4** was isolated multiple times. Due to the reproducibility of the analytical method, retention times recorded by HPLC were similar, and a total amount of 5 mg of **4** was isolated.

Characterization of 9

Compound **9** (**Figure 29**) was isolated as an amorphous solid by HPLC and had an *m/z* value of $[M+Na]^+$ 881.45 in ESI^+, corresponding to a molecular weight of 859.02 g/mol and molecular formula $C_{46}H_{66}O_{15}$. In a similar manner as described above, the MS fragmentation pattern of **9** was determined for the first time (**Figure 34**).

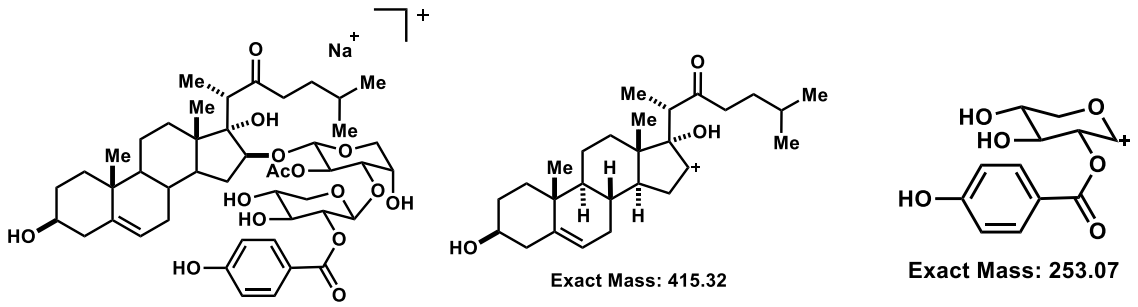

Figure 34. Sodium adduct and fragmentation pattern of 9

Analysis of the ^{1}H spectrum of **9** and comparison with OSW-1 (**Figure 35**) implied that **9** differed from OSW-1 only in terms of the aromatic acid constituent. Instead of the signals for the 4-methoxybenzoyl group, those assignable to a 4-hydroxybenzoyl residue were observed with the absence of the $-CH_3$ peak at δ 3.86 and a slight downfield-shift of the aromatic protons at δ 8.00 – 7.94 (d, 2H) and δ 6.96 – 6.91 (d, 2H).

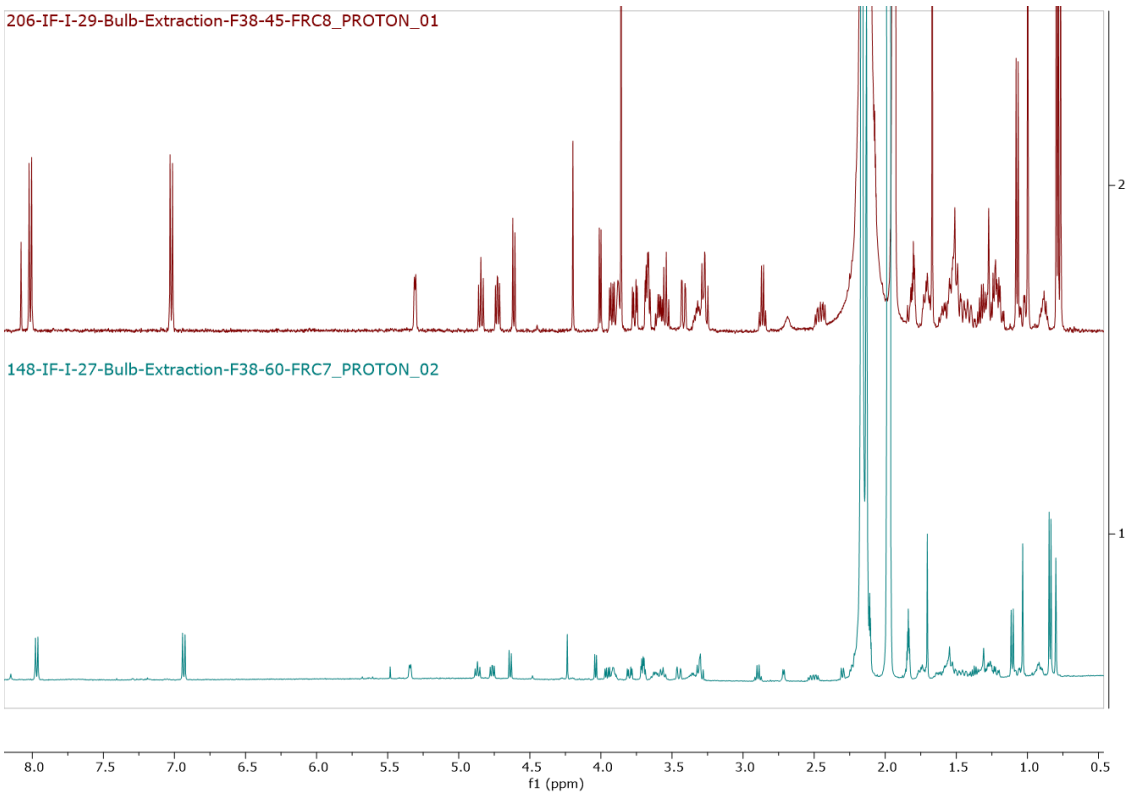

Figure 35. ^{1}H-NMR spectra comparison of OSW-1 (top) and IF-148 (bottom)

With the procedure being reiterated 8 times, **9** was isolated multiple times. Due to the reproducibility of the analytical method, retention times recorded by HPLC were similar, and a total amount of 6 mg of **9** was isolated.

Characterization of 20

Compound **20** (**Figure 29**) was isolated as an amorphous solid by HPLC and had an *m/z* value of $[M+Na]^+$ 779.40 in ESI^+ and $[M+HCOO]^-$ 791.10 in ESI^-, corresponding to a molecular weight of 756.97 g/mol and molecular formula $C_{43}H_{64}O_{11}$. In a similar manner as described above, the MS fragmentation pattern of **9** was determined for the first time (**Figure 36**).

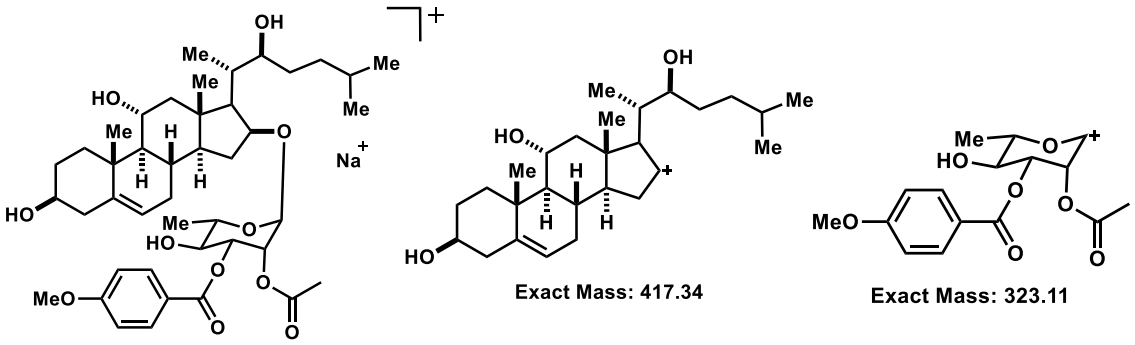

Sodium Adduct of 20
$C_{43}H_{64}O_{11}Na$
Exact Mass: 779.40

Figure 36. Sodium adduct and fragmentation pattern of 20

The ^{1}H-NMR spectrum showed signals for five steroidal methyl groups at δ 1.14 (s, 3H), 1.00 (s, 3H), 0.94 – 0.86 (m, 3H + 8H), 0.75 (dd, J = 15.9, 6.6 Hz, 6H), an olefinic proton at δ 5.38 (d, J = 5.6 Hz, 1H), and the α-L-rhamnopyranosyl anomeric proton at δ 5.34 – 5.30 (d, J= 2 Hz, 1H). Moreover, the aglycone was slightly modified with the presence of a hydroxyl group at the C-11 position showed by a proton signal at δ 4.66 (br. s, 1H). Two acyl moieties were linked to the rhamnoside, namely a p-methoxybenzoyl group at the C-3 position and an acetyl group linked at the C-2 position, supported by the presence

of proton signals at δ 7.93 – 7.88 (d, J = 8.8 Hz, 2H), 7.00 – 6.94 (d, J = 8.8 Hz, 2H), 3.84 (s, 3H, -OMe) and 1.61 (s, 3H, Ac). Reduction of the C-22 ketone present in OSW-1 to a C-22 hydroxyl group was demonstrated by the up-field shift of the C-20 proton at δ 3.27 (s, 1H), the presence of a hydroxyl proton at δ 4.60 (br. s, 1H) and by the cluster of signal at δ 4.17-4.10 (m, 1H) indicative of the C-22 proton. With the procedure being reiterated 8 times, **20** was isolated multiple times. Due to the reproducibility of the analytical method, retention times recorded by HPLC were similar, and a total amount of 4 mg of **20** was isolated.

Structural Elucidation of IF-111

Compound **IF-111 (Figure 29)** was isolated as an amorphous solid by HPLC and had an *m/z* value of $[M+Na]^+$ 893.20 in ESI^+, corresponding to a molecular weight of 871.03 g/mol and molecular formula $C_{47}H_{66}O_{15}$. In a similar manner as described above, the MS fragmentation pattern of **IF-111** was determined for the first time (**Figure 37**).

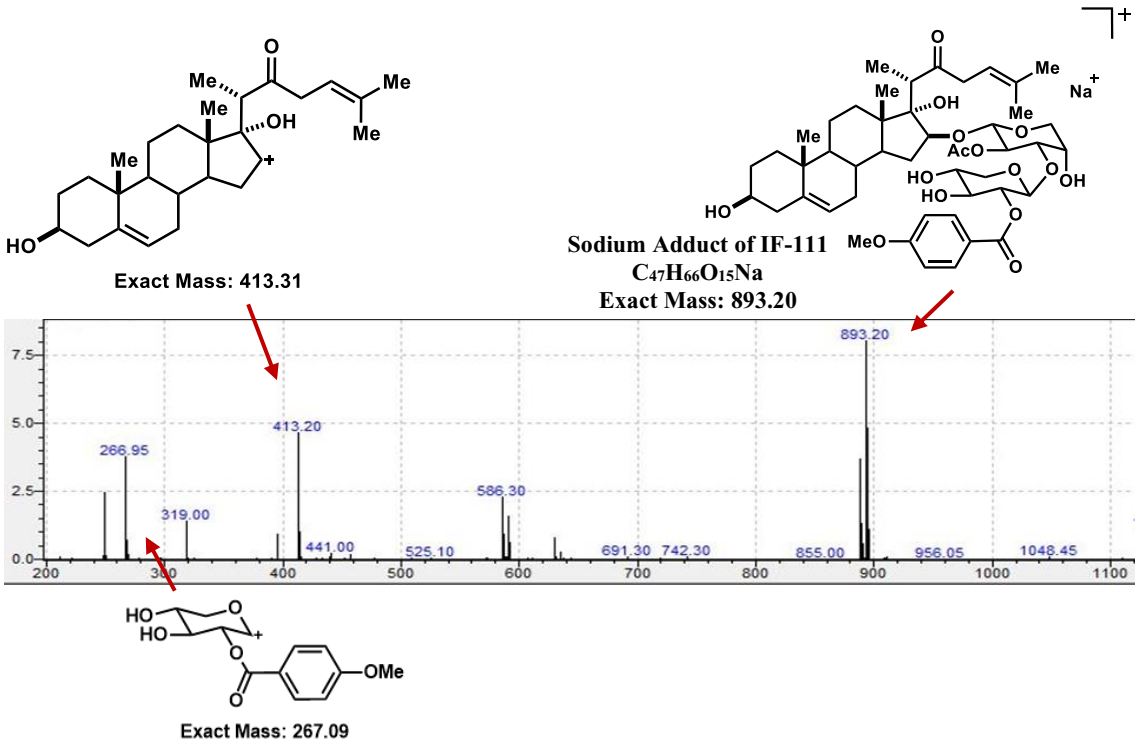

Figure 37. Mass spectrum and fragmentation pattern of IF-111 (new compound)

Analysis of the ^{1}H spectrum of **IF-111** and comparison with OSW-1 (**Figure 40**) implied that **IF-111** differed from OSW-1 by 2 protons. This correlates with the peak signal appearing at δ 5.45 (dd, 2H), indicative of an additional alkene (**Figure 38**).

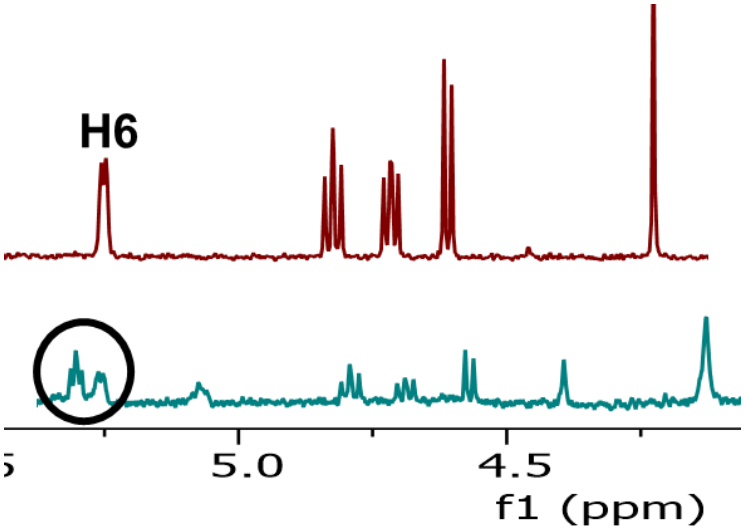

Figure 38. Zoom of the ^{1}H-NMR alkene region of IF-111 (bottom) compared to OSW-1 (top)

The position of the alkene was investigated by observing the side chain region in the low ppm values, as the steroid core proton signals were unchanged. Three positions for the alkene were hypothesized (**IF-111A**, **IF-111B**, **IF-111C**, **Figure 39**).

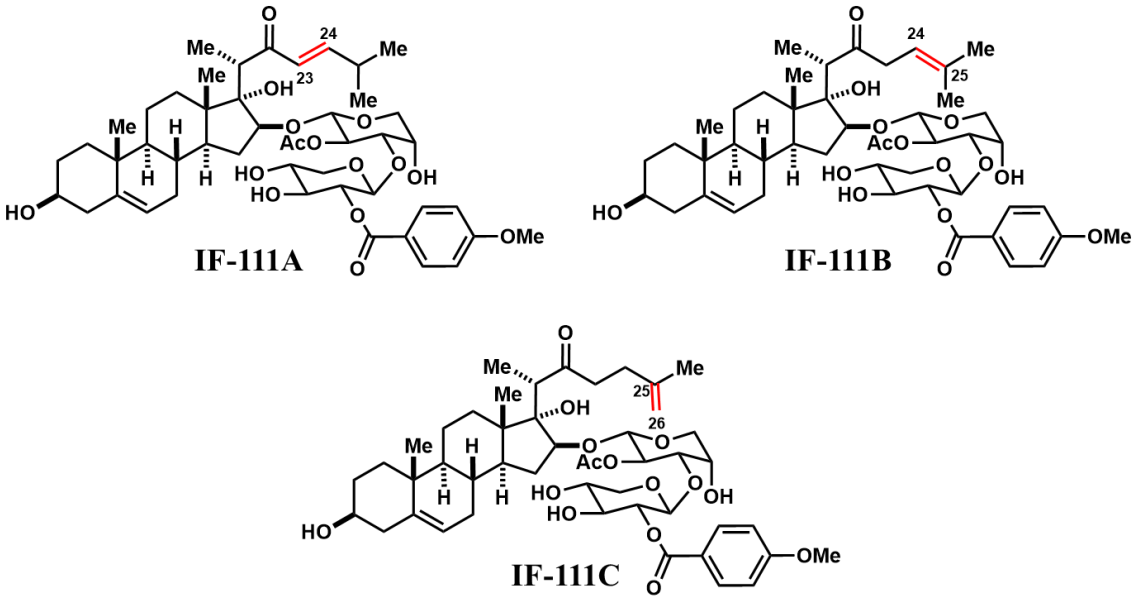

Figure 39. Three possible positions of the additional alkene on IF-111

The C26 and C27 protons in the cluster of signals at δ 0.81 – 0.75 (m, 9H) in OSW-1 were modified to a unique singlet of 6 equivalent protons at δ 0.90 (s, 6H). Moreover, the C25 proton in the region between δ 1.28 – 1.16 (m, 4H) does not appear in **IF-111**. The alkene was thus hypothesized to be positioned at the Δ–C24-C25 position.

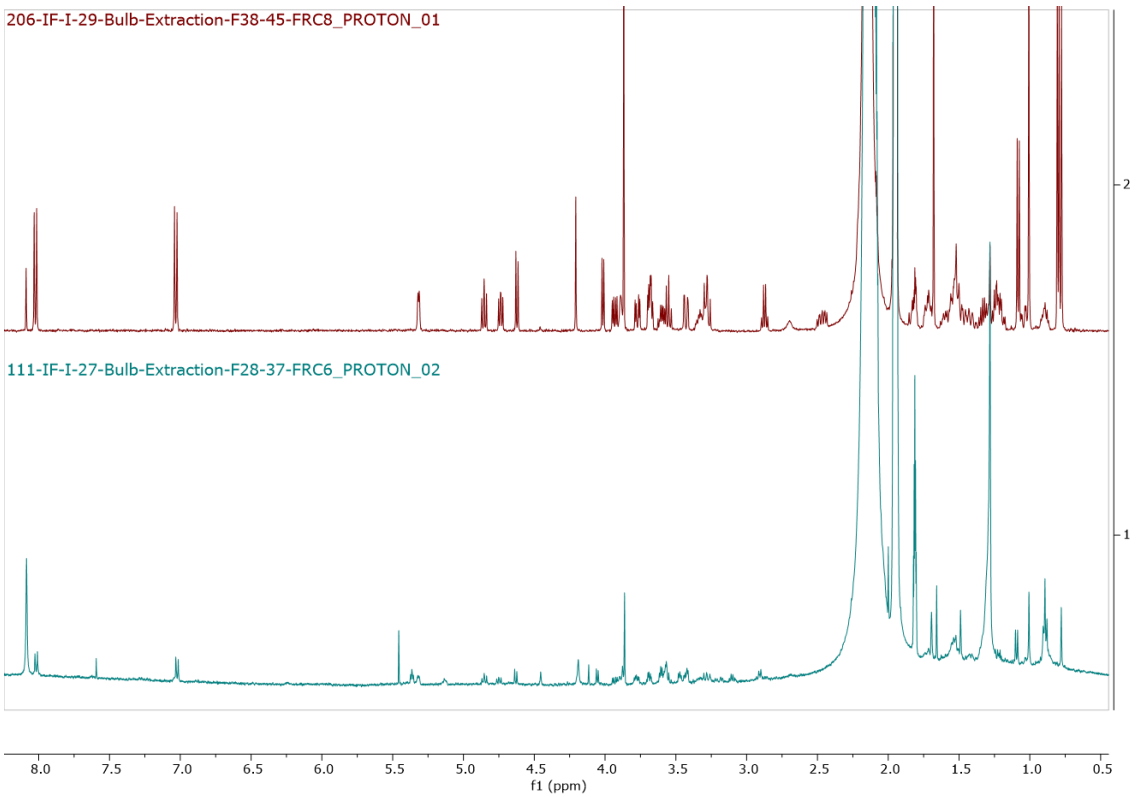

Figure 40. ^{1}H-NMR spectra comparison of OSW-1 (top) and IF-111 (bottom)

The isolated amount of compound **IF-111** was insufficient (2 mg) for ^{13}C and 2D NMR analyses to confirm the putative structure.

II.4 Conclusions and Future Directions

I have developed a novel and efficient analytical method to isolate and characterize several OSW-1 analogs. This reproducible method will allow for the isolation of OSW-1-related compounds on demand from the *O. saundersiae* bulbs. One new OSW-1-related natural product, previously unreported, has been putatively

identified. In particular, the newly isolated natural product differs from OSW-1 by the presence of an unsaturation at the C24-25 position of the aliphatic side chain. Future isolations using the established method will provide sufficient material to confirm the structures through ^{13}C NMR and 2D NMR analysis. I have additionally identified several parameters that could be further modulated to improve the isolation of OSW-1-related natural products, including exploring extraction solvent with different polarities (e.g, EtOH, EtOAc, hexanes, petroleum ether, etc…), the purification solvent system (e.g, MeOH/DCM, $CHCl_3$/AcOH/MeOH/H_2O), and the analytical method conditions (e.g, isocratic, altered gradient, MS parameters). Further, it would be interesting to process not only bulbs, but also leaves, flowers and stems of the *O. saundersiae* plant, to establish a basis of comparison and potentially discover new OSW-1 analogs to supplement SAR studies. Moreover, the analytical method can still be optimized. This can especially be done through reducing the analytical time requirements of sample analysis, and by using a succession of columns to increase the purity of compounds. Otherwise, mixtures of compounds can be tested for their activity through bioassay-guided fractionation to identify bioactive extracts more efficiently and isolate pure active compounds with potential increased binding affinity to OSBP and ORP4L. Even though cytotoxic activities of analogs have been reported for a tremendous amount of natural and synthetic analogs, many of these compounds have not been tested on resistant cancer-cell lines (e.g. ovarian cancer), which is currently investigated in our lab.

Additionally, creating molecular networks of all these steroidal saponins through the Global Natural Products Social Networking platform (GNPS) is a source of new opportunities related to the fields of analytical chemistry and metabolomics. Molecular

networking organizes the tandem MS/MS data as a relational spectral network thereby mapping the chemistry that was detected in an MS/MS-based metabolomics experiment.[138] This has never been reported before for these compounds and is a worthy objective. If implemented to this research, these networks could provide more insight into biological activities. Molecular networking is just beginning to be recognized but is already studied for the discovery of therapeutic leads, monitoring drug metabolism, clinical diagnostics, and emerging applications in precision medicine.[138,139]

Most importantly, since there are currently no existing co-crystal structures of OSBP and ORP4L bound to OSW-1 or a related analog, achieving this objective would significantly enhance our understanding of OSW-1's mechanism of action within cells, and ultimately lead to the development of potent antiviral and anticancer precision therapeutics capable of providing new therapies in human disease.

The library of OSW-1-related natural products produced from this research, in addition to compounds currently being characterized, will be tested for binding to OSBP and ORP4L in the near future. This will allow us to further supplement current SAR studies of OSW-1 in regard to OSBP and ORP4L, progressively guiding us toward the understanding of the compound's molecular interactions with the proteins. Ultimately, the results collected from biological testing will promote the development of selective anti-viral and anti-cancer therapeutics with improved pharmacokinetic and pharmacodynamic properties.

II.5 Materials and Methods

II.5.1 General Experimental Procedure

Lyophilization of plant material was performed using 2.5 L FreeZone Labconco Lyophilizer. Flash column chromatography was performed as described by Still *et al*.[137] employing E. Merck silica gel 60 (230-400 mesh ASTM). TLC analyses and preparative TLC (pTLC) purification were performed on 250 µm Silica Gel 60 F254 plates purchased from EM Science and Fluka Analytical. All solvents were used as purchased without further purification. Automated purifications were performed on Biotage Isolera One purification system using manually packed columns of 5G, 10G, 25G, or 50G of oven dried silica. ^{1}H and ^{13}C NMR spectra were recorded on a 400 MHz or 500 MHz Varian VNMRS DirectDrive spectrometer equipped with an indirect observe probe. Chemical shifts for proton and carbon resonances are reported in ppm (δ) relative to the residual protons in chloroform (δ 7.26), in acetonitrile [δ 1.94 (5)] and in methanol [δ 3.31 (5), δ 4.78] as references. High-resolution mass spectrometry (HRMS) analysis was performed using Agilent 6538 high-mass-resolution QTOF mass spectrometer. HPLC purification was performed on Shimadzu LCMS 2020 system [LC-20AP (pump), SPD-M20A (diode array detector), LCMS-2020 (mass spectrometer)]. Semi-preparative HPLC purification was performed using Phenomenex Luna C-18(2) column, 5 µm particle size (250 mm x 4.6 mm), supported by Phenomenex Security Guard cartridge kit C18 (4.0 mm x 3.0 mm); Phenomenex Luna C-8(2) column, 5 µm particle size (250 mm x 4.6 mm), supported by Phenomenex Security Guard cartridge kit C8 (4.0 mm x 3.0 mm) and HPLC-grade solvents (≥ 99.5%).

II.5.2 Plant Material

The *Ornithogalum Saundersiae* bulbs were cultivated in the OU greenhouse (Department of Microbiology and Plant Biology) by Mr. Lynn Nichols. Light was natural unless temperatures were above 98°F. In that case, there was 35% shading. Plants were fertilized every other week with 20-10-20 350 ppm N. Soil mix was 8 parts bm7 (35% composted bark, 10% perlite, 55% peat moss), 1 part turface (calcinated clay) and 1 part topsoil. Plants were harvested on June 21st, 2019 and stored at 0°C.

II.5.3 Extraction and Isolation

Fresh *Ornithogalum saundersiae* bulbs were lyophilized overnight, physically ground using mortar and pestle, and extracted with 750 mL of hot MeOH using Soxhlet apparatus. The extract was concentrated under reduced pressure, and the crude methanolic residue was diluted with 100 mL of DI H_2O and extracted 3 times with 30 mL of n-BuOH. The n-BuOH-soluble phase was fractionated on automated silica gel column using Biotage Isolera, with linear gradient elution from 0-30% MeOH/$CHCl_3$ and washed with EtOAc. Fractions with similar TLC profiles were combined and divided into 8 subfractions (A-H). Subfractions D and E were further separated by HPLC-MS with a stepped gradient from 70/30 to 85/15 to 100/0 MeCN/H_2O (with 0.1% formic acid) to yield compounds D1 (1.6 mg), D2 (3 mg), D3 (2.5 mg), D4 (3 mg), D5 (1 mg), D6 (2 mg), D7 (1.6 mg), D8 (1.3 mg), E1 (2 mg), E2 (1.6 mg), E3 (1.3 mg), E4 (2 mg), E5 (1 mg), E6 (< 1 mg), E7 (1 mg), E8 (4 mg) and E9 (< 1 mg). LC-MS samples were prepared by adding a volume of a 50/50 MeOH/MeCN solution such that the concentration was ~ 10 mg/mL. Further analysis of these compounds and other fractions is now under way.

II.5.4 LC-MS Analysis Parameters

LC-MS instrument parameters can be found as follows in **Table 4**.

MS	
Acquisition Time (min)	33 min
Acquisition Mode	Scan
m/z Range	200 – 1100
Voltage (kV)	30
INTERFACE	
DL Temperature (°C)	250
Heat Block Temperature (°C)	400
Nebulizing Gas Flow (mL/min)	1.5
Drying Gas Flow (mL/min)	15
PUMP	
Solvent A	Acetonitrile (MeCN)
Solvent B	Water + 0.1% Formic Acid
Total Flow (mL/min)	2.2
Mode	Binary Gradient

Table 4. LC-MS Instrument Parameters

LC gradient was set according to **Table 5**.

Time (min)	**%MeCN**
0	**70**
3	**70**
17	**85**
25	**100**
33	**70**

Table 5. LC-MS Gradient

II.5.5 Compound Data Summary

2 (OSW-1): 3β,17α-Dihydroxy-16β-[[O-(2-O-(4methoxybenzoyl)-β-D-xylopyranosyl)-(1 → 3)-2-O-acetyl-α-L-arabinopyranosyl]oxy]cholest-5-en-22-one

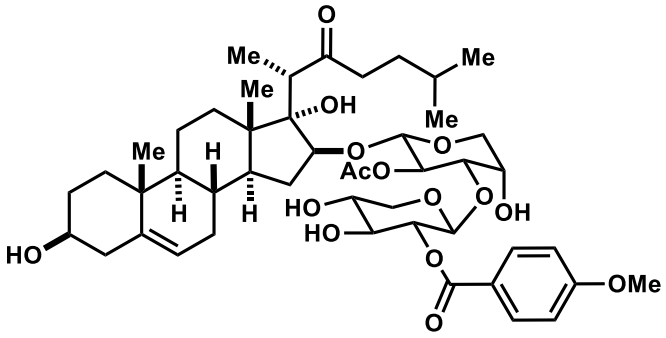

Molecular formula: $C_{47}H_{68}O_{15}$; ESI-MS (positive mode): *m/z* $[M+Na]^+$ 895.25, $[M+H]^+$ 873.25; ESI-MS (negative mode): *m/z* $[M+HCOO]^-$ 917.15; M = 873.03 g/mol; ^{1}H-NMR (500 MHz, Acetonitrile-d_3) δ 8.05 – 7.97 (d, J = 8 Hz, 2H), 7.06 – 6.98 (d, J = 8 Hz, 2H), 5.31 (d, J = 5.0 Hz, 1H), 4.87 – 4.81 (t, 1H), 4.73 (dd, J = 8.3, 6.2 Hz, 1H), 4.61 (d, J = 7.7 Hz, 1H), 4.20 (s, 1H), 4.01 (d, J = 6.2 Hz, 1H), 3.92 (dd, J = 11.5, 5.1 Hz, 1H), 3.88 (m, 1H), 3.86 (s, 3H), 3.76 (dd, J = 12.4, 4.2 Hz, 1H), 3.67 (dt, J = 8.9, 4.6 Hz, 2H), 3.63 – 3.56 (m, 1H), 3.54 (t, J = 8.8 Hz, 1H), 3.42 (dd, J = 12.4, 2.3 Hz, 1H), 3.31 (s, 1H), 3.26 (d, J = 9.7 Hz, 1H), 2.86 (q, J = 7.4 Hz, 1H), 2.69 (s, 1H), 2.46 (m, 1H), 1.82 (m, 2H), 1.74 – 1.68 (m, 2H), 1.67 (s, 3H), 1.61 – 1.56 (m, 1H), 1.53 (m, 2H), 1.50 (d, J = 9.7 Hz, 2H), 1.43 (d, J = 12.0 Hz, 1H), 1.41 – 1.29 (m, 2H), 1.28 – 1.16 (m, 4H), 1.07 (d, J = 7.4 Hz, 3H), 1.03 (dd, J = 13.6, 3.8 Hz, 1H), 1.00 (s, 3H), 0.88 (m, 1H), 0.81 – 0.75 (m, 9H). See **Appendix P** for NMR spectrum.

3: (3β,16β)-3,17-Dihydroxy-22-oxocholest-5-en-16-yl 2-O-acetyl-3-O-[2-O-(3,4-dimethoxybenzoyl)-β-D-xylopyranosyl]-α-L-arabinopyranoside)

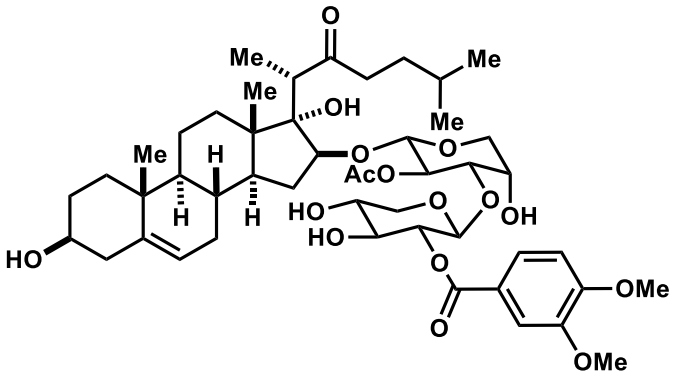

Molecular formula: $C_{48}H_{70}O_{16}$; ESI-MS (positive mode): *m/z* $[M+Na]^+$ 925.30; ESI-MS (negative mode): *m/z* $[M+HCOO]^-$ 947.10 ; M = 903.07 g/mol; ^{1}H-NMR (500 MHz, Acetonitrile-d_3) δ 7.73 (dd, J = 8.5, 2.0 Hz, 1H), 7.61 (d, J = 2.0 Hz, 1H), 7.06 (d, J = 8.5 Hz, 1H), 5.34 (d, J = 5.1 Hz, 1H), 4.88 (t, J = 8.2 Hz, 1H), 4.79 – 4.73 (dd, 1H), 4.66 (d, J = 7.7 Hz, 1H), 4.22 (s, 1H), 4.04 (d, J = 6.0 Hz, 1H), 3.96 (dd, J = 11.5, 4.9 Hz, 1H), 3.90 (2s, 6H), 3.79 (dd, J = 12.3, 4.5 Hz, 1H), 3.74 – 3.69 (m, 2H), 3.68 – 3.62 (m, 1H), 3.59 (d, J = 8.9 Hz, 2H), 3.45 (dd, J = 11.2 Hz, 2.0 Hz, 1H), 3.30 (t, J = 11.2 Hz, 2H), 2.89 (q, J = 7.4 Hz, 1H), 2.72 (s, 1H), 2.47 (m, 1H), 1.74 (m, 7H), 1.62 (m, 3H), 1.50 (m, 5H), 1.43 (m, 1H), 1.38 (m, 2H), 1.26 (4H, m), 1.10 (d, J=7.4, 3H), 1.05 (m, 1H), 1.03 (s, 3H), 0.92 (s, 1H), 0.92 (m, 1H), 0.81 – 0.79 (m, 9H). See **Appendix Q** for NMR spectrum.

4: 3β,17α-Dihydroxy-16β-[[O-(2-O-(E-cinnamoyl)-β-D-xylopyranosyl)-(1 → 3)-2-O-acetyl-α-L-arabinopyranosyl] oxy]-cholest-5-en-22-one

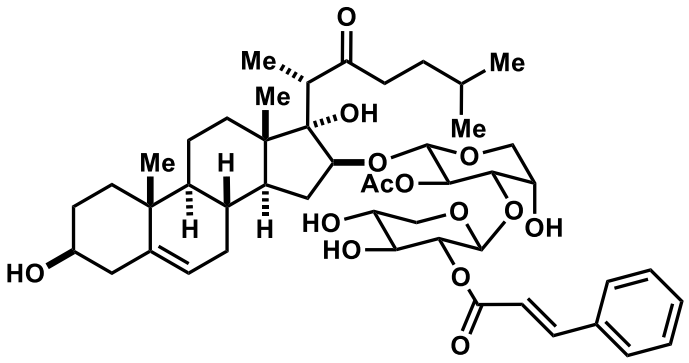

Molecular formula: $C_{48}H_{68}O_{14}$; ESI-MS (positive mode): *m/z* $[M+Na]^+$ 891.50; M = 869.06 g/mol; ^{1}H-NMR (500 MHz, Acetonitrile-d_3) δ 7.73 (d, J = 16.1 Hz, 1H), 7.65 (m, 2H), 7.46 – 7.40 (m, 3H), 6.52 (d, J = 16.0 Hz, 1H), 5.29 (d, J = 5 Hz, 1H), 4.83 – 4.78 (m, 1H), 4.75 (t, J = 8.5 Hz, 1H), 4.53 (d, J = 7.7 Hz, 1H), 4.21 (s, 1H), 4.04 (d, J = 6.6 Hz, 1H), 3.89 (dd, J = 11.6, 5.3 Hz, 1H), 3.77 (dd, J = 12.6, 3.7 Hz, 1H), 3.73 – 3.64 (m, 2H), 3.56 (m, 1H), 3.45 (dd, J = 17.1, 10.6 Hz, 1H), 3.24 (d, J = 10.8 Hz, 2H), 2.94 (q, J = 7.4 Hz, 1H), 2.69 (m, 1H), 2.34 (m, 1H), 1.99 (s, 3H), 1.72 (m, 2H), 1.52 (m, 5H), 1.36 (m, 1H), 1.33 (m, 2H), 1.22 (m, 2H), 1.20 – 1.19 (m, 1H), 1.14 (m, 2H), 1.09 (d, J = 7.4 Hz, 4H), 1.05 (s, 1H), 0.99 (s, 3H), 0.88 (m, 1H), 0.78 – 0.76 (m, 9H). See **Appendix R** for NMR spectrum.

9: 3β,17α-Dihydroxy-16β-[[O-(2-O-(4-hydroxybenzoyl)-β-D-xylopyranosyl)-(1 → 3)-2-O-acetyl-α-L-arabinopyranosyl] oxy]-cholest-5-en-22-one

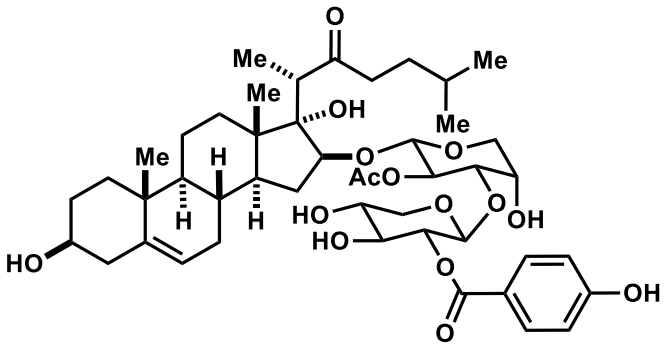

Molecular formula: $C_{46}H_{66}O_{15}$; ESI-MS (positive mode): *m/z* $[M+Na]^+$ 881.25; M = 859.02 g/mol; ^{1}H-NMR (500 MHz, Acetonitrile-d_3) δ 8.00 – 7.94 (d, J = 8 Hz, 2H), 6.96 – 6.91 (d, J= 8 Hz, 2H), 5.34 (d, J = 5.0 Hz, 1H), 4.87 (t, J = 8.3 Hz, 1H), 4.76 (dd, J = 8.3, 6.2 Hz, 1H), 4.64 (d, J = 7.7 Hz, 1H), 4.24 (s, 1H), 4.04 (d, J = 6.2 Hz, 1H), 3.95 (dd, J = 11.6, 5.1 Hz, 1H), 3.91 (s, 1H), 3.80 (dd, J = 12.4, 4.2 Hz, 1H), 3.70 (dt, J = 7.8, 3.9 Hz, 2H), 3.66 – 3.60 (m, 1H), 3.56 (t, J = 8.9 Hz, 1H), 3.45 (d, J = 12.3 Hz, 1H), 3.34 (d, J = 13.3 Hz, 1H), 3.28 (s, 1H), 2.89 (q, J = 7.4 Hz, 1H), 2.71 (d, J = 4.7 Hz, 1H), 2.51 (m, 1H), 2.29 (m, 1H), 1.74 (m, 2H), 1.70 (s, 3H), 1.62 (m, 1H), 1.58 (m, 2H), 1.54 (d, J = 10.0 Hz, 2H), 1.47 (m, 1H), 1.37 (dt, J = 13.2, 6.7 Hz, 2H), 1.31 – 1.23 (m, 4H), 1.11 (d, J = 7.4 Hz, 3H), 1.09 – 1.05 (m, 1H), 1.03 (s, 3H), 0.92 (m, 1H), 0.84 (d, J = 6.5 Hz, 6H), 0.80 (s, 3H). See **Appendix S** for NMR spectrum.

20: 3,11α,22-Trihydroxycholest-5-en-16β-yl,2-O-acetyl-3-O-p-methoxybenzoyl-α-L-rhamnopyranoside

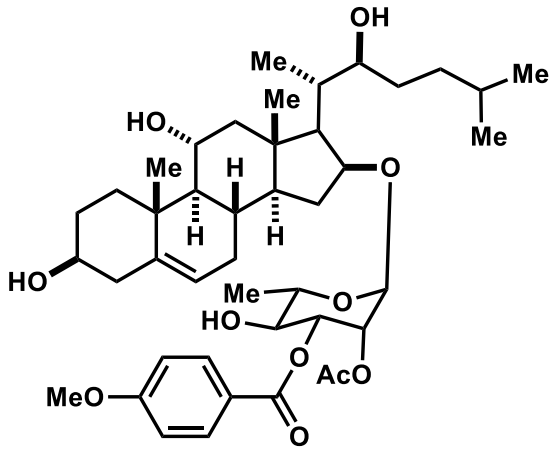

Molecular formula $C_{43}H_{64}O_{11}$; ESI-MS (positive mode): *m/z* $[M+Na]^+$ 779.40; ESI-MS (negative mode): *m/z* $[M+HCOO]^-$ 791.10; M = 756.97 g/mol; ^{1}H-NMR (500 MHz, Acetonitrile-d_3) δ 7.93 – 7.88 (d, J = 8.8 Hz, 2H), 7.00 – 6.94 (d, J = 8.8 Hz, 2H), 5.38 (d, J = 5.6 Hz, 1H), 5.34 – 5.30 (d, J= 2 Hz, 1H), 5.14 (dd, J = 9.7, 3.4 Hz, 1H), 5.11 (t, J = 2.5 Hz, 1H), 4.85 (dd, J = 3.5, 1.6 Hz, 1H), 4.66 (br. s, 1H), 4.60 (br.s, 1H), 4.17-4.10 (m, 1H), 3.95 (m, 1H), 3.84 (s, 3H), 3.80 – 3.75 (m, 1H), 3.72 – 3.54 (m, 4H), 3.46 (m, 2H), 3.43 (s, 2H), 3.27 (s, 1H), 2.70 (m, 1H), 2.58 – 2.55 (td, J = 3.5 Hz, J = 13.9 Hz, 1H), 1.69 (s, 3H), 1.61 (s, 3H), 1.47 (m, 7H), 1.14 (s, 3H), 1.00 (s, 3H), 0.94 – 0.86 (m, 11H), 0.75 (dd, J = 15.9, 6.6 Hz, 6H). See **Appendix T** for NMR spectrum.

IF-111: 3β,17α-Dihydroxy-16β-[[O-(2-O-(4methoxybenzoyl)-β-D-xylopyranosyl)-(1 → 3)-2-O-acetyl-α-L-arabinopyranosyl]oxy]cholest-5,24-diene-22-one

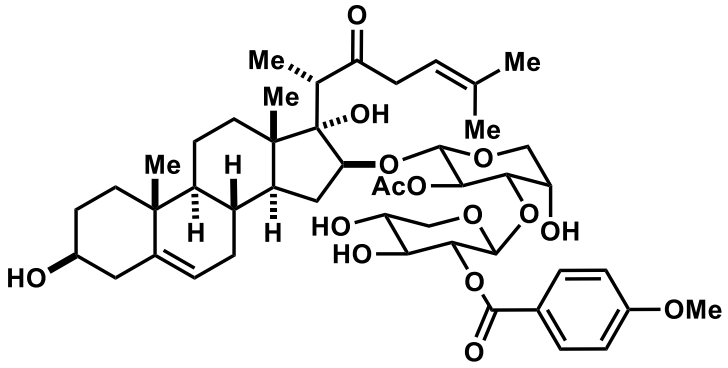

Molecular formula: $C_{47}H_{66}O_{15}$; ESI-MS (positive mode): *m/z* $[M+Na]^+$ 893.20; ESI-MS (negative mode): *m/z* $[M+HCOO]^-$ 915.10; M = 871.03 g/mol; ^{1}H-NMR (500 MHz, Acetonitrile-d_3) δ 8.03 – 8.00 (d, J = 8 Hz, 2H), 7.35 – 7.01 (d, J = 8 Hz, 2H), 5.36 (d, J = 5.2 Hz, 1H), 5.32 (d, J = 5.0 Hz, 1H), 4.87 – 4.82 (t, 1H), 4.75 (dd, J = 8.3, 6.2 Hz, 1H), 4.61 (d, J = 7.7 Hz, 1H), 4.19 (s, 1H), 4.06 (m, 2H), 3.86 (s, 3H), 3.77 (m, 1H), 3.70 (m, 1H), 3.61 (t, J = 4.6 Hz, 2H), 3.56 (m, 1H), 3.47 (t, J = 8.8 Hz, 1H), 3.42 (dd, J = 12.4, 2.3 Hz, 1H), 3.27 (m, 1H), 3.11 (q, J = 9.7 Hz, 1H), 2.91 (d, J = 7.4 Hz, 1H), 2.69 (m, 1H), 1.72 (m, 2H), 1.74 – 1.68 (m, 2H), 1.66 (s, 3H), 1.53 (m, 2H), 1.51 (m, 5H), 1.22 (m, 4H), 1.07 (d, J = 7.4 Hz, 3H), 1.03 (dd, J = 13.6, 3.8 Hz, 1H), 1.02 (s, 3H), 0.88 (m, 10H), 0.76 (s, 3H). See **Appendix U** for NMR spectrum.

References

1. Auwal, M. S.; Saka, S.; Mairiga, I. A.; Sanda, K. A.; Shuaibu, A.; Ibrahim, A. Preliminary Phytochemical and Elemental Analysis of Aqueous and Fractionated Pod Extracts of Acacia Nilotica (Thorn Mimosa). *Vet. Res. forum an Int. Q. J.* **2014**, *5* (2), 95–100.
2. Yuan, H.; Ma, Q.; Ye, L.; Piao, G. The Traditional Medicine and Modern Medicine from Natural Products. *Molecules* **2016**, *21* (5), 559–576.
3. Mushtaq, S.; Abbasi, B. H.; Uzair, B.; Abbasi, R. Natural Products as Reservoirs of Novel Therapeutic Agents. *EXCLI J.* **2018**, *17*, 420–451.
4. Newman, D. J.; Cragg, G. M. Natural Products as Sources of New Drugs over the Nearly Four Decades from 01/1981 to 09/2019. *J. Nat. Prod* **2020**, *83*, 770–803.
5. Klayman, D. L. et al. Isolation of Artemisinin (Qinghaosu) From Artemisia Annua Growing in the United States. *J. Nat. Prod.* **1984**, *47* (4), 715–717.
6. Wall, M. E. The Discovery of Camptothecin and Taxol. *Am. Chem. Soc.* **2003**.
7. Heinrich, M.; Teoh, H. L. Galanthamine from Snowdrop - The Development of a Modern Drug against Alzheimer's Disease from Local Caucasian Knowledge. *J. Ethnopharmacol.* **2004**, *92* (2–3), 147–162.
8. Carlson, E. E. Natural Products as Chemical Probes. *ACS Chem. Biol.* **2010**, *5* (7), 639–653.
9. Shen, B. A New Golden Age of Natural Products Drug Discovery. *Cell* **2015**, *163* (6), 1297–1300.
10. Challinor, V. L.; De Voss, J. J. Open-Chain Steroidal Glycosides, a Diverse Class of Plant Saponins. *Nat. Prod. Rep.* **2013**, *30* (3), 429–454.

11. Ashour, A. S.; El Aziz, M. M. A.; Gomha Melad, A. S. A Review on Saponins from Medicinal Plants: Chemistry, Isolation, and Determination. *J. Nanomedicine Res.* **2019**, *7* (4), 282–288.

12. El Barky, A.; Hussein, S. A.; Alm-Eldeen, A.-E.; Hafez, A.; Mohamed, T. *Diabetes Management Saponins and Their Potential Role in Diabetes Mellitus*; 2017; Vol. 7.

13. Sobolewska Agnieszka Galanty Karolina Grabowska Justyna Makowska-Wa, D.; Wróbel-Biedrawa Irma Podolak, D. Saponins as Cytotoxic Agents. *Phytochem. Rev.* **2020**, *19*, 139–189.

14. Sparg, S. G.; Light, M. E.; Van Staden, J. Biological Activities and Distribution of Plant Saponins. *J. Ethnopharmacol.* **2004**, *94* (2–3), 219–243.

15. Akinmoladun, A. C.; Olaleye, M. T.; Farombi, E. O. *Cardiotoxicity and Cardioprotective Effects of African Medicinal Plants*; Elsevier Inc., 2014.

16. Plančić, M.; Božin, B.; Kladar, N.; Rat, M.; Srđenović, B. Phytochemical Profile and Biological Activities of the Genus Ornithogalum L. (Hyacinthaceae). *Biol. Serbica* **2014**, *36* (1), 3–17.

17. Tang, Y.; Li, N.; Duan, J. A.; Tao, W. Structure, Bioactivity, and Chemical Synthesis of OSW-1 and Other Steroidal Glycosides in the Genus Ornithogalum. *Chem. Rev.* **2013**, *113* (7), 5480–5514.

18. Podolak, I.; Galanty, A.; Sobolewska, D. Saponins as Cytotoxic Agents: A Review. *Phytochemistry Reviews*. Phytochem Rev September 2010, pp 425–474.

19. Kubo, S.; Mimaki, Y.; Terao, M.; Sashida, Y.; Nikaido, T.; Ohmoto, T. Acylated Cholestane Glycosides from the Bulbs of Ornithogalum Saundersiae.

Phytochemistry **1992**, *31* (11), 3969–3973.

20. Iguchi, T.; Kuroda, M.; Naito, R.; Watanabe, T.; Matsuo, Y.; Yokosuka, A.; Mimaki, Y. Cholestane Glycosides from Ornithogalum Saundersiae Bulbs and the Induction of Apoptosis in HL-60 Cells by OSW-1 through a Mitochondrial-Independent Signaling Pathway. *J. Nat. Med.* **2019**, *73* (1), 131–145.
21. Chen, Q. W.; Gong, T.; Zhang, P. C.; Kong, J. Q. Seven New 1-Oxygenated Cholestane Glycosides from Ornithogalum Saundersiae. *J. Asian Nat. Prod. Res.* **2020**, *22* (3), 201–216.
22. Kuroda, M.; Mimaki, Y.; Sashida, Y.; Nikaido, T.; Ohmoto, T. Structure of a Novel 22-Homo-23-Norcholestane Trisaccharide from Ornithogalum Saundersiae. *Tetrahedron Lett.* **1993**, *34* (38), 6073–6076.
23. Kuroda, M.; Mimaki, Y.; Sashida, Y.; Hirano, T.; Oka, K.; Dobashi, A. A Novel Cholestane Glycoside with Inhibitory Activity on Proliferation of Human PBL from O. Saundersiae Bulbs. *Chem. Pharm. Bull.* **1995**, *43* (7), 1257–1259.
24. Mimaki, Y.; Kuroda, M.; Sashida, Y.; Hirano, T.; Oka, K.; Dobashi, A.; Koshino, H.; Uzawa, J. Three Novel Rearranged Cholestane Glycosides from Ornithogalum Saundersiae Bulbs and Their Cytostatic Activities on Leukemia HL-60 and MOLT-4 Cells. *Tetrahedron Lett.* **1996**, *37* (8), 1245–1248.
25. Hirano, T.; Oka, K.; Mimaki, Y.; Kuroda, M.; Sashida, Y. Potent Growth Inhibitory Activity of a Novel Ornithogalum Cholestane Glycoside on Human Cells: Induction of Apoptosis in Promyelocytic Leukemia HL-60 Cells. *Life Sci.* **1996**, *58* (9), 789–798.
26. Mimaki, Y. Structures and Biological Activities of Plant Glycosides. *Nat. procuts*

Commun. **2006**, *1* (3), 247–253.

27. Kuroda, M.; Mimaki, Y.; Sashida, Y. Saundersiosides C-H, Rearranged Cholestane Glycosides from the Bulbs of Ornithogalum Saundersiae and Their Cytostatic Activity on HL-60 Cells. *Phytochemistry* **1999**, *52* (3), 435–443.
28. Kuroda, M.; Mimaki, Y.; Yokosuka, A.; Sashida, Y.; Beutler, J. A. Cytotoxic Cholestane Glycosides from the Bulbs of Ornithogalum Saundersiae. *J. Nat. Prod.* **2001**, *64* (1), 88–91.
29. Iguchi, T.; Kuroda, M.; Naito, R.; Watanabe, T.; Matsuo, Y.; Yokosuka, A.; Mimaki, Y. Structural Characterization of Cholestane Rhamnosides from Ornithogalum Saundersiae Bulbs and Their Cytotoxic Activity against Cultured Tumor Cells. *Molecules* **2017**, *22* (8).
30. Morzycki, J. W.; Wojtkielewicz, A. Synthesis of a Highly Potent Antitumor Saponin OSW-1 and Its Analogues. *Phytochem. Rev.* **2005**, *4* (2–3), 259–277.
31. Yan, K.; Gao, L. N.; Cui, Y. L.; Zhang, Y.; Zhou, X. The Cyclic AMP Signaling Pathway: Exploring Targets for Successful Drug Discovery (Review). *Mol. Med. Rep.* **2016**, *13* (5), 3715–3723.
32. Lerner, A.; Epstein, P. M. Cyclic Nucleotide Phosphodiesterases as Targets for Treatment of Haematological Malignancies. *Biochem. J.* **2006**, *393* (1), 21–41.
33. Mimaki, Y.; Kuroda, M.; Kameyama, A.; Sashida, Y.; Hirano, T.; Oka, K.; Mafkawa, R.; Wada, T.; Sug, K.; Beutler, J. A. Cholestane Glycosides with Potent Cytotoxic Activities on Various Tumor Cells from Ornithogalum Saundersiae Bulbs. *Bioorganic Med. Chem. Lett.* **1997**, *7* (5), 633–636.
34. Zhang, Y.; Fang, F.; Fan, K.; Zhang, Y.; Zhang, J.; Guo, H.; Yu, P.; Ma, J.

Effective Cytotoxic Activity of OSW-1 on Colon Cancer by Inducing Apoptosis in Vitro and in Vivo. *Oncol. Rep.* **2017**, *37* (6), 3509–3519.

35. Zhou, Y.; Garcia-Prieto, C.; Carney, D. A.; Xu, R. hua; Pelicano, H.; Kang, Y.; Yu, W.; Lou, C.; Kondo, S.; Liu, J.; Harris, D. M.; Estrov, Z.; Keating, M. J.; Jin, Z.; Huang, P. OSW-1: A Natural Compound with Potent Anticancer Activity and a Novel Mechanism of Action. *J. Natl. Cancer Inst.* **2005**, *97* (23), 1781–1785.

36. Zhu, J.; Xiong, L.; Yu, B.; Wu, J. Apoptosis Induced by a New Member of Saponin Family Is Mediated through Caspase-8-Dependent Cleavage of Bcl-2. *Mol. Pharmacol.* **2005**, *68* (6), 1831–1838.

37. Péresse, T.; Kovacs, D.; Subra, M.; Bigay, J.; Antonny, B.; Mesmin, B. et al. Molecular and Cellular Dissection of the Oxysterol-Binding Protein Cycle through a Fluorescent Inhibitor. *J. Biol. Chem.* **2020**, *295* (13), 4277–4288.

38. Zhong, W.; Xu, M.; Li, C.; Olkkonen, V. M.; Lei, P.; Yan, D. et al. ORP4L Extracts and Presents PIP 2 from Plasma Membrane for PLCβ3 Catalysis: Targeting It Eradicates Leukemia Stem Cells. *Cell Rep.* **2019**, *26* (8), 2166-2177.e9.

39. Olkkonen, V. M. OSBP-Related Proteins: Liganding by Glycerophospholipids Opens New Insight into Their Function. *Molecules* **2013**, *18* (11), 13666–13679.

40. Burgett, A. W. G.; Shair, M. D. et al. Natural Products Reveal Cancer Cell Dependence on Oxysterol-Binding Proteins. *Nat. Chem. Biol.* **2011**, *7* (9), 639–647.

41. Garcia-Prieto, C.; Ahmed, K. B. R.; Chen, Z.; Zhou, Y.; Hammoudi, N.; Kang, Y.; Lou, C.; Mei, Y.; Jin, Z.; Huang, P. Effective Killing of Leukemia Cells by the Natural Product OSW-1 through Disruption of Cellular Calcium Homeostasis. *J.*

Biol. Chem. **2013**, *288* (5), 3240–3250.

42. Charman, M.; Colbourne, T. R.; Pietrangelo, A.; Kreplak, L.; Ridgway, N. D. Oxysterol-Binding Protein (OSBP)-Related Protein 4 (ORP4) Is Essential for Cell Proliferation and Survival. *J. Biol. Chem.* **2014**, *289* (22), 15705–15717.

43. Shah, A. Development of Novel Anticancer Agents Based on Natural Products. **2015**, 1–205.

44. Li, J. W.; Xiao, Y. L.; Lai, C. F.; Lou, N.; Ma, H. L.; Zhu, B. Y.; Zhong, W. Bin; Yan, D. G. Oxysterol-Binding Protein-Related Protein 4L Promotes Cell Proliferation by Sustaining Intracellular Ca 2+ Homeostasis in Cervical Carcinoma Cell Lines. *Oncotarget* **2016**, *7* (40), 65849–65861.

45. Zhong, W.; Olkkonen, V. M.; Yan, D. et al. ORP4L Is Essential for T-Cell Acute Lymphoblastic Leukemia Cell Survival. *Nat. Commun.* **2016**, *7*, 1–14.

46. Kimura, M.; Sasaki, K.; Fukutani, Y.; Yoshida, H.; Ohsawa, I.; Yohda, M.; Sakurai, K. Anticancer Saponin OSW-1 Is a Novel Class of Selective Golgi Stress Inducer. *Bioorganic Med. Chem. Lett.* **2019**, *29* (14), 1732–1736.

47. Liu, H.; Huang, S. Role of Oxysterol-Binding Protein-Related Proteins in Malignant Human Tumours. *World J. Clin. Cases* **2020**, *8* (1), 1–10.

48. Albulescu, L.; Strating, J. R. P. M.; Thibaut, H. J.; Van Der Linden, L.; Shair, M. D.; Neyts, J.; Van Kuppeveld, F. J. M. Broad-Range Inhibition of Enterovirus Replication by OSW-1, a Natural Compound Targeting OSBP. *Antiviral Res.* **2015**, *117*, 110–114.

49. Albulescu, L.; Weber-Boyvat, M.; Olkkonen, V. M.; van Kuppeveld, F. J. M.; Strating, J. R. P. M. et al. Uncovering Oxysterol-Binding Protein (OSBP) as a

Target of the Anti-Enteroviral Compound TTP-8307. *Antiviral Res.* **2017**, *140*, 37–44.

50. Jaworski, C. J.; Moreira, E.; Li, A.; Lee, R.; Rodriguez, I. R. A Family of 12 Human Genes Containing Oxysterol-Binding Domains. *Genomics* **2001**, *78* (3), 185–196.

51. Lehto, M.; Laitinen, S.; Chinetti, G.; Johansson, M.; Ehnholm, C.; Staels, B.; Ikonen, E.; Olkkonen, V. M. The OSBP-Related Protein Family in Humans. *J. Lipid Res.* **2001**, *42* (8), 1203–1213.

52. Anniss, A. M.; Apostolopoulos, J.; Dworkin, S.; Purton, L. E.; Sparrow, R. L. An Oxysterol-Binding Protein Family Identified in the Mouse. *DNA Cell Biol.* **2002**, *21* (8), 571–580.

53. Raychaudhuri, S.; Prinz, W. A. The Diverse Functions of Oxysterol-Binding Proteins. *Annu. Rev. Cell Dev Biol* **2010**, *26*, 157–177.

54. Olkkonen, V. M.; Zhou, Y.; Yan, D.; Vihervaara, T. Oxysterol-Binding Proteins-Emerging Roles in Cell Regulation. *Eur. J. Lipid Sci. Technol.* **2012**, *114* (6), 634–643.

55. Weber-Boyvat, M.; Zhong, W.; Yan, D.; Olkkonen, V. M. Oxysterol-Binding Proteins: Functions in Cell Regulation beyond Lipid Metabolism. *Biochem. Pharmacol.* **2013**, *86* (1), 89–95.

56. Kentala, H.; Weber-Boyvat, M.; Olkkonen, V. M. *OSBP-Related Protein Family: Mediators of Lipid Transport and Signaling at Membrane Contact Sites*; Elsevier Inc., 2016; Vol. 321.

57. Levine, T. P.; Munro, S. The Pleckstrin Homology Domain of Oxysterol-Binding

Protein Recognises a Determinant Specific to Golgi Membranes. *Curr. Biol.* **1998**, *8* (13), 729–739.

58. Furuita, K.; Jee, J. G.; Fukada, H.; Mishima, M.; Kojima, C. Electrostatic Interaction between Oxysterol-Binding Protein and VAMP-Associated Protein a Revealed by NMR and Mutagenesis Studies. *J. Biol. Chem.* **2010**, *285* (17), 12961–12970.

59. Manik, M. K.; Yang, H.; Tong, J.; Im, Y. J. Structure of Yeast OSBP-Related Protein Osh1 Reveals Key Determinants for Lipid Transport and Protein Targeting at the Nucleus-Vacuole Junction. *Structure* **2017**, *25* (4), 617-629.e3.

60. Olkkonen, V. M. OSBP-Related Protein Family in Lipid Transport over Membrane Contact Sites. *Lipid Insights* **2015**, *2015*, 1–9.

61. Wyles, J. P.; Perry, R. J.; Ridgway, N. D. Characterization of the Sterol-Binding Domain of Oxysterol-Binding Protein (OSBP)-Related Protein 4 Reveals a Novel Role in Vimentin Organization. *Exp. Cell Res.* **2007**, *313* (7), 1426–1437.

62. Kandutschs, A. A.; Thompson, E. B. Cytosolic Proteins That Bind Oxygenated Sterols. *Biol. Chem.* **1980**, *255* (22), 10813–10826.

63. Soffientini, U.; Graham, A. Intracellular Cholesterol Transport Proteins: Roles in Health and Disease. *Clin. Sci.* **2016**, *130* (21), 1843–1859.

64. Roberts, B. L.; Severance, Z. C.; Bensen, R. C.; Le-McClain, A. T.; Malinky, C. A.; Mettenbrink, E. M.; Nuñez, J. I.; Reddig, W. J.; Blewett, E. L.; Burgett, A. W. G. Differing Activities of Oxysterol-Binding Protein (OSBP) Targeting Anti-Viral Compounds. *Antiviral Res.* **2019**, *170* (June), 104548.

65. Wang, A. P.; Weng, J.; Anderson, R. G. W.; Science, S.; Series, N.; Mar, N. OSBP

Is a Cholesterol-Regulated Scaffolding Protein in Control of ERK1 / 2 Activation. *Science (80-.).* **2005**, *307* (5714), 1472–1476.

66. Wang, P. Y.; Weng, J.; Lee, S.; Anderson, R. G. W. The N Terminus Controls Sterol Binding While the C Terminus Regulates the Scaffolding Function of OSBP. *J. Biol. Chem.* **2008**, *283* (12), 8034–8045.

67. Wang, C.; JeBailey, L.; Ridgway, N. D. Oxysterol-Binding-Protein (OSBP)-Related Protein 4 Binds 25-Hydroxycholesterol and Interacts with Vimentin Intermediate Filaments. *Biochem. J.* **2002**, *361* (3), 461–472.

68. Tong, J.; Yang, H.; Yang, H.; Eom, S. H.; Im, Y. J. Structure of Osh3 Reveals a Conserved Mode of Phosphoinositide Binding in Oxysterol-Binding Proteins. *Structure* **2013**, *21* (7), 1203–1213.

69. Beh, C. T.; Cool, L.; Phillips, J.; Rine, J. Overlapping Functions of the Yeast Oxysterol-Binding Protein Homologues. *Genetics* **2001**, *157* (3), 1117–1140.

70. Im, Y. J.; Raychaudhuri, S.; Prinz, W. A.; Hurley, J. H. Structural Mechanism for Sterol Sensing and Transport by OSBP-Related Proteins. *Nature* **2005**, *437* (7055), 154–158.

71. Suchanek, M.; Hynynen, R.; Wohlfahrt, G.; Lehto, M.; Johansson, M.; Saarinen, H.; Radzikowska, A.; Thiele, C.; Olkkonen, V. M. The Mammalian Oxysterol-Binding Protein-Related Proteins (ORPs) Bind 25-Hydroxycholesterol in an Evolutionary Conserved Pocket. *Biochem. J.* **2007**, *405* (3), 473–480.

72. Singh, R. P.; Brooks, B. R.; Klauda, J. B. Binding and Release of Cholesterol in the Osh4 Protein of Yeast. *Proteins Struct. Funct. Bioinforma.* **2009**, *75* (2), 468–477.

73. Bukiya, A. N.; Dopico, A. M. Common Structural Features of Cholesterol Binding Sites in Crystallized Soluble Proteins. *J. Lipid Res.* **2017**, *58* (6), 1044–1054.

74. Moser, B. R. Review of Cytotoxic Cephalostatins and Ritterazines: Isolation and Synthesis. *J. Nat. Prod.* **2008**, *71* (3), 487–491.

75. Komiya, T.; Yoshida, M.; Fukuoka, M.; Nakagawa, K. et al. Ritterazine B, a New Cytotoxic Natural Compound, Induces Apoptosis in Cancer Cells. *Cancer Chemother. Pharmacol.* **2003**, *51* (3), 202–208.

76. Beutler, J. A.; Shoemaker, R. H.; Johnson, T.; Boyd, M. R. Cytotoxic Geranyl Stilbenes from Macaranga Schweinfurthii. *J. Nat. Prod.* **1998**, *61* (12), 1509–1512.

77. Tasdemir, D.; Mangalindan, G. C.; Ireland, C. M. et al. Bioactive Isomalabaricane Triterpenes from the Marine Sponge Rhabdastrella Globostellata. *J. Nat. Prod.* **2002**, *65* (2), 210–214.

78. Du, X.; Turner, N.; Yang, H. The Role of Oxysterol-Binding Protein and Its Related Proteins in Cancer. *Semin. Cell Dev. Biol.* **2018**, *81*, 149–153.

79. Olkkonen, V. M. ORP4L: Can Targeting an MCS Component Provide Tools for Eradication of Leukemia? *Contact* **2019**, *2*, 251525641984052.

80. Lehto, M.; Olkkonen, V. M. The OSBP-Related Proteins: A Novel Protein Family Involved in Vesicle Transport, Cellular Lipid Metabolism, and Cell Signalling. *Biochim. Biophys. Acta - Mol. Cell Biol. Lipids* **2003**, *1631* (1), 1–11.

81. Mesmin, B.; Bigay, J.; Moser Von Filseck, J.; Lacas-Gervais, S.; Drin, G.; Antonny, B. A Four-Step Cycle Driven by PI(4)P Hydrolysis Directs Sterol/PI(4)P Exchange by the ER-Golgi Tether OSBP. *Cell* **2013**, *155* (4), 830.

82. Pietrangelo, A.; Ridgway, N. D. Bridging the Molecular and Biological Functions

of the Oxysterol-Binding Protein Family. *Cell. Mol. Life Sci.* **2018**, *75* (17), 3079–3098.

83. Strating, J. R. P. M.; van der Linden, L.; Albulescu, L.; Bigay, J.; Shair, M. D.; Olkkonen, V. M.; van Kuppeveld, F. J. M. et al. Itraconazole Inhibits Enterovirus Replication by Targeting the Oxysterol-Binding Protein. *Cell Rep.* **2015**, *10* (4), 600–615.

84. Park, I. W.; Ndjomou, J.; Wen, Y.; Liu, Z.; Ridgway, N. D.; Kao, C. C.; He, J. J. Inhibition of HCV Replication by Oxysterol-Binding Protein-Related Protein 4 (ORP4) through Interaction with HCV NS5B and Alteration of Lipid Droplet Formation. *PLoS One* **2013**, *8* (9), 1–18.

85. Meutiawati, F.; Bezemer, B.; Strating, J. R. P. M.; Overheul, G. J.; Žusinaite, E.; van Kuppeveld, F. J. M.; van Cleef, K. W. R.; van Rij, R. P. Posaconazole Inhibits Dengue Virus Replication by Targeting Oxysterol-Binding Protein. *Antiviral Res.* **2018**, *157*, 68–79.

86. Wang, H.; Perry, J. W.; Lauring, A. S.; Neddermann, P.; De Francesco, R.; Tai, A. W. Oxysterol-Binding Protein Is a Phosphatidylinositol 4-Kinase Effector Required for HCV Replication Membrane Integrity and Cholesterol Trafficking. *Gastroenterology* **2014**, *146* (5), 1373-1385.e11.

87. Lin, J.-Y.; Kung, Y.-A.; Shih, S.-R. Antivirals and Vaccines for Enterovirus A71.

88. Amako, Y.; Sarkeshik, A.; Hotta, H.; Yates, J.; Siddiqui, A. Role of Oxysterol Binding Protein in Hepatitis C Virus Infection. *J. Virol.* **2009**, *83* (18), 9237–9246.

89. Pietrangelo, A.; Ridgway, N. D. Bridging the Molecular and Biological Functions of the Oxysterol-Binding Protein Family. *Cell. Mol. Life Sci.* **2018**, *75* (17), 3079–

3098.

90. Bugert, J. J.; Hucke, · F; Zanetta, · P; Bassetto, · M; Brancale, · A. Antivirals in Medical Biodefense. *Virus Genes* **2020**, 1–18.

91. Litterman, N.; Lipinski, C.; Ekins, S.; Lipinski, C. A. Small Molecules with Antiviral Activity against the Ebola Virus. **2015**.

92. Bauer, L.; Albulescu, L.; van Kuppeveld, F. J. M.; Strating, J. R. P. M. et al. Structure-Activity Relationship Study of Itraconazole, a Broad-Range Inhibitor of Picornavirus Replication That Targets Oxysterol-Binding Protein (OSBP). *Antiviral Res.* **2018**, *156*, 55–63.

93. Mesmin, B.; Bigay, J.; Polidori, J.; Jamecna, D.; Lacas-Gervais, S.; Antonny, B. Sterol Transfer, PI 4P Consumption, and Control of Membrane Lipid Order by Endogenous OSBP . *EMBO J.* **2017**, *36* (21), 3156–3174.

94. Altan-Bonnet, N. Lipid Tales on Viral Replication and Transmission. *Trends Cell Biol.* **2017**, *27* (3), 201–213.

95. Burgett, A. W. G.; Kothapalli, N. R.; Wu, S.; Severance, Z. C.; Bensen, R. C.; Le, A. T.; Roberts, B. L.; Nuñez, J. I.; Ma, H.; Standke, S. J.; Yang, Z.; Reddig, W. J.; Blewett, E. L. Transient Compound Treatment Induces a Multigenerational Reduction of Oxysterol-Binding Protein (OSBP) Levels and Prophylactic Antiviral Activity. *ACS Chem. Biol.* **2019**.

96. Cragg, G. M.; Newman, D. J. Antineoplastic Agents from Natural Sources: Achievements and Future Directions. *Expert Opin. Investig. Drugs* **2000**, *9* (12), 2783–2797.

97. Suggitt, M.; Bibby, M. C. 50 Years of Preclinical Anticancer Drug Screening:

Empirical to Target-Driven Approaches. *Clin. Cancer Res.* **2005**, *11* (3), 971–981.

98. Gottesman, M. M. Mechanisms of Cancer Drug Resistance. *Annu. Rev. Med.* **2002**, *53* (1), 615–627.

99. Mimaki, Y.; Kuroda, M.; Kameyama, A.; Sashida, Y.; Hirano, T.; Oka, K.; Koike, K.; Nikaido, T. A New Cytotoxic Cholestane Bisdesmoside from Ornithogalum Saundersiae Bulbs. *Biosci. Biotechnol. Biochem.* **1996**, *60* (6), 1049–1050.

100. Mimaki, Y.; Kuroda, M.; Sashida, Y.; Kameyama, A.; Hirano, T.; Oka, K.; Dobashi, A. A New Rearranged Cholestane Glycoside. *Bioorganic Med. Chem. Lett.* **1996**, *6* (22), 2635–2638.

101. Kuroda, M.; Mimaki, Y.; Sashida, Y.; Hirano, T.; Oka, K.; Dobashi, A.; Li, H. Y.; Harada, N. Novel Cholestane Glycosides from the Bulbs of Ornithogalum Saundersiae and Their Cytostatic Activity on Leukemia HL-60 and MOLT-4 Cells. *Tetrahedron* **1997**, *53* (34), 11549–11562.

102. Iguchi, T.; Kuroda, M.; Naito, R.; Watanabe, T.; Matsuo, Y.; Yokosuka, A.; Mimaki, Y. Cholestane Glycosides from Ornithogalum Saundersiae Bulbs and the Induction of Apoptosis in HL-60 Cells by OSW-1 through a Mitochondrial-Independent Signaling Pathway. *J. Nat. Med.* **2019**, *73* (1), 131–145.

103. Chen, Q. W.; Zhang, X.; Gong, T.; Gao, W.; Yuan, S.; Zhang, P. C.; Kong, J. Q. Structure and Bioactivity of Cholestane Glycosides from the Bulbs of Ornithogalum Saundersiae Baker. *Phytochemistry* **2019**, *164* (March), 206–214.

104. Deng, S.; Yu, B.; Lou, Y.; Hui, Y. First Total Synthesis of an Exceptionally Potent Antitumor Saponin, OSW-1. *J. Org. Chem.* **1999**, *64*, 202–208.

105. Morzycki, J. W.; Wojtkielewicz, A. Synthesis of a Cholestane Glycoside OSW-1

with Potent Cytostatic Activity. *Carbohydr. Res.* **2002**, *337* (14), 1269–1274.

106. Xue, J.; Liu, P.; Pan, Y.; Guo, Z. A Total Synthesis of OSW-1. *J. Org. Chem.* **2008**, *73* (1), 157–161.

107. Yu, W.; Jin, Z. A New Strategy for the Stereoselective Introduction of Steroid Side Chain via α-Alkoxy Vinyl Cuprates: Total Synthesis of a Highly Potent Antitumor Natural Product OSW-1 [2]. *J. Am. Chem. Soc.* **2001**, *123* (14), 3369–3370.

108. Wojtkielewicz, A.; Długosz, M.; Maj, J.; Morzycki, J. W.; Nowakowski, M.; Renkiewicz, J.; Strnad, M.; Swaczynová, J.; Wilczewska, A. Z.; Wójcik, J. New Analogues of the Potent Cytotoxic Saponin OSW-1. *J. Med. Chem.* **2007**, *50* (15), 3667–3673.

109. Zheng, D.; Zhou, L.; Guan, Y.; Chen, X.; Zhou, W.; Chen, X.; Lei, P. Synthesis of Cholestane Glycosides Bearing OSW-1 Disaccharide or Its 1→4-Linked Analogue and Their Antitumor Activities. *Bioorganic Med. Chem. Lett.* **2010**, *20* (18), 5439–5442.

110. Guan, Y.; Zheng, D.; Zhou, L.; Wang, H.; Yan, Z.; Wang, N.; Chang, H.; She, P.; Lei, P. Synthesis of 5(6)-Dihydro-OSW-1 Analogs Bearing Three Kinds of Disaccharides Linking at 15-Hydroxy and Their Antitumor Activities. *Bioorganic Med. Chem. Lett.* **2011**, *21* (10), 2921–2924.

111. Maj, J.; Morzycki, J. W.; Rárová, L.; Oklešťková, J.; Strnad, M.; Wojtkielewicz, A. Synthesis and Biological Activity of 22-Deoxo-23-Oxa Analogues of Saponin OSW-1. *J. Med. Chem.* **2011**, *54* (9), 3298–3305.

112. Sakurai, K.; Takeshita, T.; Hiraizumi, M.; Yamada, R. Synthesis of OSW-1 Derivatives by Site-Selective Acylation and Their Biological Evaluation. *Org.*

Lett. **2014**, *16* (24), 6318–6321.

113. Liu, C.; Wang, A. peng; Jin, L.; Guo, Y.; Li, Y.; Zhao, Z.; Lei, P. Synthesis, Conformational Analysis and SAR Research of OSW-1 Analogues. *Tetrahedron* **2016**, *72* (27–28), 4091–4102.

114. Sakurai, K.; Hiraizumi, M.; Isogai, N.; Komatsu, R.; Shibata, T.; Ohta, Y. Synthesis of a Fluorescent Photoaffinity Probe of OSW-1 by Site-Selective Acylation of an Inactive Congener and Biological Evaluation. *Chem. Commun.* **2017**, *53* (3), 517–520.

115. Komatsu, R.; Sakurai, K. Development of Chemical Probes for Functional Analysis of Anticancer Saponin OSW-1. *Chem. Rec.* **2019**, *19* (12), 2362–2369.

116. Xu, Q. H.; Peng, X. W.; Tian, W. S. A New Strategy for Synthesizing the Steroids with Side Chains from Steroidal Sapogenins: Synthesis of the Aglycone of OSW-1 by Using the Intact Skeleton of Diosgenin. *Tetrahedron Lett.* **2003**, *44* (52), 9375–9377.

117. Deng, L.-H.; Wu, H.; Yu, B.; Jiang, M.-R.; Wu, J.-R. Synthesis of 5,6-Dihydro-OSW-1 and Its Antitumor Activities. *Chinese J. Chem.* **2004**, *22* (9), 994–998.

118. Deng, L.; Wu, H.; Yu, B.; Jiang, M.; Wu, J. Synthesis of OSW-1 Analogs with Modified Side Chains and Their Antitumor Activities. *Bioorganic Med. Chem. Lett.* **2004**, *14* (11), 2781–2785.

119. Morzycki, J. W.; Wojtkielewicz, A.; Wołczyński, S. Synthesis of Analogues of a Potent Antitumor Saponin OSW-1. *Bioorganic Med. Chem. Lett.* **2004**, *14* (12), 3323–3326.

120. Matsuya, Y.; Masuda, S.; Ohsawa, N.; Adam, S.; Tschamber, T.; Eustache, J.;

Kamoshita, K.; Sukenaga, Y.; Nemoto, H. Synthesis and Antitumor Activity of the Estrane Analogue of OSW-1. *European J. Org. Chem.* **2005**, No. 5, 803–808.

121. Shi, B.; Tang, P.; Hu, X.; Liu, J. O.; Yu, B. OSW Saponins: Facile Synthesis toward a New Type of Structures with Potent Antitumor Activities. *J. Org. Chem.* **2005**, *70* (25), 10354–10367.

122. Qin, H. J.; Tian, W. S.; Lin, C. W. A Highly Efficient Synthesis of 22-Deoxy-OSW-1 by Utilizing the Intact Skeleton of Diosgenin. *Tetrahedron Lett.* **2006**, *47* (19), 3217–3219.

123. Tang, P.; Mamdani, F.; Hu, X.; Liu, J. O.; Yu, B. Synthesis of OSW Saponin Analogs with Modified Sugar Residues and Their Antiproliferative Activities. *Bioorganic Med. Chem. Lett.* **2007**, *17* (4), 1003–1007.

124. Fukaya, K.; Urabe, D.; Hiraizumi, M.; Noguchi, K.; Matsumoto, T.; Sakurai, K. Computational and Experimental Analysis on the Conformational Preferences of Anticancer Saponin OSW-1. *J. Org. Chem.* **2020**, *85* (2), 339–344.

125. Guo, C.; Fuchs, P. L. The First Synthesis of the Aglycone of the Potent Anti-Tumor Steroidal Saponin OSW-1. *Tetrahedron Lett.* **1998**, *39* (10), 1099–1102.

126. Appendino, G.; Banfi, L. Molecular Diversity and Natural Products. *Mol Divers* **2011**, *15*, 291–292.

127. Harvey, A. L. Natural Products in Drug Discovery. *Drug Discov. Today* **2008**, *13* (19–20), 894–901.

128. Sasidharan, S.; Chen, Y.; Saravanan, D.; Sundram, K. M.; Latha, L. Y.; Bedong-semeling, J.; Nasi, B. A. Extraction, Isolation and Characterization of Bioactive Compounds from Plants Extracts. *Afr J Tradit Complement Altern Med* **2011**, *8*

(1), 1–10.

129. Amit Koparde, A.; Chandrashekar Doijad, R.; Shripal Magdum, C. Natural Products in Drug Discovery. *Intech* **2019**.

130. Nawaz, H.; Shad, M. A.; Rehman, N.; Andaleeb, H.; Ullah, N. Effect of Solvent Polarity on Extraction Yield and Antioxidant Properties of Phytochemicals from Bean (Phaseolus Vulgaris) Seeds. *Brazilian J. Pharm. Sci.* **2020**, *56*.

131. Rasul, M. Extraction, Isolation and Characterization of Natural Products from Medicinal Plants. *Int. J. Basic Sci. Appl. Comput.* **2018**, *2* (6), 1–6.

132. Resolution and Peak Separation https://www.shimadzu.com/an/hplc/support/lib/lctalk/resol-1.html.

133. Kasai, Hiroko, F.; Tsubuki, M.; Matsuo, S.; Honda, T. Analysis of Antitumor Active OSW-1 and Its Analogues by Liquid Chromatography Coupled with Electrospray and Atmospheric Pressure Chemical Ionization Quadrupole Mass Spectrometry. *Rapid Commun. Mass Spectrom.* **2007**, *21*, 1100–1114.

134. Kasai, H.; Tsubuki, M.; Shimada, K.; Nambara, T.; Honda, T. Analyses of Biologically Active Steroids: Antitumor Active OSW-1 and Cardiotonic Marinobufotoxin, by Matrix-Assisted Laser Desorption/Ionization Quadrupole Ion Trap Time-of-Flight Tandem Mass Spectrometry. *Chem. Pharm. Bull.* **2009**, *57* (9), 948–956.

135. Bouslimani, A.; Sanchez, L. M.; Garg, N.; Dorrestein, P. C. Mass Spectrometry of Natural Products: Current, Emerging and Future Technologies. *Nat. Prod. Rep.* **2014**, *31* (6), 718–729.

136. Merck. LC-MS Contaminants. How to Identify and Avoid Contaminants in LC-

MS.

137. Still, W. C.; Kahn, M.; Mitra, A. Rapid Chromatographic Technique for Preparative Separations with Moderate Resolution. *J. Org. Chem.* **1978**, *43* (14), 2923–2925.

138. Quinn, R. A.; Nothias, L. F.; Vining, O.; Meehan, M.; Esquenazi, E.; Dorrestein, P. C. Molecular Networking As a Drug Discovery, Drug Metabolism, and Precision Medicine Strategy. *Trends Pharmacol. Sci.* **2017**, *38* (2), 143–154.

139. Nothias, L. F.; Nothias-Esposito, M.; Da Silva, R.; Touboul, D.; Costa, J.; Paolini, J.; Alexandrov, T.; Litaudon, M.; Dorrestein, P. C. et al. Bioactivity-Based Molecular Networking for the Discovery of Drug Leads in Natural Product Bioassay-Guided Fractionation. *J. Nat. Prod.* **2018**, *81* (4), 758–767.

Appendix

Appendix A. Isolated OSW-1 analogs with Structure A

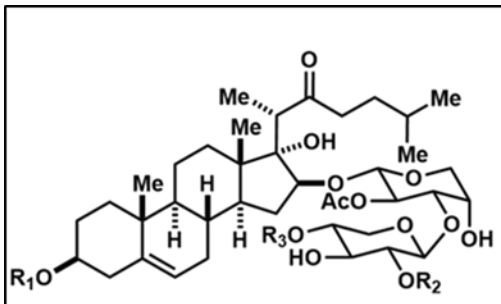

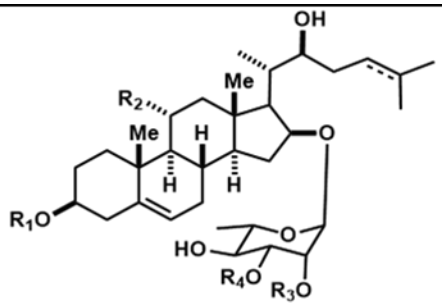

	R_1	R_2	R_3
1	H	H	H
2 (OSW-1)	H	PMBz	H
3	H	DMBz	H
4	H	CNM	H
5	glc	PMBz	H
6	glc	CNM	H
7	H	DMBz	glc
8	H	TMBz	glc
9	H	PHBz	H
10	H	TMBz	H
11	glc	PHBz	H

		R_1	R_2	R_3	R_4
12	Δ^{24}	H	OH	H	H
13	Δ^{24}	H	OH	H	Ac
14	Δ^{24}	H	OH	Ac	Ac
15		H	OH	H	H
16		H	OH	H	Ac
17		H	OH	Ac	H
18		H	OH	Ac	Ac
19		H	OH	Ac	TMBz
20		H	OH	Ac	PMBz
21		glc	OH	Ac	H
22		glc	OH	Ac	Ac
23		glc	OH	Ac	PMBz
24		glc	OH	Ac	TMBz
25	Δ^{24}	H	OH	Ac	H
26	Δ^{24}	glc	OH	Ac	Ac
27	Δ^{24}	glc	OH	Ac	PMBz
28	Δ^{24}	glc	OH	Ac	TMBz
29	Δ^{24}	$glc^2 \rightarrow {}^1rha$	OH	Ac	Ac
30		glc	H	Ac	Ac
31	Δ^{24}	H	H	Ac	H
32	Δ^{24}	glc	H	Ac	Ac

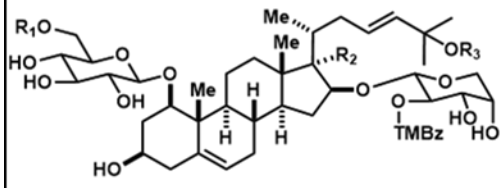

	R_1	R_2	R_3
33	H	OH	H
34	glc	H	H
35	H	H	H
36	H	H	Me

PHBz: p-hydroxybenzoyl
PMBz: p-methoxybenzoyl
DMBz: 3,4-dimethexobenzoyl
TMBz: 3,4,5-trimethoxybenzoyl
CNM: (E)-cinnamoyl
Ac: Acetyl
glc: β–D-glucopyranosyl
rha: α-L-rhamnopyranosyl

Appendix B. Cytotoxic activities of compounds with Structure A (NT: not tested)

Compounds	IC_{50} values (nM)	
	HL-60	A549
1	3.4 ± 0.076	98 ± 8.0
2 (OSW-1)	0.061 ±0.002	0.65 ± 0.018
3	0.19 ±0.0026	1.7 ± 005
4	0.077 ±0.0070	0.68 ±0.057
5	0.24	NT
6	0.12	NT
7	16	NT
8	14	NT
9	0.20 ± 0.0074	3.6 ± 0.37
10	0.55 ± 0.013	6.2 ± 0.10
11	NT	NT
12	inactive	NT
13	109	NT
14	2670 ± 310	NT
15	inactive	NT
16	0.99	NT
17	inactive	NT
18	7120 ± 270	NT
19	50 ± 10	270 ± 40
20	60 ± 2	370 ± 90
21	inactive	NT
22	inactive	NT
23	1570 ± 100	NT
24	inactive	NT
25	inactive	NT
26	inactive	NT
27	7720 ± 420	NT
28	5330 ± 330	NT
29	5940 ± 100	NT
30	90 ± 10	2410 ± 170
31	160 ± 20	1840 ± 310
32	80 ± 10	980 ± 90
33	20 (LC_{50} value, nM)	NT
34	inactive	inactive
35	inactive	inactive
36	inactive	inactive

Appendix C. Isolated OSW-1 analogs with Structure B

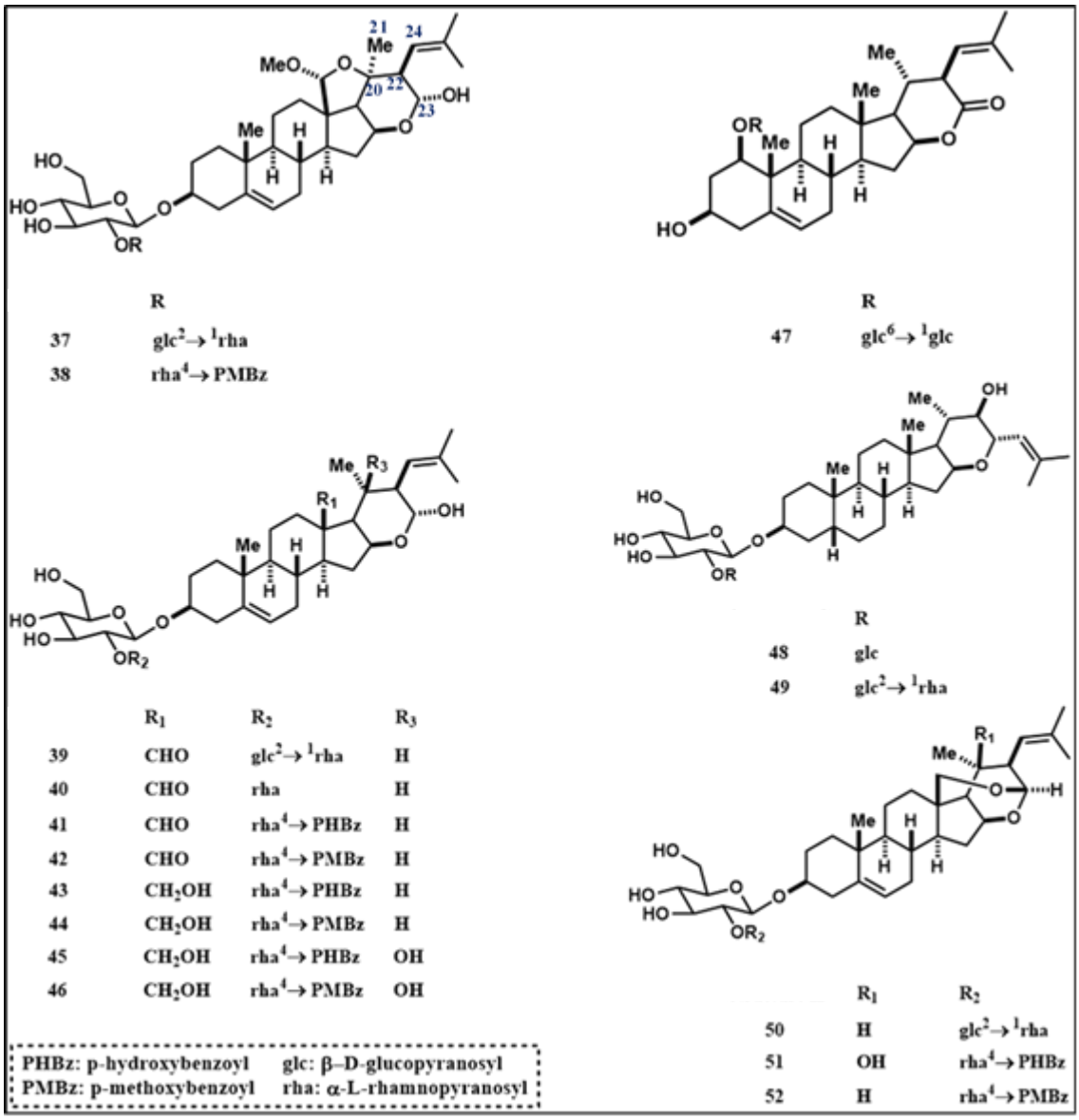

	R
37	glc[2]→ [1]rha
38	rha[4]→ PMBz

	R
47	glc[6]→ [1]glc

	R
48	glc
49	glc[2]→ [1]rha

	R_1	R_2	R_3
39	CHO	glc[2]→ [1]rha	H
40	CHO	rha	H
41	CHO	rha[4]→ PHBz	H
42	CHO	rha[4]→ PMBz	H
43	CH_2OH	rha[4]→ PHBz	H
44	CH_2OH	rha[4]→ PMBz	H
45	CH_2OH	rha[4]→ PHBz	OH
46	CH_2OH	rha[4]→ PMBz	OH

	R_1	R_2
50	H	glc[2]→ [1]rha
51	OH	rha[4]→ PHBz
52	H	rha[4]→ PMBz

PHBz: p-hydroxybenzoyl glc: β–D-glucopyranosyl
PMBz: p-methoxybenzoyl rha: α-L-rhamnopyranosyl

Appendix D. Cytotoxic activities of compounds with Structure B (NT: not tested)

Compounds	IC_{50} values (nM)		
	HL-60	MOLT-4	A549
37	1,800	1,300	NT
38	9.2	3.2	NT
39	inactive	inactive	NT
40	inactive	inactive	NT
41	21	18	1,010 ± 17
42	19	NT	NT
43	63	NT	4930 ± 60
44	52	NT	NT
45	37 ± 4.4	NT	1,030 ± 69
46	90 ± 14	NT	500 ± 53
47	inactive	inactive	NT
48	790 ± 17	NT	5,790 ± 280
49	inactive	NT	inactive
50	58 ± 2.0	NT	900 ± 11
51	67 ± 0.23	NT	850 ± 15
52	170 ± 5.1	NT	5,500 ± 170

Appendix E. Cytotoxic activities of 15 new isolated OSW-1 analogs by Chen *et al.*

New Compounds	IC_{50} values (nM)				
	A549	BGC-823	HCT-116	HepG2	MCF7
53	inactive	inactive	inactive	inactive	inactive
54	inactive	inactive	inactive	inactive	inactive
55	inactive	inactive	inactive	inactive	inactive
56	inactive	inactive	inactive	inactive	inactive
57	inactive	inactive	inactive	inactive	200
58	inactive	inactive	inactive	inactive	inactive
59	inactive	inactive	inactive	inactive	inactive
60	inactive	inactive	inactive	inactive	inactive
61	inactive	inactive	inactive	inactive	inactive
62	inactive	inactive	inactive	inactive	inactive
63	inactive	inactive	inactive	inactive	inactive
64	inactive	inactive	inactive	inactive	inactive
65	inactive	inactive	inactive	inactive	inactive
66	inactive	inactive	inactive	inactive	inactive
67	inactive	inactive	inactive	inactive	inactive

Appendix F. Modified steroidal nucleus analogs 68 and 69 and their cytotoxic activities (NT: Not Tested)

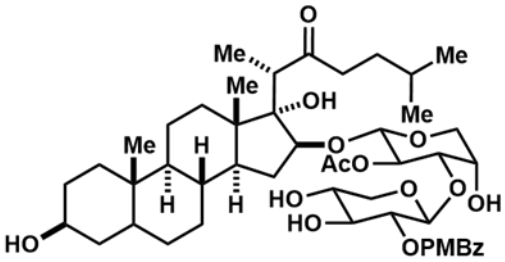

68

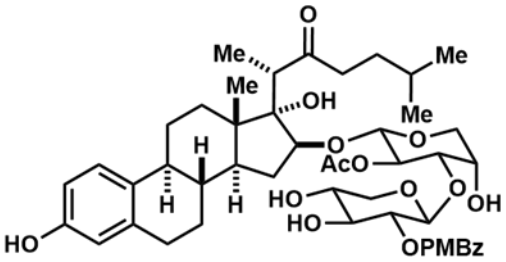

69

Compounds	IC_{50} values (nM)								
	AGS	7404	MCF7	NCI-H460	T470	MDA-MB-231	A498	PC-3	DLD1
68	710	25	29	NT	NT	NT	NT	NT	NT
69	NT	NT	NT	439	709	1010	430	1400	1180

Appendix G. Modified side chain analogs 70-101 and their cytotoxic activities (NT: Not Tested)

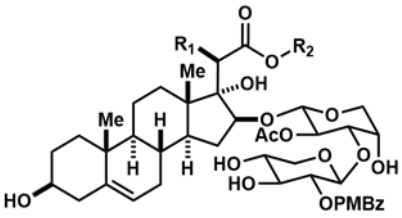

	R_1	R_2
70	Me	CH_2CH_3
71	H	$(CH_2)_{11}CH_3$

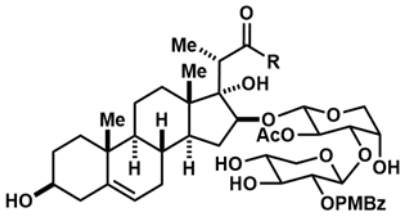

	R
82	H
83	i-C_3H_7
84	n-C_4H_9
85	i-C_4H_9
86	CH_3
87	$CH_2CH_2CH_3$
88	C_5H_{11}

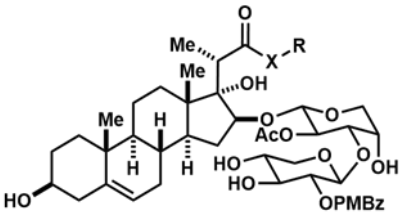

	X	R
72	O	$CH_2CH(CH_3)_2$
73	O	CH_2CH_3
74	O	$(CH_2)_{11}CH_3$
75	O	$(CH_2)_6CH_3$
76	O	$(CH_2)_{17}CH_3$
77	O	$CH_2CH=CH_2$
78	O	$CH_2CH=CH(CH_2)_8OBz$
79	S	i-C_3H_7
80	NH	i-C_3H_7
81	NCH_3	OCH_3

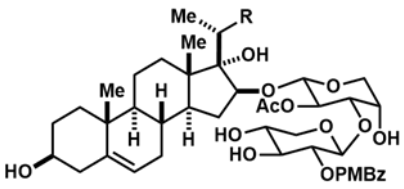

	R
89	CH_3
90	$O(CH_2)_4CH_3$
91	$(CH_2)_3CH(CH_3)_2$

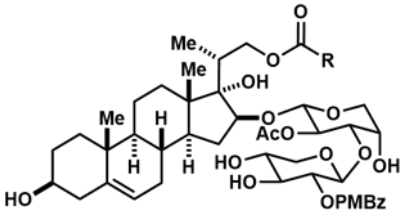

	R
92	C_4H_9
93	C_6H_{13}
94	C_8H_{17}
95	$C_{11}H_{23}$
96	$C_{13}H_{27}$
97	$C_{17}H_{35}$
98	$CH=CHCH_3$
99	$C_4H_8CH=CH_2$
100	C_6H_5
101	p-$C_6H_4OCH_3$

Compounds	IC_{50} values (nM) or *TCS_{50} (10^{-3} µM)					
	Hela	Jurkat T	MCF7	MDA-MB-231	Ishikawa	AGS
70	3.4	4.2	130	NT	NT	NT
71	inactive	73	1400	NT	NT	NT
72	230	0.68	900	NT	NT	NT
73	240	5.3	inactive	NT	NT	NT
74	3.3	7.3	140	NT	NT	NT
75	2	1.4	2600	NT	NT	NT
76	inactive	inactive	inactive	NT	NT	NT
77	65	2.7	100	NT	NT	NT
78	40	3	190	NT	NT	NT
79	1.3	0.9	5200	NT	NT	NT
80	8.4	5.3	1800	NT	NT	NT
81	12	35	inactive	NT	NT	NT
82	NT	NT	inactive	inactive	inactive	NT
83	NT	NT	inactive	inactive	inactive	NT
84	NT	NT	inactive	inactive	inactive	NT
85	NT	NT	inactive	inactive	inactive	NT
86	NT	NT	6610	NT	NT	6980
87	*12	NT	20	NT	NT	1920
88	*8	NT	*40	NT	NT	NT
89	inactive	NT	inactive	NT	NT	NT
90	*350	NT	*860	NT	NT	NT
91	NT	NT	60	NT	NT	1380
92	inactive	NT	inactive	NT	NT	NT
93	inactive	NT	inactive	NT	NT	NT
94	inactive	NT	inactive	NT	NT	NT
95	inactive	NT	inactive	NT	NT	NT
96	inactive	NT	inactive	NT	NT	NT
97	inactive	NT	inactive	NT	NT	NT
98	inactive	NT	inactive	NT	NT	NT
99	inactive	NT	inactive	NT	NT	NT
100	inactive	NT	inactive	NT	NT	NT
101	inactive	NT	inactive	NT	NT	NT

Compounds	IC_{50} values (nM) or *TCS_{50} (10^{-3} µM)							
	7404	CEM	G361	HOS	A549	T98	HCT116	BJ
70	NT	NT	NT	NT	NT	NT	NT	NT
71	NT	NT	NT	NT	NT	NT	NT	NT
72	NT	NT	NT	NT	NT	NT	NT	NT
73	NT	NT	NT	NT	NT	NT	NT	NT
74	NT	NT	NT	NT	NT	NT	NT	NT
75	NT	NT	NT	NT	NT	NT	NT	NT
76	NT	NT	NT	NT	NT	NT	NT	NT
77	NT	NT	NT	NT	NT	NT	NT	NT
78	NT	NT	NT	NT	NT	NT	NT	NT
79	NT	NT	NT	NT	NT	NT	NT	NT
80	NT	NT	NT	NT	NT	NT	NT	NT
81	NT	NT	NT	NT	NT	NT	NT	NT
82	NT	NT	NT	NT	NT	NT	NT	NT
83	NT	NT	NT	NT	NT	NT	NT	NT
84	NT	NT	NT	NT	NT	NT	NT	NT
85	NT	NT	NT	NT	NT	NT	NT	NT
86	2900	NT	NT	NT	NT	NT	NT	NT
87	32	*0.5	*3100	*140	*0.9	NT	NT	NT
88	NT	*0.2	*1400	*42	*0.5	NT	NT	NT
89	NT	*1300	inactive	NT	NT	NT	NT	NT
90	NT	*<200	*1900	1800	*<200	NT	NT	NT
91	63	NT	NT	NT	NT	NT	NT	NT
92	NT	inactive	inactive	inactive	inactive	inactive	inactive	inactive
93	NT	inactive	inactive	inactive	inactive	inactive	inactive	inactive
94	NT	7200	inactive	inactive	inactive	inactive	inactive	7000
95	NT	6300	8000	inactive	inactive	7000	inactive	5000
96	NT	inactive	inactive	inactive	inactive	inactive	inactive	inactive
97	NT	inactive	inactive	inactive	inactive	inactive	inactive	inactive
98	NT	inactive	inactive	inactive	inactive	inactive	inactive	inactive
99	NT	inactive	inactive	inactive	inactive	inactive	inactive	inactive
100	NT	inactive	inactive	inactive	inactive	inactive	inactive	inactive
101	NT	inactive	inactive	inactive	inactive	inactive	inactive	inactive

Appendix H. Modified disaccharide analogs 102-105 and their cytotoxic activities (NT: Not Tested)

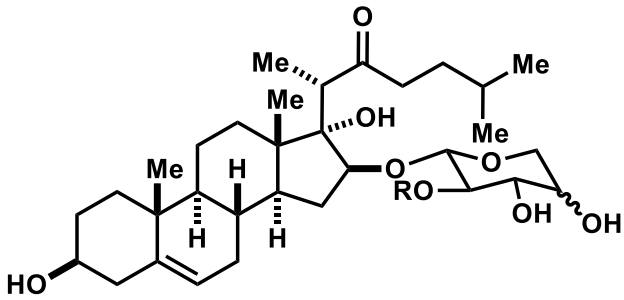

		R
102	4R-L-arabinopyranosyl	Ac
103	4S-L-arabinopyranosyl	Ac
104	4R-D-xylopyranosyl	PMBz
105	4S-D-xylopyranosyl	PMBz

Compounds	TCS_{50} values (10^{-3} μM)							
	CEM	MCF7	K562	ARN8	G361	Hela	HOS	A549
102	NT	NT	NT	NT	NT	NT	NT	NT
103	200	1300	430	inactive	2200	570	inactive	inactive
104	NT	NT	NT	NT	NT	NT	NT	NT
105	inactive	inactive	inactive	inactive	3500	inactive	inactive	inactive

Appendix I. OSW-1 analogs with modified side chains and disaccharide moieties

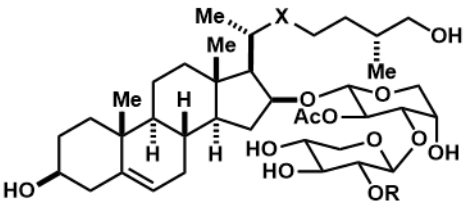

	X	R
106	CHOH (S)	PMBz
107	C=O	PMBz
108	CHOH (S)	CNM
109	C=O	CNM
110	CH_2	CNM

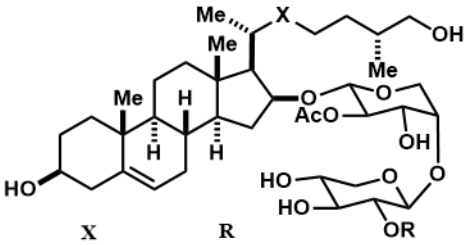

	X	R
111	CHOH (S)	PMBz
112	C=O	PMBz
113	CHOH (S)	CNM
114	C=O	CNM
115	CH_2	CNM

Appendix J. OSW-1 sulfur-containing analogs identified by HPLC-MS

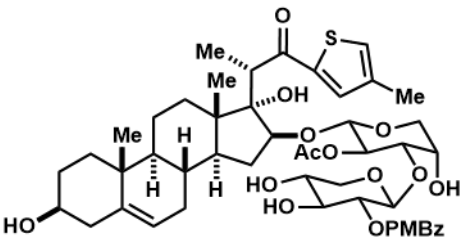

116 ThOSW-1

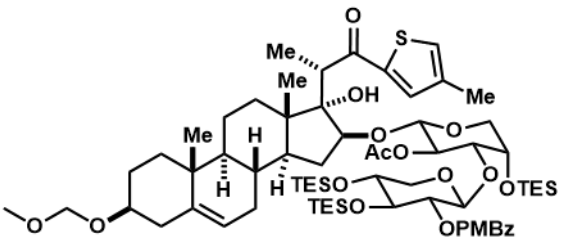

117 SiThOSW-1

Appendix K. Selected Analytical method comparison. Stepped gradient 75/25 to 85/15 to 100/0 MeOH/H_2O (left) and stepped gradient 70/30 to 85/15 to 100/0 MeCN/H_2O

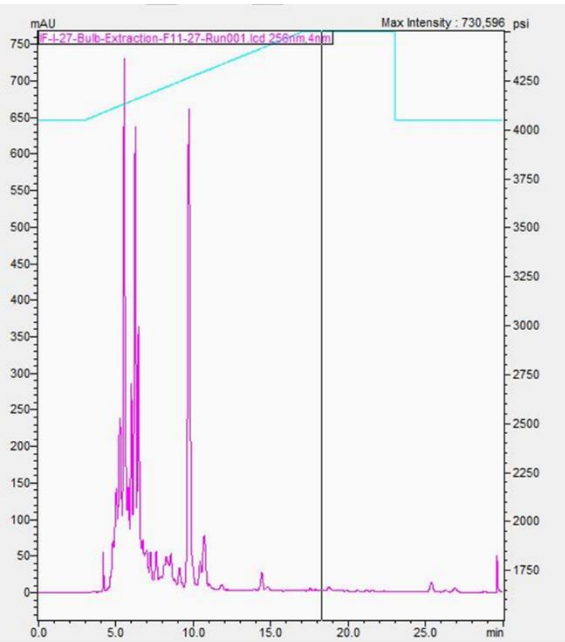

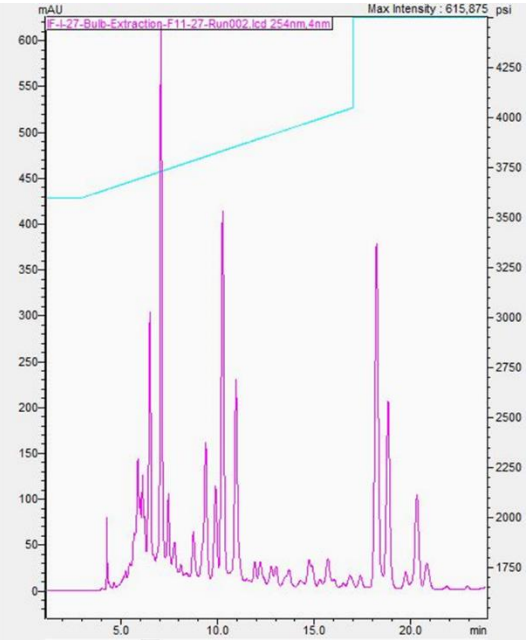

Appendix L. Compounds LC-MS data IF-I-27 Fractions F1-4, F5-10 and F11-27

Column Fraction	FRC	λ Max (nm)	RT (min) at 254 nm	MS Peaks/Fragments	Mass (mg)	Characterization/Remarks (Y/N/Solvent Pb /2D needed)
F1-4	1	218	8.873	**ESI+** : 238.10 ; 391.15 ; 413.20 ; 439.00 ; 453.95 ; 672.95 / **ESI-** : 455.90 ; 561.20	~ 1	Solvent Pb
	2	200	9.490	**ESI+** : 227.00 ; 268.05 / **ESI-** : 384.70 ; 520.70	~ 1	Solvent Pb
	3	252	10.458	**ESI+** : 208.00 ; 239.30 ; 410.75	~ 1	Solvent Pb
	4	274	11.949	**ESI+** : 204.05 ; 482.65 ; 756.25 ; 848.05	~ 1	Solvent Pb
F5-10	1	236	6.44	**ESI+** : 209.00 ; 303.05 ; 581.35 / **ESI-** : 448.00	< 1	N
	2	254	7.105	**ESI+** : 214.65 ; 370.75 ; 676.90 ; 754.70 ; 784.15 ; 825.25	< 1	N
	3	309	7.488	**ESI+**: Uninterpretable	< 1	N
	4	305	7.742	**ESI+**: Uninterpretable	< 1	Solvent Pb
	5	218	8.894	**ESI+** : 237.85 ; 345.05 ; 359.10 ; 391.15 ; 413.15 ; 454.15	< 1	Solvent Pb
	6	265	9.513	**ESI+** : 227.00 ; 267.95 ; 279.00 ; 342.05 ; 450.30	< 1	N
	7	254	10.482	**ESI+** : 208.00 ; 455.55 ; 515.15 ; 790.35 ; 899.60	< 1	N
	8	274	11.977	**ESI+** : 507.85 / **ESI-** : 365.30 ; 612.65	< 1	N
	9	258	13.763	**ESI+** : 241.10 ; 387.05 ; 507.10 ; 547.20 ; 1066.30 ; 1071.10	< 1	N
	10	228	14.778	**ESI+** : 241.00 ; 386.95 ; 507.20 ; 547.35 ; 1066.10 ; 1071.20	< 1	N
F11-27	1	283	6.460	**ESI+**: Uninterpretable	< 1	Solvent Pb
	2	254	7.125	**ESI+** : 301.20 ; 371.15 ; 465.95 ; 544.55 / **ESI-** : 323.50 ; 521.00 ; 663.05	< 1	Solvent Pb
	3	309	7.515	**ESI+** : 231.05 ; 283.20 ; 511.55 ; 974.40	< 1	Not pure (2 products)
	4	216	8.858	**ESI+** : 359.10 ; 391.10 ; 413.10 ; 453.90 ; 791.30 ; 807.20	~ 1	Not pure (2 products)
	5	266	9.513	**ESI+** : 341.40 ; 383.00 ; 400.95 ; 837.30 / **ESI-** : 859.15	~ 1	More product/2D Needed
	6	266	10.049	**ESI+** : 271.15 ; 382.95 ; 400.85 ; 627.25 ; 839.25 / **ESI-** : 520.70 ; 621.20 ; 649.15 ; 861.00	~ 1	More product/2D Needed
	7	257	10.404	**ESI+** : 323.00 ; 515.20 ; 777.30	~ 1	More product/2D Needed
	8	256	11.112	**ESI+** : 323.00 ; 426.25 ; 779.40 / **ESI-** : 280.40 ; 586.80 ; 791.10	~ 2	More product needed
	9	262	15.947	**ESI+** : 278.85 ; 296.85 ; 383.25 ; 415.25 ; 925.20 / **ESI-** : 947.05	~ 1	More product/2D Needed
	10	257	18.481	**ESI+** : 248.85 ; 266.95 ; 415.25 ; 441.15 ; 895.25 / **ESI-** : 917.15	~ 2	**Y : OSW-1 (IF-141)**
	11	257	19.065	**ESI+** :266.80 ; 415.20 ; 571.20 ; 895.20 / **ESI-** : 917.20	~ 2	Not pure (2 products)
	12	276	20.638	**ESI+** : 262.90 ; 415.30 ; 774.80 ; 891.35 / **ESI-** : 301.55 ; 447.00 ; 913.15	< 1	**Y (3) More product/2D Needed**

Appendix M. Compound LC-MS data IF-I-27 Fractions F28-37, F38-60 and F61-69

Column Fraction	FRC	λ Max (nm)	RT (min) at 254 nm	MS Peaks/Fragments	Mass (mg)	Characterization/Remarks (Y/N/Solvent Pb/2D/Purity)
F28-37	1	253	6.921	ESI+ : 226.95 ; 341.00 ; 699.30 / ESI- : 681.35	~ 3	Not pure (2 products)
	2	264	9.211	ESI+ : 279.00 ; 383.10 ; 443.25 ; 809.30 ; 837.25 / ESI- : 609.20 ; 677.10	~ 3	Not pure (2 products)
	3	267	9.953	ESI+ : 383.00 ; 401.00 ; 839.25 ; 880.25 / ESI- : 621.20 ; 861.10	~ 2	Not pure (2 products)
	4	256	10.978	ESI+ : 265.60 ; 340.95 ; 779.30 / ESI- : 520.65	~ 4	More product/2D needed
	5	246	14.442	ESI+ : 277.20 ; 415.20 ; 488.90 ; 853.30 ; 881.50 / ESI- : 313.45 ; 857.05 ; 875.20	~ 1	Not pure
	6	257	15.345	ESI+ : 266.95 ; 413.20 ; 441.00 ; 586.30 ; 893.20 / ESI- : 869.00 ; 915.10	~ 1	Y (4) More product/2D needed
	7	262	15.756	ESI+ : 278.90 ; 296.95 ; 415.20 ; 542.25 ; 925.30 / ESI- : 947.10	< 1	Y (2) More product/2D needed
	8	257	18.279	ESI+ : 248.95 ; 267.00 ; 415.25 ; 441.00 ; 895.25 / ESI- : 917.10 ; 985.10	~ 4	Y : OSW-1 (IF-113)
	9	257	19.591	ESI+ : 266.95 ; 484.25 ; 576.40 ; 581.35 ; 874.35 ; 879.30 ; 895.40	~ 1	N (More product needed)
	10	278	20.434	ESI+ : 262.90 ; 415.15 ; 891.25 / ESI- : 913.15	< 1	Y (3) Not pure (2 products)
F38-60	1	257	4.655	ESI+ : 450.70 ; 580.05 ; 663.45 / ESI- : 414.85 ; 522.10	< 0.5	N
	2	265	5.057	ESI+ : 245.00 ; 298.00 ; 308.00 ; 339.00 ; 476.05 ; 832.55 / ESI- : 286.90 ; 354.90 ; 639.05	< 0.5	N
	3	257	6.690	ESI+ : 271.05 ; 280.95 ; 344.20 ; 379.00 ; 397.15 ; 415.25 ; 459.70 ; 585.25 ; 603.30 ; 851.25 ; 873.15 ; 935.20 / ESI- : 665.20 ; 733.05 ;931.05	~ 5	N (multiple products)
	4	258	7.503	ESI+ : Uninterpretable / ESI- : 819.25 ; 917.15	~ 1	N (OSW-1/analog with ESI- ?)
	5	257	8.359	ESI+ : 267.30 ; 325.20 ; 415.20 ; 577.35 ; 1017.30 ; 1057.30 / ESI- : 607.15 ; 657.10 ;	~ 1	Not pure (2 products & M=1034?)
	6	257	8.742	ESI+ : 281.00 ; 415.30 ; 492.40 ; 557;70 ; 719.30 / ESI- : 281.60 ; 695.00 ; 741.20 ; 809.10 ; 915.20 ; 1039.60	~ 1	More product/2D needed
	7	257	11.859	ESI+ : 235.00 ; 252.95 ; 415.20 ; 432.15 ; 881.25 / ESI- : 857.05 ; 971.00	~ 2	Y (1) OSW-1 analog with PHBz
	8	257	16.982	ESI+ : 262.75 ; 324.35; 415.10 ; 525.35 ; 877.30 ; 937.10 ; 1016.35 / ESI- : 899.20	< 1	More product needed
	9	257	18.372	ESI+ : 248.95 ; 267.00 ; 415.20 ; 895.35 / 917.50	< 0.5	Y : OSW-1
F61-69	1	257	5.985	ESI+ : 427.15 ; 1041.05 / ESI- : 391.85 ; 772.90 ; 932.65	~ 6	N
	2	257	6.533	ESI+ : 323.00 ; 353.10 ; 571.40 ; 756.25 ; 854.90 ; 909.20 ; 939.15 / ESI- : 329.00 ; 921.25 ; 998.80	~ 4	N
	3	257	7.520	ESI+ : 249.05 ; 267.05 ; 281.05 ; 397.25 ; 415.30 ; 577.25 ; 1017.15 ; 1057.25 / ESI- : 871.05 ; 917.00 ; 985.30 ; 1068.85 ; 1079.05	~ 4	N
	4	257	9.065	ESI+ : 263.00 ; 280.90 ; 393.05 ; 411.10 ; 414.50 ; 443.10 ; 893.00 ; 1054.25 / ESI- : 868.90 ; 914.95 ; 983.05	~ 2	N
	5	258	10.557	ESI+ : 217.45 ; 266.95 ; 397.20 ; 415.20 ; 891.00 ; 1016.95 ; 1058.05 / ESI- : 313.90 ; 353.50 ; 1068.85	~ 3	N
	6	257	12.180	ESI+ : 267.00 ; 414.15 ; 429.00 ; 896.15 ; 1052.35 ; 1057.05 / ESI- : 335.10 ; 695.80 ; 887.15 ; 1069.05	~ 2	N

Appendix N. Compound LC-MS data IF-I-27 Fractions F70-72 and Wash

Column Fraction	FRC	λ Max (nm)	RT (min) at 254 nm	MS Peaks/Fragments	Mass (mg)	Characterization/Remarks (Y/N/Solvent Pb /2D needed)
F70-72	1	257	4.697	**ESI+** : 268.10	< 1	N
	2	263	4.804	**ESI+** : 268.10 ; 318.30 ; 446.15 ; 468.15 / **ESI-** : 444.05 ; 679.30 ; 703.85	< 1	N
	3	257	5.708	**ESI+** : 281.10 ; 397.30 ; 415.25 ; 577.35 ; 923.35 ; 1041.40 / **ESI-** : 775.20 ; 871.40 ; 935.20 ; 945.20 ; 1013.15	~ 6	N
	4	257	6.514	**ESI+** : 295.20 ; 353.15 ; 939.35 ; 999.50 ; 1164.95 / **ESI-** : 329.15 ; 857.20	~ 3	N
	5	249	6.957	**ESI+** : 267.05 ; 393.25 ; 411.30 ; 573.25 ; 879.35 / **ESI-** : 347.75 ; 855.25 ; 969.20	~ 3	OSW-1 without C17 hydroxyl
	6	257	7.498	**ESI+** : 267.15 ; 415.25 ; 577.35 ; 1017.40 ; 1057.50 / **ESI-** : 985.25 ; 1069.15 ; 1079.15	~ 2	N
	7	257	9.040	**ESI+** : 281.10 ; 393.05 ; 442.90 ; 561.25 ; 893.35 / **ESI-** : 402.80 ; 869.25 ; 915.20 ; 983.20	~ 1	N
	8	257	12.245	**ESI+** : 215.95 ; 415.30 ; 429.10 ; 1053.45 ; 1057.35 / **ESI-** : 1069.25	~ 2	N
Wash	1	257	4.690	**ESI+** : 268.05 ; 316.20 / **ESI-** : 785.20	~ 1	N
	2	266	5.077	**ESI+** : 309.10 ; 316.30 ; 327.05 ; 943.30 / **ESI-** : 955.05 ; 965.15 ; 1033.15	~ 3	Not pure (2 products)
	3	257	5.702	**ESI+** : 266.95 ; 316.20 ; 397.25 ; 415.25 ; 577.35 ; 923.35 ; 1036.50 ; 1041.30 / **ESI-** : 478.25 ; 935.20 ; 945.20 ; 1013.15	~ 3	N
	4	257	6.508	**ESI+** : 256.40 ; 295.25 ; 353.15 ; 415.15 ; 477.05 ; 571.30 ; 899.40 / **ESI-** : 329.15 ; 860.30	~ 1	Not pure (2 products)
	5	257	6.945	**ESI+** : 267.10 ; 330.25 ; 353.25 ; 393.50 ; 554.55 ; 879.30 ; 991.30 / **ESI-** : 395.70 ; 547.80 ; 855.20 ; 968.10	~ 2	N
	6	257	7.492	**ESI+** : 281.25 ; 397.35 ; 415.30 ; 577.25 ; 923.30 ; 1017.35 ; 1057.30 / **ESI-** : 899.40 ; 945.30 ; 1013.20 ; 1079.35	~ 1	N
	7	257	7.975	**ESI+** : 253.00 ; 397.15 ; 448.00 ; 415.30 ; 1043.35 / **ESI-** : 1019.25 ; 1054.90	~ 1	N
	8	257	12.234	**ESI+** : 415.25 ; 429.20 ; 538.85 ; 717.95 ; 1052.45 ; 1057.35 ; 1078.80 / **ESI-** : 696.50 ; 1069.30 ; 1079.15	~ 1	N

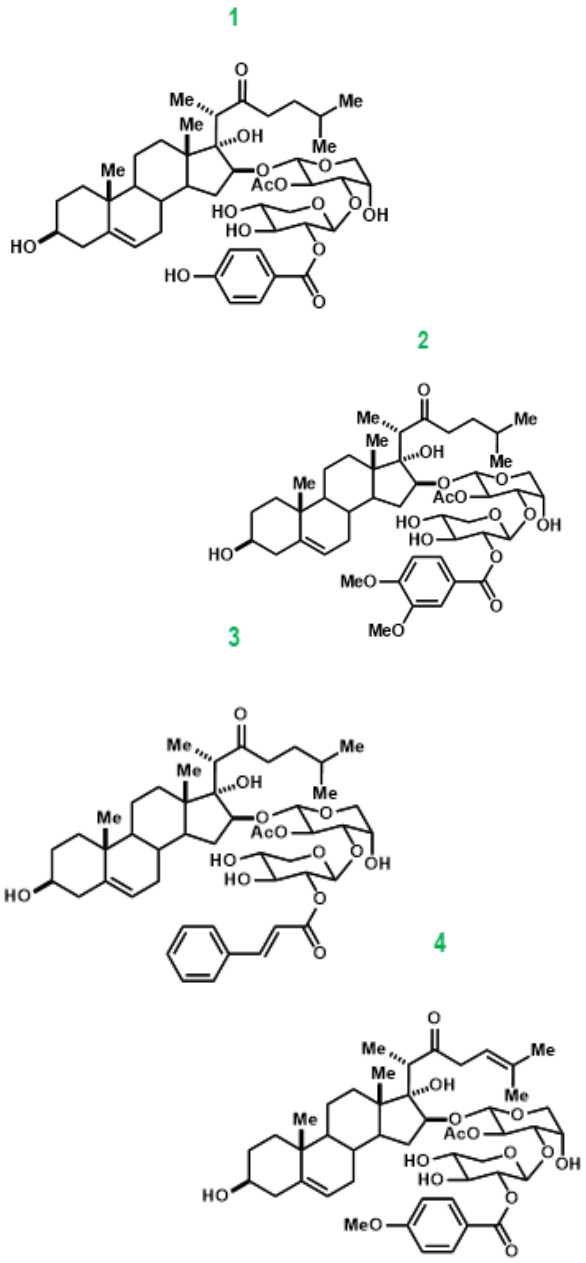

Appendix O. Compound LC-MS data IF-I-29 Fractions F26-37, F38-45, F46-53 and F54-68

Column Fraction	FRC	λ Max (nm)	RT (min) at 254 nm	MS Peaks/Fragments	Mass (mg)	Characterization/Remarks (Y/N/Solvent Pb /2D needed)
F26-37	1	279	5.783	**ESI+** : 284.10 ; 413.35 ;701.45	1.6	N
	2	266	9.151	**ESI+** : 279.10 ; 383.15 ; 401.20 ; 837.60	3	N
	3	257	9.996	**ESI+** : 323.10 ; 341.10 ; 405.35 ; 777.45	2.5	**Y : D3/IF-193**
	4	256	10.687	**ESI+** : 323.15 ; 341.10 ; 559.70 ; 779.40	3	**Y : D4/ IF-194**
	5	262	15.793	**ESI+** : 279.05 ; 296.95 ; 415.45 ; 671.50 ; 925.50	1	N
	6	257	18.699	**ESI+** : 249.00 ; 267.05 ; 415.35 ; 441.10 ; 895.55 / **ESI-** : 917.40	2	**Y : OSW-1 (D6 & IF-196)**
	7	277	21.327	**ESI+** : 245.25 ; 263.05 ; 415.35 ; 891.45 / **ESI-** : 913.50	1.6	**Y : 3 (D7 & IF-197)**
	8	241	25.952	**ESI+** : 324.30 ; 484.30 ; 489.05 ; 583.45 ; 671.40	1.3	N
F38-45	1	266	9.665	**ESI+** : 271.55 ; 383.25 ; 401.20 ; 415.10 ; 839.50	2	N
	2	257	9.991	**ESI+** : 224.25 ; 323.10 ; 747.90 ; 777.45	1.6	N
	3	256	10.670	**ESI+** : 244.85 ; 323.10 ; 341.10 ; 415.50 ; 761.40 ; 779.40	1.3	**Y : E3/IF-201**
	4	257	11.471	**ESI+** : 235.10 ; 253.05 ; 415.40 ; 881.50	2	**Y : E4/IF-202**
	5	256	12.471	**ESI+** : 248.85 ; 319.05 ; 415.50 ; 761.10 ; 775.70	1	N
	6	257	14.976	**ESI+** : 267.00 ; 413.25 ; 869.30 ; 893.40	<1	N
	7	262	15.387	**ESI+** : 266.05 ; 297.00 ; 415.40 ; 588.30 ; 925.45	1	**Y : 2 (E7/IF-205)**
	8	257	17.893	**ESI+** : 249.00 ;267.05 ; 415.35 ; 895.45	4	**Y : E8/IF-208**
	9	278	20.040	**ESI+** : 245.05 ; 263.15 ; 415.35 ; 757.40 ; 891.50	<1	Y : E9/IF-207
F46-53	1	258	4.463	**ESI+** : 314.15 ;1019.35	Pending	Pending
	2	265	6.187	**ESI+** : 367.70 ; 383.10 ; 427.25 ; 487.20 ; 999.55 / **ESI-** : 1021.50	Pending	Pending
	3	257	6.532	**ESI+** : 241.10 ; 323.05 ; 409.15 ; 939.45 / **ESI-** : 931.25	Pending	Pending
	4	257	7.538	**ESI+** : 267.10 ; 281.00 ; 397.35 ; 415.30 ; 577.45 ; 1017.55 ; 1057.45 / **ESI-** : 1079.40	Pending	Pending
	5	258	9.079	**ESI+** : 262.75 ; 281.10 ; 397.35 ; 415.20 ; 561.20 ; 893.30 ; 1013.80 ; 1053.65 / **ESI-** : 867.35 ; 915.30	Pending	Pending
	6	257	9.648	**ESI+** : 273.70 ; 363.30 ; 409.35 ; 441.35 ; 571.35 ; 857.50 ; 895.25 ; 918.40 ; 965;40 / **ESI-** : 945.25	Pending	Pending
	7	257	13.219	**ESI+** : 281.10 ; 413.35 ; 561.25 ; 909.35 / **ESI-** : 931.40	Pending	Pending
F54-68	1	266	5.070	**ESI+** : 309.15 ; 327.10 ; 943.60 / **ESI-** : 965.40	Pending	Pending
	2	258	6.519	**ESI+** : 267.10 ; 323.15 ; 413.40 ; 571.35 ; 939.55	Pending	Pending
	3	257	7.508	**ESI+** : 249.15 ; 267.25 ; 281.00 ; 397.30 ; 415.40 ; 577.45 ; 1017.55 ; 1057.60 / **ESI-** : 1079.45	Pending	Pending
	4	257	9.059	**ESI+** : 212.55 ; 281.10 ; 343.35 ; 443.40 ; 574.45 ; 894.45 / **ESI-** : 915.35 ; 983.45	Pending	Pending

Appendix P. NMR Spectrum of 2 (OSW-1)

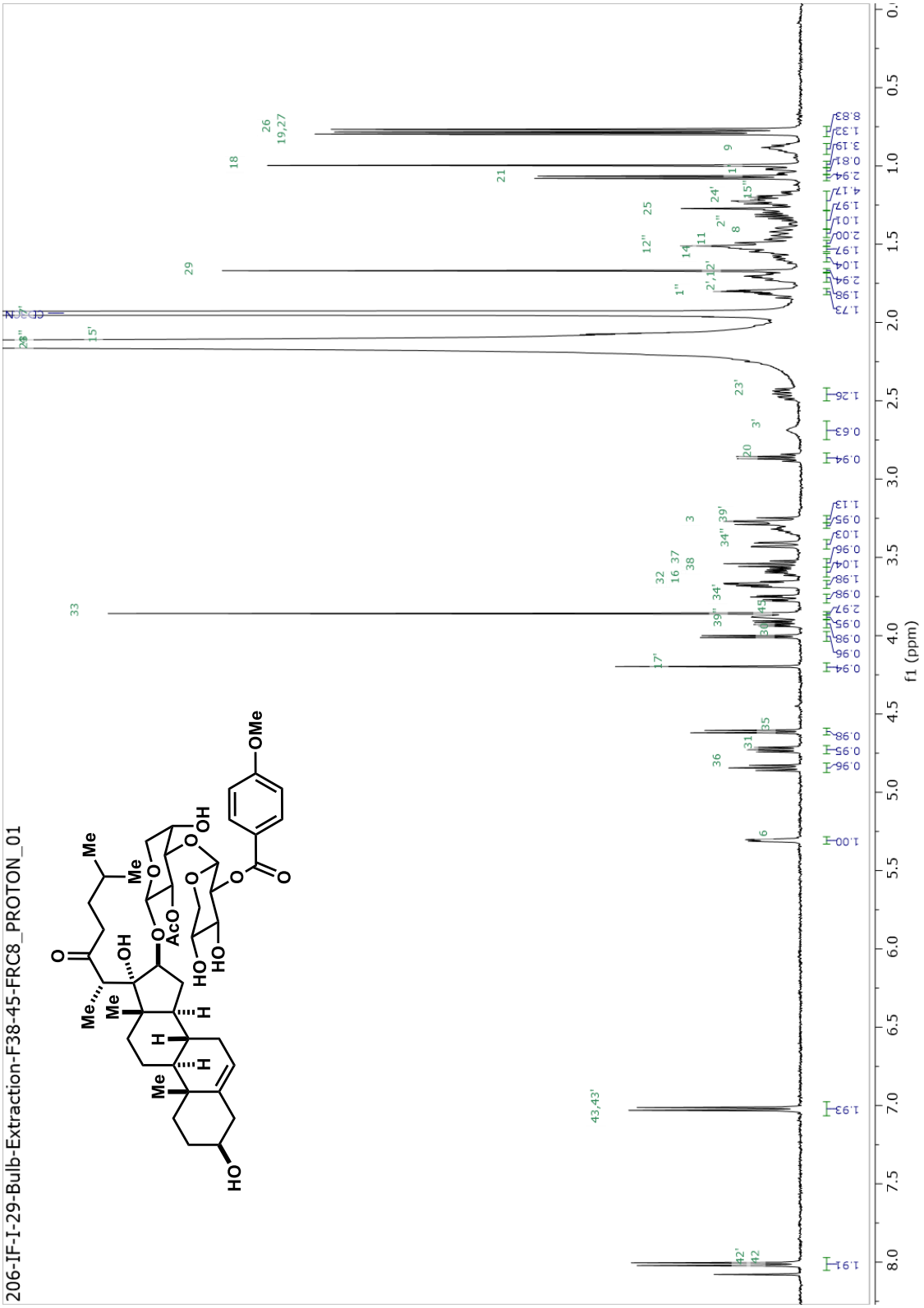

Appendix Q. NMR Spectrum of 3 (DMBz Analog)

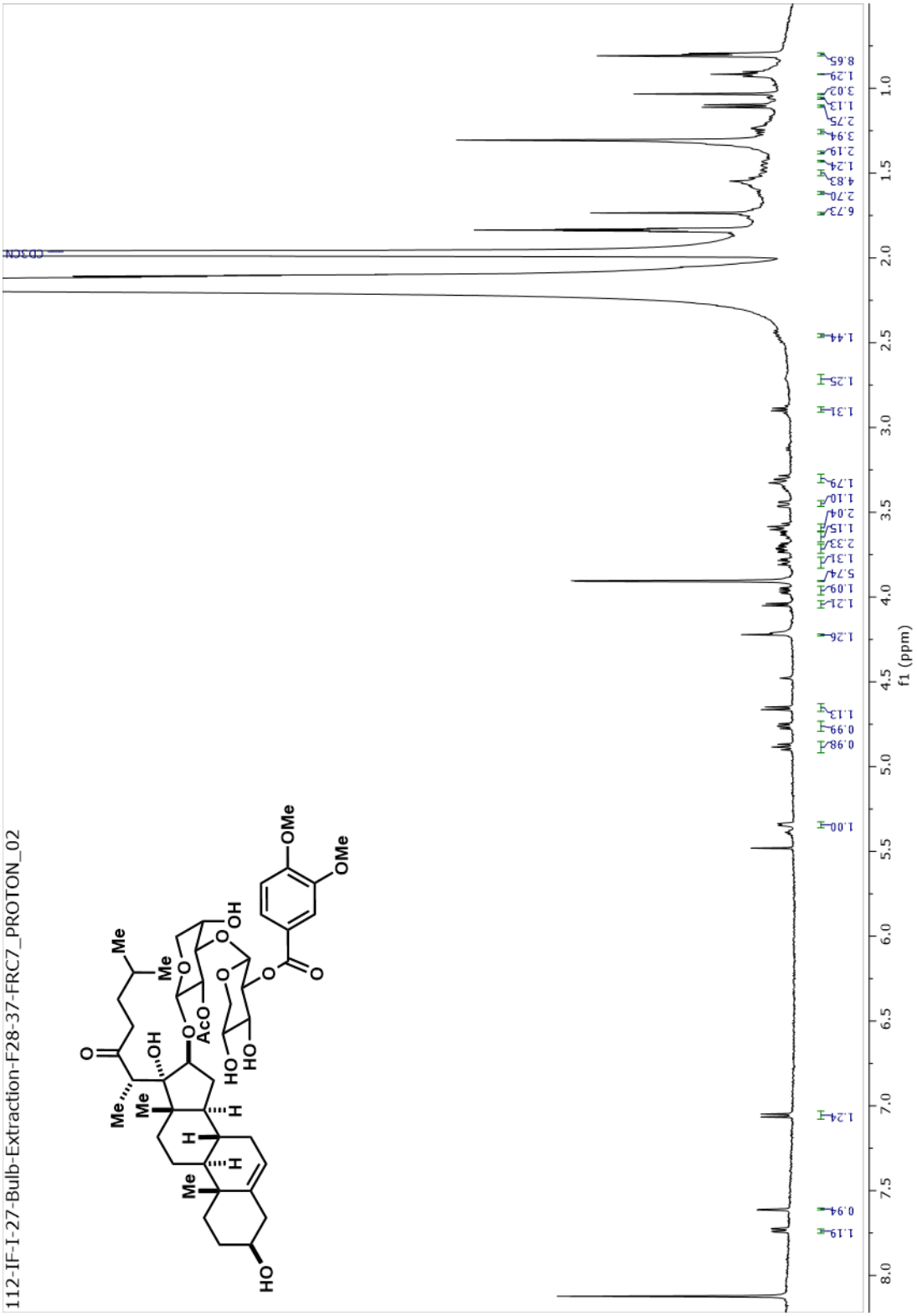

Appendix R. NMR Spectrum of 4 (E-CNM Analog)

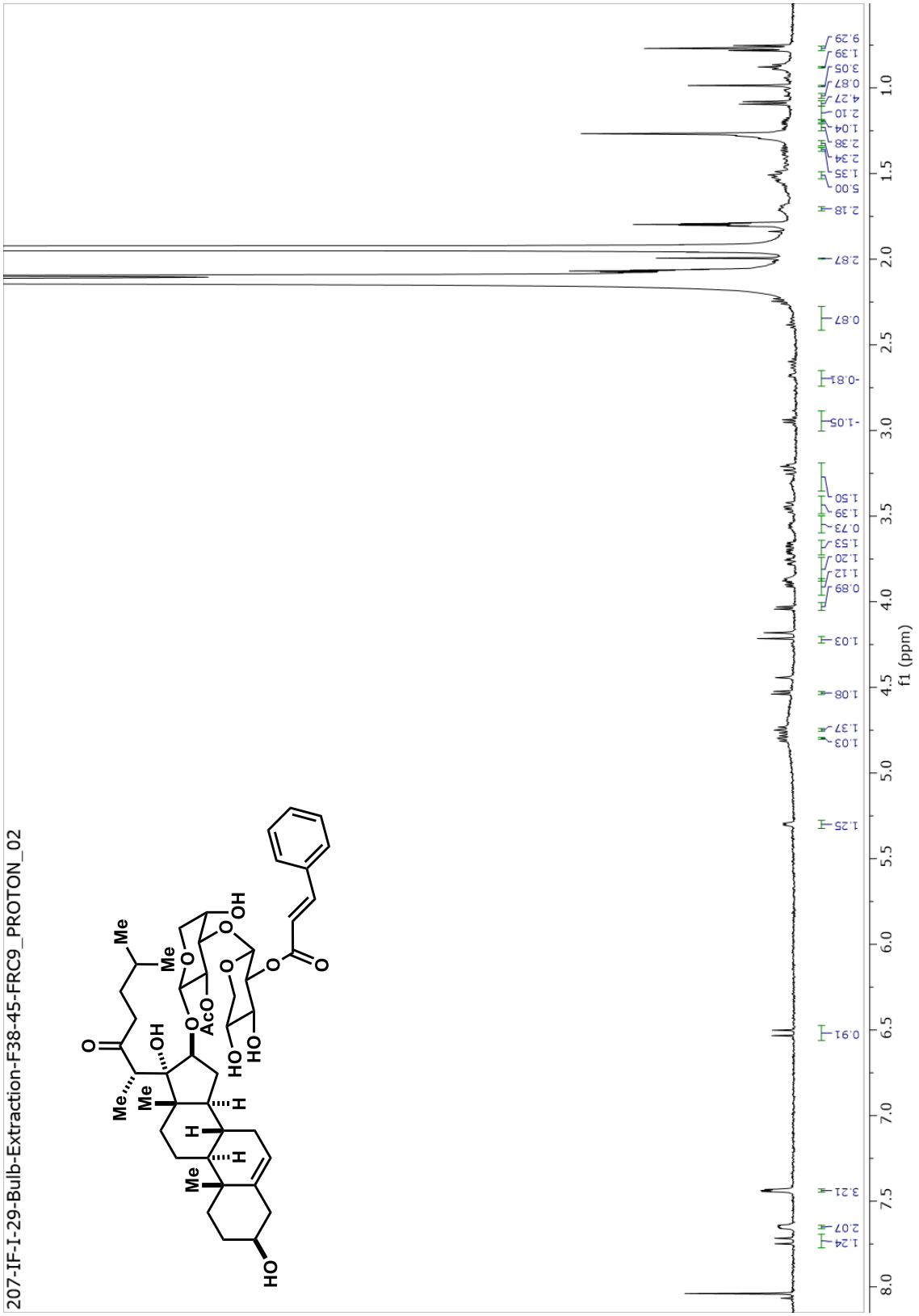

Appendix S. NMR Spectrum of 9 (PHBz Analog)

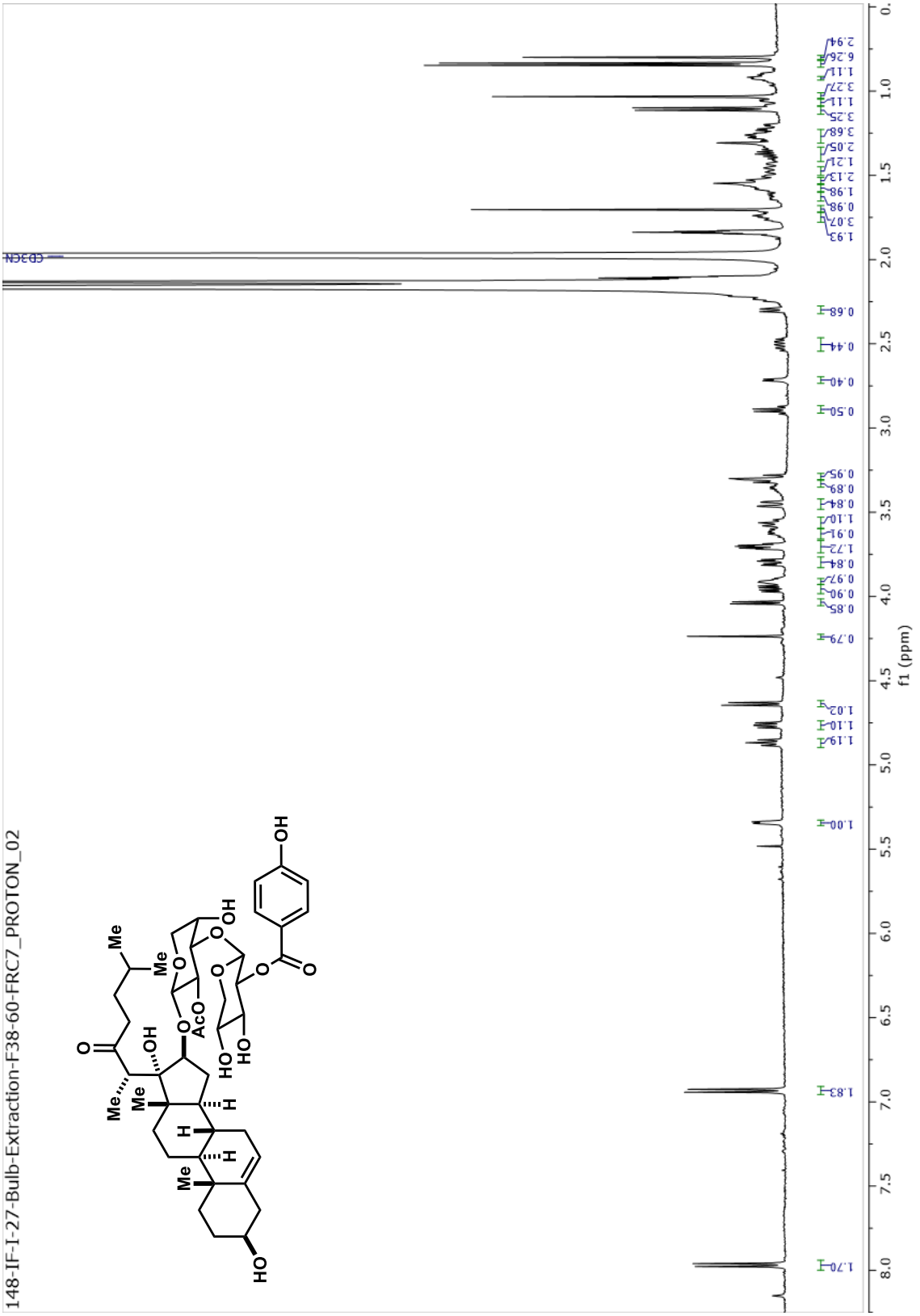

Appendix T. NMR Spectrum of 20 (Cholestane Rhamnoside)

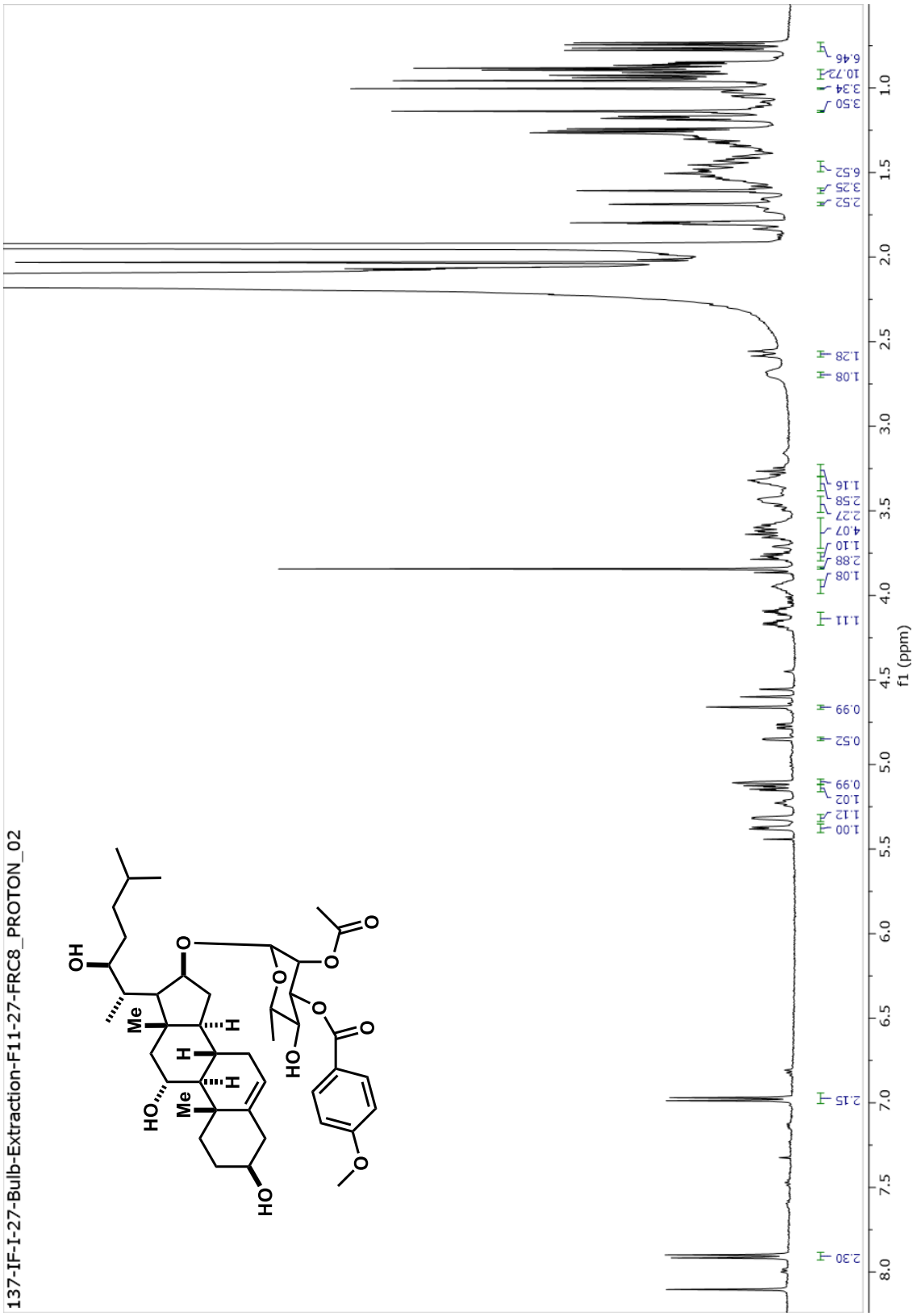

Appendix U. NMR Spectrum of IF-111 (Novel C24-C25 Unsaturated Analog)